NAVAL POSTGRADUATE SCHOOL
Monterey, California

THESIS

SIMULATION OF THE BOHAI SEA CIRCULATION AND THERMOHALINE STRUCTURE USING COHERENS MODEL

by

Rodrigo S. Obino

June 2002

Thesis Advisor:	Peter C. Chu
Second Reader:	Steven D. Haeger (NAVO)

Approved for public release; distribution is unlimited

THIS PAGE INTENTIONALLY LEFT BLANK

REPORT DOCUMENTATION PAGE			Form Approved OMB No. 0704-0188
Public reporting burden for this collection of information is estimated to average 1 hour per response, including the time for reviewing instruction, searching existing data sources, gathering and maintaining the data needed, and completing and reviewing the collection of information. Send comments regarding this burden estimate or any other aspect of this collection of information, including suggestions for reducing this burden, to Washington headquarters Services, Directorate for Information Operations and Reports, 1215 Jefferson Davis Highway, Suite 1204, Arlington, VA 22202-4302, and to the Office of Management and Budget, Paperwork Reduction Project (0704-0188) Washington DC 20503.			
1. AGENCY USE ONLY *(Leave blank)*	**2. REPORT DATE** June 2002	**3. REPORT TYPE AND DATES COVERED** Master's Thesis	
4. TITLE AND SUBTITLE: Simulation of the Bohai Sea Circulation and Thermohaline Structure Using COHERENS Model			**5. FUNDING NUMBERS**
6. AUTHOR(S) Rodrigo de S. Obino			
7. PERFORMING ORGANIZATION NAME(S) AND ADDRESS(ES) Naval Postgraduate School Monterey, CA 93943-5000			**8. PERFORMING ORGANIZATION REPORT NUMBER**
9. SPONSORING /MONITORING AGENCY NAME(S) AND ADDRESS(ES) N/A			**10. SPONSORING/MONITORING AGENCY REPORT NUMBER**
11. SUPPLEMENTARY NOTES The views expressed in this thesis are those of the author and do not reflect the official policy or position of the Department of Defense or the U.S. Government.			
12a. DISTRIBUTION / AVAILABILITY STATEMENT Approved for public release; distribution is unlimited			**12b. DISTRIBUTION CODE**

13. ABSTRACT ***(maximum 200 words)***

The goals of this work are to simulate the Bohai Sea circulation and thermohaline structure and to investigate the physical mechanisms using the Coupled Hydrodynamical-Ecological Model for Regional and Shelf Seas (COHERENS) with realistic bottom topography and coastal geometry. The model-simulated seasonal variability of the circulation pattern and the thermal structure agree qualitatively with the observation. The salinity field is not as well simulated as the temperature. The thermohaline structure is vertically stratified during the summer monsoon. The sub-surface velocities are found to be compensating currents from the surface circulation.

Several experiments are performed to identify the prevailing forcing functions and Bohai Sea characteristics: (1) control run, with all the surface forcing functions (thermohaline fluxes, wind, tides) present, (2) no-thermohaline flux run, (3) no-wind run, and (4) no-tide run. The experiments show that the surface wind effect is the major forcing to drive the surface currents and the thermohaline structure, the thermohaline flux is the important driving force for the thermal structure, and the tidal mixing is responsible for the deep layer characteristics.

It is also found that a higher turbulence kinetic energy (TKE) is produced using the Mellor-Yamada turbulence closure scheme than the "k-ε" scheme. The deeper regions present higher TKE at the surface than in shallow waters. Maximum TKE for July are greater than the maximum TKE in January.

14. SUBJECT TERMS: Ocean Modeling, Simulation, Sensitivity Study, Primitive Equation Model, Shallow Sea, Circulation, GDEM, COHERENS, Sigma Coordinate, TKE	**15. NUMBER OF PAGES** 142
	16. PRICE CODE

17. SECURITY CLASSIFICATION OF REPORT	**18. SECURITY CLASSIFICATION OF THIS PAGE**	**19. SECURITY CLASSIFICATION OF ABSTRACT**	**20. LIMITATION OF ABSTRACT**
Unclassified	Unclassified	Unclassified	UL

NSN 7540-01-280-5500 Standard Form 298 (Rev. 2-89)
Prescribed by ANSI Std. 239-18

THIS PAGE INTENTIONALLY LEFT BLANK

Approved for public release; distribution is unlimited

SIMULATION OF THE BOHAI SEA CIRCULATION AND THERMOHALINE STRUCTURE USING COHERENS MODEL

Rodrigo S. Obino
Lieutenant Commander, Brazilian Navy
B.S., Brazilian Naval Academy, 1989

Submitted in partial fulfillment of the
requirements for the degree of

MASTER OF SCIENCE IN PHYSICAL OCEANOGRAPHY

from the

NAVAL POSTGRADUATE SCHOOL
June 2002

Author: Rodrigo S. Obino

Approved by: Peter C. Chu
Thesis Advisor

Steven D. Haeger (NAVO)
Second Reader

Mary L. Batteen
Chairman, Department of Oceanography

THIS PAGE INTENTIONALLY LEFT BLANK

ABSTRACT

The goals of this work are to simulate the Bohai Sea circulation and thermohaline structure and to investigate the physical mechanisms using the Coupled Hydrodynamical-Ecological Model for Regional and Shelf Seas (COHERENS) with realistic bottom topography and coastal geometry. The model-simulated seasonal variability of the circulation pattern and thermal structure agree qualitatively with the observation. The salinity field is not as well simulated as the temperature. The thermohaline structure is vertically stratified during the summer monsoon. The sub-surface velocities are found to be compensating currents from the surface circulation.

Several experiments are performed to identify the prevailing forcing functions and Bohai Sea characteristics: (1) control run, with all the surface forcing functions (thermohaline fluxes, wind, tides) present, (2) no-surface thermohaline flux run, (3) no-wind run, and (4) no-tide run. The experiments show that the surface wind effect is the major forcing to drive the surface currents and the thermohaline structure, the thermohaline flux is the important driving force for the thermal structure, and the tidal mixing is responsible for the deep layer characteristics.

It is also found that a higher turbulence kinetic energy (TKE) is produced using the Mellor-Yamada turbulence closure scheme than the "k-ε" scheme. The deeper regions present higher TKE at the surface than in shallow waters. Maximum TKE for July are greater than the maximum TKE in January.

THIS PAGE INTENTIONALLY LEFT BLANK

TABLE OF CONTENTS

THIS PAGE INTENTIONALLY LEFT BLANK

LIST OF FIGURES

THIS PAGE INTENTIONALLY LEFT BLANK

LIST OF TABLES

THIS PAGE INTENTIONALLY LEFT BLANK

ACKNOWLEDGMENTS

The author wishes to thank Dr. Peter Chu and Mr. Steven Haeger for their suggestions and guidance throughout this thesis. In addition, the author would like to express his appreciation to Mr. Chenwu Fan for providing necessary assistance in computer programming. Finally, a very special thank must go to my fiancée, Namhee, for her support during this work.

THIS PAGE INTENTIONALLY LEFT BLANK

I. INTRODUCTION

A. BACKGROUND

The Bohai Sea (BS) is a semi-enclosed sea surrounded by the Chinese mainland and the Liaodong Peninsula and connected to the northern Huanghai Sea, also called the Yellow Sea (YS), by the Bohai Strait. It is divided into four parts (Figure 1): Liaodong Gulf to the northeast, Bohai Gulf to the west, Laizhou Bay to the south and central basin. It covers an area of approximately 80,000 km^2, has a width of 300 km and a length of 500 km. It has relatively shallow waters with an average depth of 18 m (Huang et al., 1995). The depth increases gradually from the coastal area to the central basin where the maximum depth is about 30 m. The deepest region is on the northern side of the Bohai Strait where the depth reaches 60 m (Figure 2).

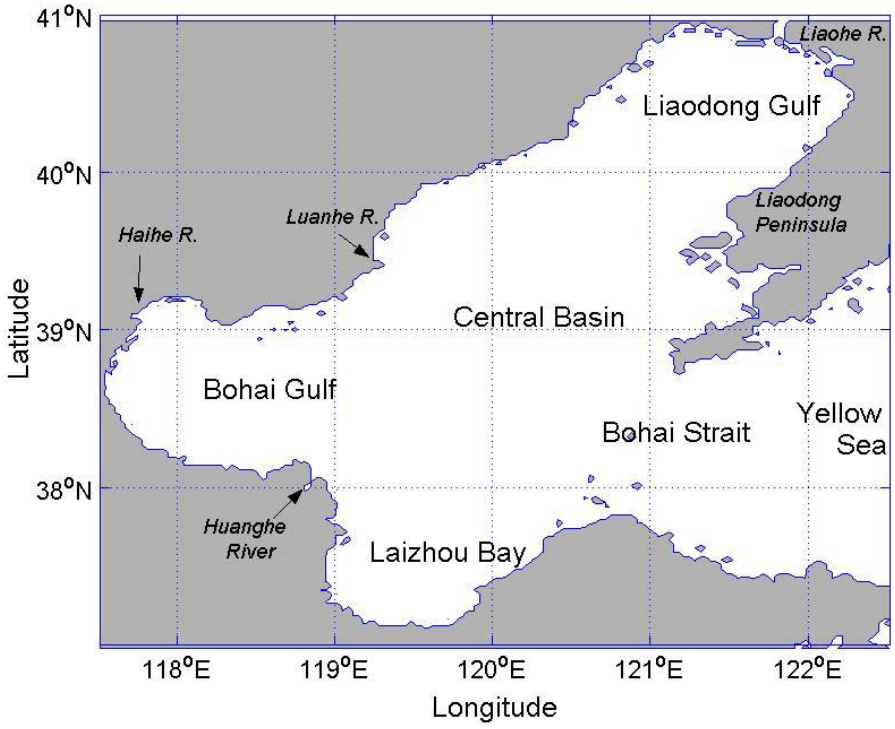

Figure 1. Bohai Sea

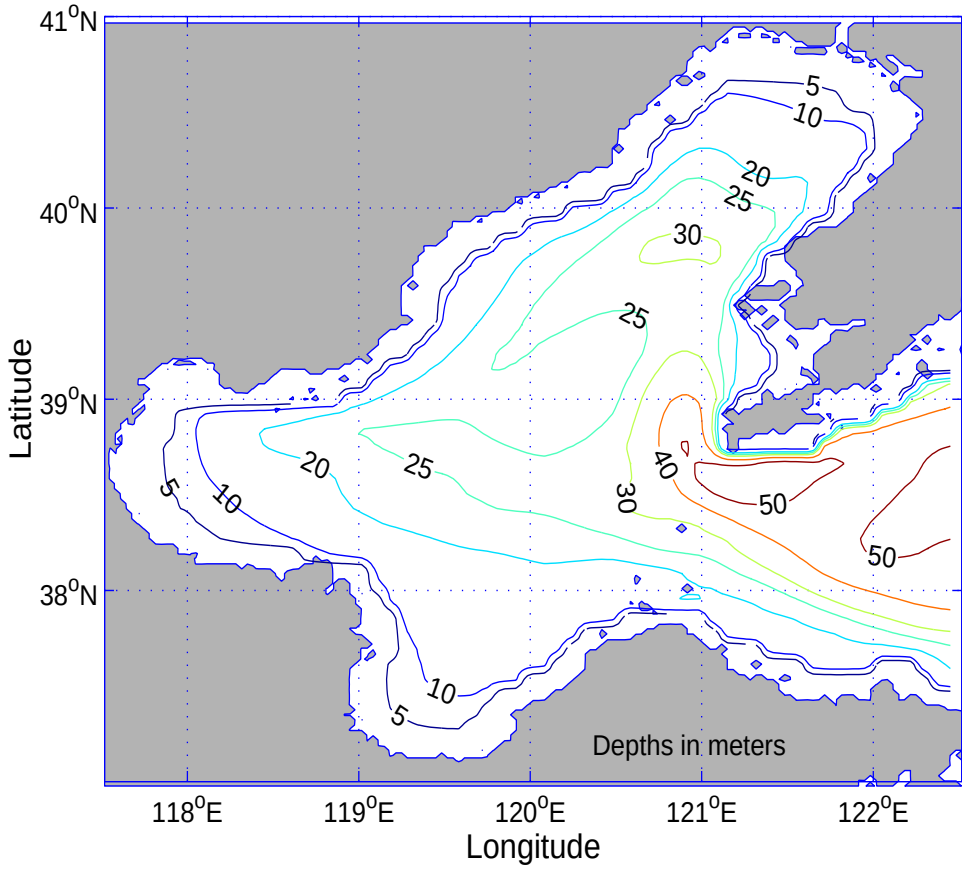

Figure 2. **Bottom topography in the Bohai Sea**

Monsoon winds, surface thermohaline fluxes (net heat flux and moisture flux), tides, and open-ocean forcing affect the BS circulation and thermohaline structure. The BS circulation is composed of the predominant extension of the Yellow Sea Warm Current, the Liaonan Coastal Current, and the southern Bohai Sea Coastal Current. The saline distribution indicates that saltier water enters the BS from the north YS through the northern Bohai Strait and less saline water leaves the BS through the southern Bohai Strait. The Yellow Sea Warm Current extension penetrates the BS like a jet and moves westward through the central basin. When it reaches the west coast, it divides into two branches. The northward branch goes towards the Liaodong Gulf forming an anticyclonic gyre while the other southward branch goes towards the Bohai Gulf to feed a cyclonic gyre (Guan, 1994). Usually, the current is stronger in the winter than in the summer (Figure 3).

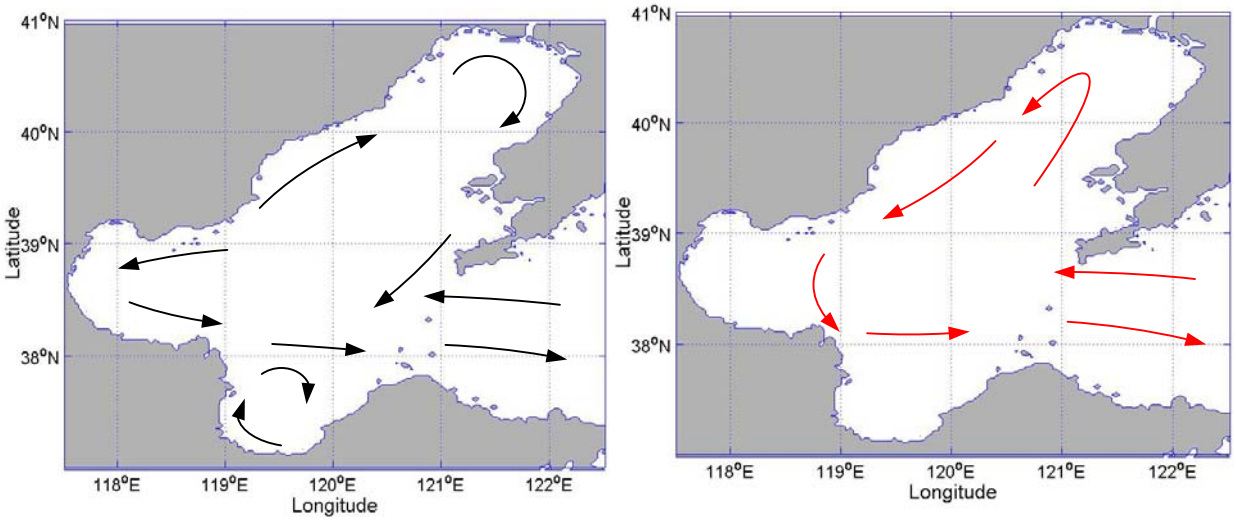

Figure 3. **Circulation in Bohai Sea during winter (black) and summer (red)**

The ocean systems in the winter are forced by frequent outbreaks of the continental Siberian High from October to March (Figure 4). The strong northerly winds following the surge of cold and dry continental air result in vertically well-mixed conditions and drive the currents southward (Su Jilan, 1998). The temperature distribution shows vertical uniformity, while the salinity is around 26-31 psu. Northerly winds prevail and the mean speed is 8.5 m/s. Winds can rise up to 25-28 m/s and the air temperature decreases sharply. Tidal currents prevail and the current velocity is generally 50-100 cm/s. Nontidal currents, represented as wind-driven currents, the coastal current and the Yellow Sea Warm Current, are weaker than the tidal currents (Wu et al., 1998). The Yellow Sea Warm Current Extension still reaches the BS. East of the Bohai Strait the salinity reaches its maximum in February-March. The distribution of water masses is basically the same for the entire water column. From November to April, the water masses have the following distribution: The Bohai Sea and Yellow Sea Mixed Water originates in the YS and reaches the Bohai Strait. The Bohai Sea Central Water dominates the central basin. The Bohai Sea Coastal Water appears to the south and southwest of the Bohai Sea Central Water. The Continental Diluted Water concentrates at the Bohai Gulf and at the Laizhou Bay (Su et al., 1994). Sea ice usually forms in

December along the coast of the BS and disappears by early March of the following year. Normally, it is limited to areas with a water depth of less than 10 m. There are also records that the BS has been almost fully covered by sea ice between January and March (Wu et al., 1998).

During the summer, an interesting feature appears as the bottom cold tongue from the Yellow Sea Cold Water at the Bohai Strait. This water mass is formed from the re-stratification in the BS and YS due to the summer warming of the surface water and weak wind mixing (Zhao, 1989). Due to the strengthening of the density circulation of the Yellow Sea Cold Water Mass and of the Liaonan Coastal Current, the westward current is strong. In Liaodong Bay, the current usually moves anticyclonically, but can be in the opposite direction if the Liaohe River discharge strengthens. The warm and moist southerly winds (Figure 4) drive northward boundary currents in the shallow waters near the coast. The stratification fluctuates with synoptic winds throughout the warm months and is destroyed around the end of summer after the northerly wind return. Tides are also very important for the circulation dynamics of the BS. Between June and October, at the upper layers, the Bohai Sea Central Water is converted into the Bohai Sea and the Yellow Sea Mixed Water. The Continental Diluted Water expands off the coast and appears at the Liaodong Gulf. At the lower layers, the distribution differs from winter with the presence of the North Yellow Sea Bottom Cold Water in the north and in the central basin. The rivers are present at the BS. The Huanghe River (or called Yellow River) is the largest one discharging on the southern shore, but changes the velocities near the estuary and has not enough strength to change the summer motion throughout the BS (Wang et al., 1993). Other major rivers discharging on the BS are the Liaohe River to the north, the Haihe River and the Luanhe River to the west.

The results of observations suggest that the tidal current dominates in the Bohai Strait and especially the M_2 tidal harmonic (Li et al., 1988; Feng et al., 1994; Fang, 1994). The current pattern, the inflow on the northern side and the outflow to the southern part, seems to be controlled by the bottom topography as discussed by Miao and Liu (1989). The transport processes of pollutants and wastes originating from the heavily populated industrialized sections of the northern and southern coasts across the straits are important for marine environmental protection and management of the area. The sea

surface temperature is considered by Jin et al. (1993) to be determinant also in oceanic fishing, communication, oceanic exploration and submarine operations.

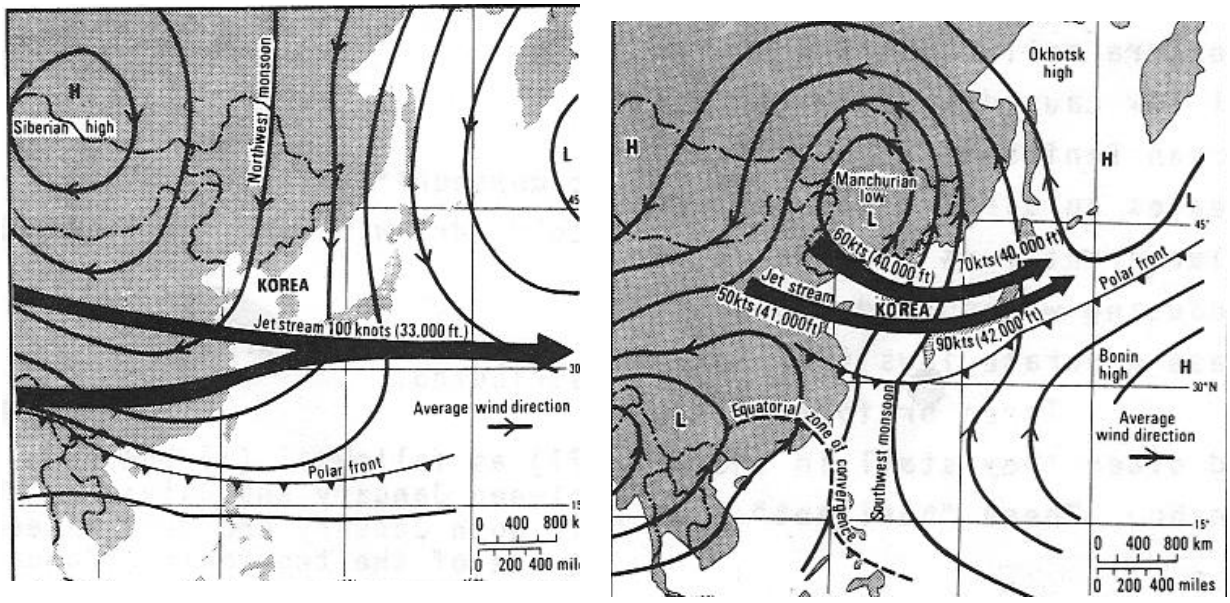

Figure 4. Wind systems for February (left) and June (right)

The tidal mixing and the wind effect cause the thermocline fluctuations, accordingly to Zhang and Wang (1992). In the BS, the thermocline thickness increases from the shallow region to the deeper area and the thermocline is considered seasonal due to the monsoon atmospheric variability (Wang et al., 1998).

B. PREVIOUS SIMULATION STUDIES

Three-dimensional hydrodynamic models for regional and shelf seas have been developed for several decades to simulate physical processes with various scales. Dou et al. (1994) used a three-dimensional hydrodynamic model to simulate the tidal circulation in the BS with the four major tidal harmonics of M_2, S_2, K_1 and O_1 specified at the eastern open boundary. The model was integrated from rest initially. The simulated co-tidal charts agree qualitatively with the observations and confirm the standing wave characteristics of the BS tides. Their numerical studies show the following results: (1)

existence of a strong current at the northern Bohai Strait, (2) anticyclonic rotation of the tidal vector dominating the BS except at the tip of the Liaodong and Bohai Gulfs, and (3) the vertical velocity strongly affected by the topography. However, no analysis of the thermohaline structure was presented.

Sun et al. (1994) used a numerical model to simulate the salinity structure and found that the bottom salinity is correlated to the bottom topography. On the Bohai Strait, the northern part defines a high-salinity tongue and the southern part a low-salinity feature. Their results were compared to the observational data only in July.

Huang et al. (1995) used the Hamburg Shelf Ocean Model (HAMSOM), a three-dimensional baroclinic primitive equation model, to investigate the barotropic processes of tides, wind-driven current and their interaction. This model was set with a spherical grid with a resolution of 5' in latitude and longitude, ten z-vertical layers and a maximum time step of 30 minutes. The model forcing functions consist of tides at the eastern open boundary at 122°30'W. The sea surface wind speed and heat flux at air-sea interface were obtained from the interpolation and objective analysis of four coastal stations. The velocity at the open boundary is controlled by Orlanski radiation condition. Five tidal components, M_2, S_2, N_2, K_1 and O_1, are used for harmonic analysis. The sea was at rest for the initial conditions.

The model simulates some phenomena such as local maximum in the sea surface at the head of the three bays during the summer due to the shallow water and low heat capacity. Cold-water belts appeared in relatively deep regions near tidal fronts. From their analysis, the dominant diurnal and semidiurnal tidal components were K_1 and M_2, and the type of tide was mixed with semidiurnal predominance. A pair of cyclonic and anticyclonic eddies in the northern Bohai Strait was noticed. Three regions of strong currents were observed in the Bohai Strait, in the central Bohai Gulf and in the eastern Liaodong Gulf. In the upper layers, the tidal currents had a small vertical variation. The water transport between the YS and BS was defined by the inflow at the surface and the outflow in the lower layers through the southern Bohai Strait during the winter, and by the inflow through the south and the outflow through the northern Bohai Strait due to a cyclonic eddy during the summer.

Since the surface winds and heat and moisture fluxes are obtained from the four coastal stations, it is reasonable to doubt the accuracy of the surface forcing functions. Also, the physical processes that determine the circulation and the thermohaline structure were not discussed in detail in their studies.

C. OBJECTIVES

The objectives of this work are to simulate the BS circulation and thermohaline structure using the synoptic forcing, to investigate the physical mechanisms, and to compare the two commonly used turbulence closures schemes, "*k–l*" scheme (or called Mellor-Yamada scheme) and "k-ε" scheme, using the Coupled Hydrodynamical-Ecological Model for Regional and Shelf Seas (COHERENS) with realistic bottom topography and coastal geometry. To do so, several experiments will be performed to identify the prevailing forcing functions and Bohai Sea characteristics: (1) control run, with all the surface forcing functions (thermohaline fluxes, wind, tides) present, (2) no-thermohaline flux run (3) no-wind run, and (4) no-tide run. The difference between the control run and the sensitivity runs (no-thermohaline flux, no-wind, and no-tides) leads to the effects of the thermohaline fluxes, winds, and tides.

THIS PAGE INTENTIONALLY LEFT BLANK

II. MODEL DESCRIPTION

A. MODEL FEATURES

COHERENS is a three-dimensional hydrodynamical model for coastal and shelf seas, coupled to sediment, contaminant and biological models (EU Marine Science and Technology Program, 1999). Developed by a multinational European group, it has primarily been implemented for the North Sea and stratified coastal seas for predicting and monitoring waste materials. The relatively easy understanding of the model structure and the flexibility due to the capability of selecting different processes, specific schemes and parameterizations, or numerous types of forcing are the advantages of the model.

The incompressible governing primitive equations of the model, derived from the Navior-Stokes equations, are given by:

- The momentum equations based on the Boussinesq approximation and hydrostatic equilibrium:

$$\frac{\partial u}{\partial t}+u\frac{\partial u}{\partial x}+v\frac{\partial u}{\partial y}+w\frac{\partial u}{\partial z}-fv=-\frac{1}{\rho_0}\frac{\partial p}{\partial x}+\frac{\partial}{\partial z}\left(\nu_T\frac{\partial u}{\partial z}\right)+\frac{\partial \tau_{xx}}{\partial x}+\frac{\partial \tau_{yx}}{\partial y} \tag{1}$$

$$\frac{\partial v}{\partial t}+u\frac{\partial v}{\partial x}+v\frac{\partial v}{\partial y}+w\frac{\partial v}{\partial z}+fu=-\frac{1}{\rho_0}\frac{\partial p}{\partial y}+\frac{\partial}{\partial z}\left(\nu_T\frac{\partial v}{\partial z}\right)+\frac{\partial \tau_{xy}}{\partial x}+\frac{\partial \tau_{yy}}{\partial y} \tag{2}$$

$$-\frac{1}{\rho}\frac{\partial p}{\partial z}=\rho g \tag{3}$$

- The continuity equation:

$$\frac{\partial u}{\partial x}+\frac{\partial v}{\partial y}+\frac{\partial w}{\partial z}=0 \tag{4}$$

- The equations of temperature and salinity:

$$\frac{\partial T}{\partial t}+u\frac{\partial T}{\partial x}+v\frac{\partial T}{\partial y}+w\frac{\partial T}{\partial z}=\frac{1}{\rho_0 c_p}\frac{\partial I}{\partial z}+\frac{\partial}{\partial z}\left(\lambda_T\frac{\partial T}{\partial z}\right)+\frac{\partial}{\partial x}\left(\lambda_H\frac{\partial T}{\partial x}\right)+\frac{\partial}{\partial y}\left(\lambda_H\frac{\partial T}{\partial y}\right) \tag{5}$$

$$\frac{\partial S}{\partial t}+u\frac{\partial S}{\partial x}+v\frac{\partial S}{\partial y}+w\frac{\partial S}{\partial z}=\frac{\partial}{\partial z}\left(\lambda_T\frac{\partial S}{\partial z}\right)+\frac{\partial}{\partial x}\left(\lambda_H\frac{\partial S}{\partial x}\right)+\frac{\partial}{\partial y}\left(\lambda_H\frac{\partial S}{\partial y}\right) \tag{6}$$

In the Cartesian coordinates (x,y,z) equations, t is time, T is temperature, S is salinity, ρ is density, p is pressure, (u,v,w) are velocity components, f is Coriolis frequency, ν_T and λ_T are vertical eddy viscosity and diffusion coefficients, λ_H is the horizontal diffusion coefficient for salinity and temperature, c_p is specific heat of seawater at constant pressure and I is solar irradiance.

The horizontal Reynolds stress tensor components are expressed as follows:

$$\tau_{xx} = 2\nu_T \frac{\partial u}{\partial x} \tag{7}$$

$$\tau_{xy} = \tau_{yx} = \nu_T \left(\frac{\partial u}{\partial y} + \frac{\partial v}{\partial x} \right) \tag{8}$$

$$\tau_{yy} = 2\nu_T \frac{\partial v}{\partial y} \tag{9}$$

ν_T is the horizontal diffusion coefficient.

The equations of momentum and continuity are solved numerically using the mode-splitting technique, which requires a special treatment and coupling between the external barotropic mode and the internal baroclinic mode. The sea surface elevation and the depth-integrated velocities are calculated by the external mode, while the three-dimension currents, temperature and salinity are determined by the internal mode. In the vertical, the equations are discretized over the bottom topography using a terrain-following coordinate, or sigma (σ) coordinate (Phillips, 1957). This coordinate system tries to solve the problems from the combined influences of steep topography and strong stratification. The σ-coordinate varies between 0 at the bottom (z = -h) and 1 at the surface ($z = \eta$), according to the formula below:

$$\sigma = \frac{z+h}{\eta+h} = \frac{z+h}{H} \tag{10}$$

where H is the total water depth, h is the mean water depth and η is the sea surface elevation.

The relationship between the original vertical velocity and the "new" pseudo-vertical velocity in the new coordinate system is defined as:

$$\omega = w - u\sigma\frac{\partial H}{\partial x} + \frac{\partial \eta}{\partial x} - v\sigma\frac{\partial H}{\partial y} + \frac{\partial \eta}{\partial y} - \left(\sigma\frac{\partial \eta}{\partial t} + \frac{\partial \eta}{\partial t}\right) \quad (11)$$

The model program has many switches that allow the user to select the kind of model grid, enable/disable different processes, set the forcings and boundary conditions, and enable/disable biology, contaminant, particle and sediment modules.

The spherical coordinates (λ, φ, z) were selected for the model formulation where the longitude (λ) is positive when east, the latitude (φ) is positive when north and the z-axis is directed upwards along the vertical. The surface (z = 0) represents the mean sea water level.

The BS coastline and bottom depth are obtained from the Naval Oceanographic Office Digital Bathymetry with 5' resolution (DBDB5) database. The domain of the model is from 37.0°N to 41.0°N and from 117.5°N to 122.5°N. The 62 x 50 points horizontal grid was set with a resolution around 0.082 degrees, approximately, 5' or 9 km, and 16 vertical sigma levels. The Arakawa staggered C-scheme (Arakawa and Lamb, 1977) was used for horizontal finite differencing. Horizontal advection and diffusion terms are discretized explicitly in time, vertical advection is taken semi-implicitly, and vertical diffusion is treated fully implicitly. The model was run with an external mode time step of 15 seconds and an internal model time step of 10 minutes between January 1st and December 31st of 2000.

The vertical eddy viscosity and diffusion coefficients are determined with an parameterization or a turbulence closure scheme. The "k-ε" turbulence closure scheme, two equation models developed by Luyten et al. (1996), was used for most runs. The "k-l" level 2.5 turbulence closure scheme developed by Mellor and Yamada (1982), with the Galperin et al. (1988) modifications, was applied to compare with the previous theory. The Smagorinsky (1963) formulation is used to parameterize horizontal diffusion coefficients. The type of advection scheme selected for horizontal and vertical advection of momentum and scalars parameters was the Total Variation Diminishing (TVD) scheme with a superbee limiter.

B. INITIAL AND BOUNDARY CONDITIONS

Initial conditions for the spin-up run consisted of climatological June-July temperature and salinity data derived from the Navy's Generalized Digital Environmental Model (GDEM) database and interpolated to the model grid. All three components of velocity and the sea surface elevation were initially set equal to zero. It was discovered that 180 days were sufficient for the model to reach a quasi-steady state under the imposed conditions. The initial conditions for all subsequent runs used the parameters values at the end of the spin-up simulation.

The surface horizontal current was obtained from the wind stress as a function of the wind components. The model uses the free surface boundary condition. A quadratic friction law was used for the slip boundary conditions to calculate the horizontal bottom currents. In the heat equation (5), the solar radiation was absorbed in the upper layers. The bottom boundary conditions for scalars, temperature and salinity, were calculated by considering zero flux normal to the ocean floor ($I_b = 0$).

The eastern open boundary is controlled monthly by temperature and salinity vertical sections provided by GDEM and by the amplitudes and phases from eight tidal harmonics constituents, M_2, S_2, N_2, K_2, K_1, O_1, P_1 and Sa obtained from the International Hydrographic Organization (IHO) database. A zero normal gradient condition was applied to the open boundaries (Orlanski, 1976). At the coastal boundaries, there are no currents, and advective and diffusive fluxes. The climatological data was interpolated in time to each internal time step.

C. EXTERNAL FORCINGS

The following meteorological surface data for 1999 and 2000 were obtained from the reanalysis of the National Center for Environmental Prediction (NCEP), defined on a 2.5° global grid spacing and interpolated to the model grid: wind components at 10 m, air temperature, pressure, relative humidity, cloudiness and precipitation rate. The downward solar radiation and the upward non-solar radiation fluxes were derived from the input parameters and applied to the heat equation. Figures 5 through 10 illustrate the field of parameters for January 15 and July 15 2000 at local time 0200 and 1400. The air

temperature plots illustrate the seasonal changes due to the monsoon and the land effect that cools the northern part of the BS during winter and warms the region in summer. The wind is another important element to determine the surface fluxes and shows dramatic changes along the year. In winter, the winds flow south- and southwestward, while in summer, they blow north- and northwestward.

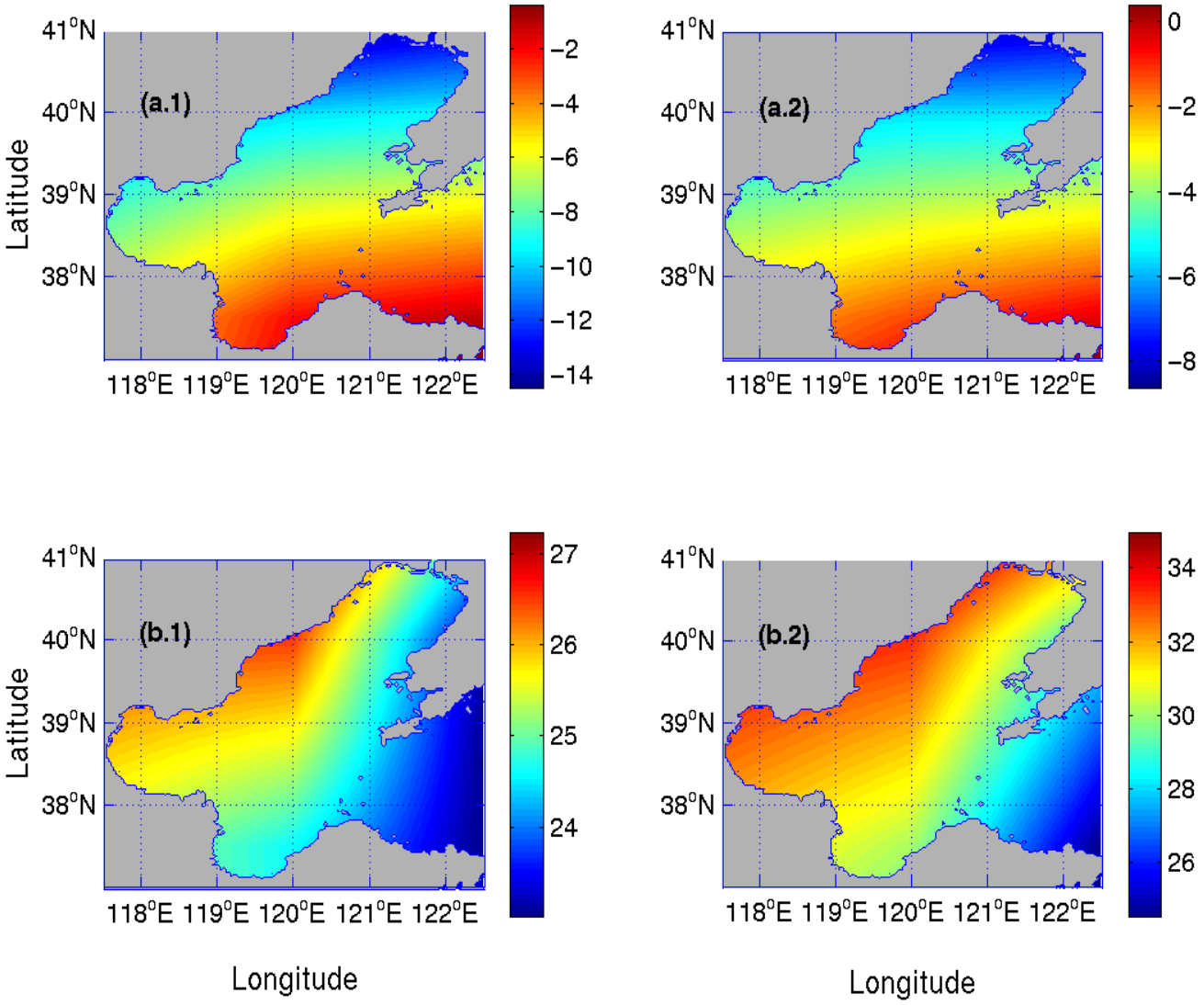

Figure 5. Air temperature (°C) at the sea surface for (a1) January 15, 2000 at 2 a.m. L.T., (a2) January 15, 2000 at 2 p.m. L.T., (b1) July 15, 2000 at 2 a.m. L.T., and (b2) July 15, 2000 at 2 p.m. L.T..

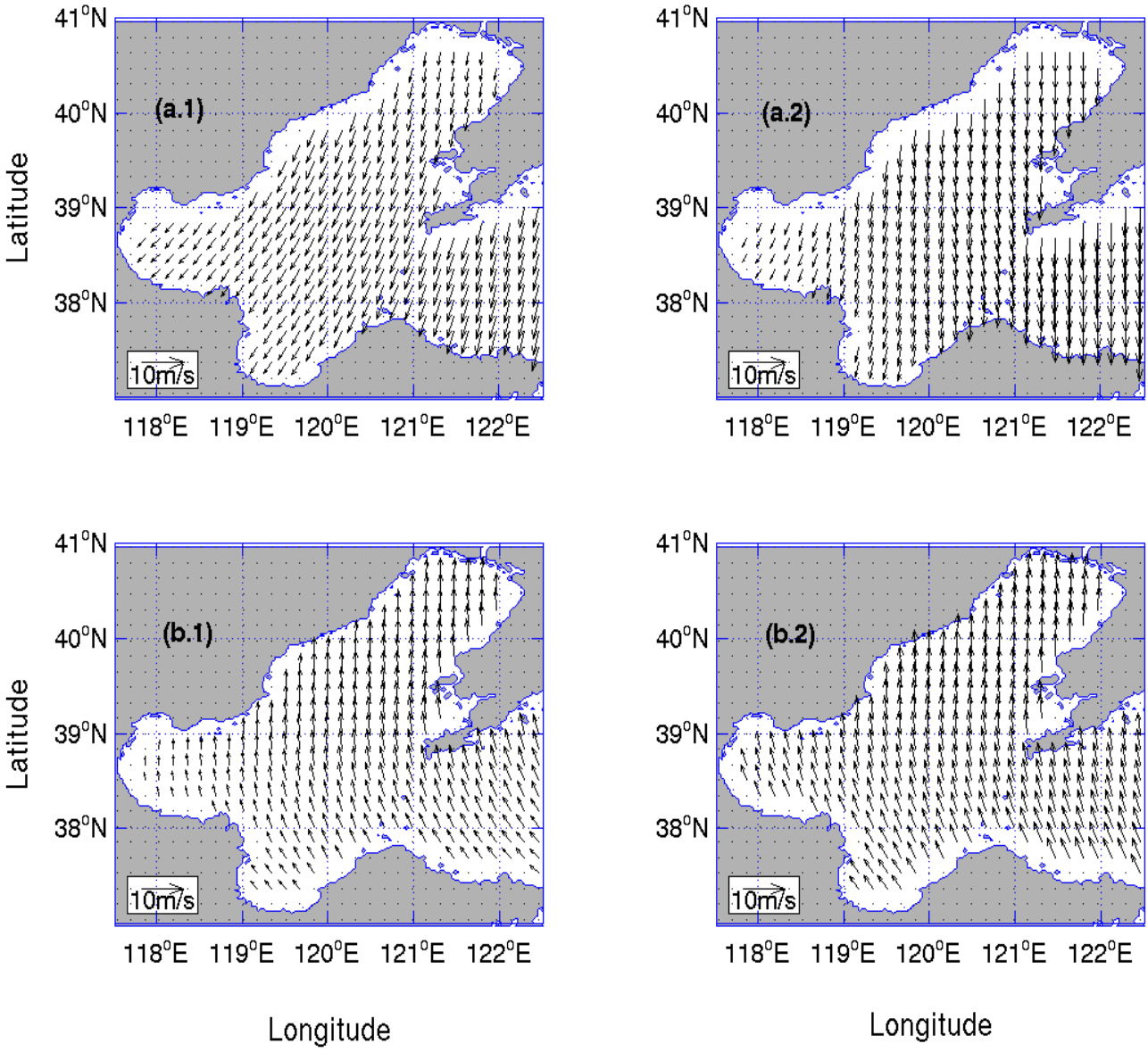

Figure 6. Wind speed at the 10 m height for (a1) January 15, 2000 at 2 a.m. L.T., (a2) January 15, 2000 at 2 p.m. L.T., (b1) July 15, 2000 at 2 a.m. L.T., and (b2) July 15, 2000 at 2 p.m. L.T..

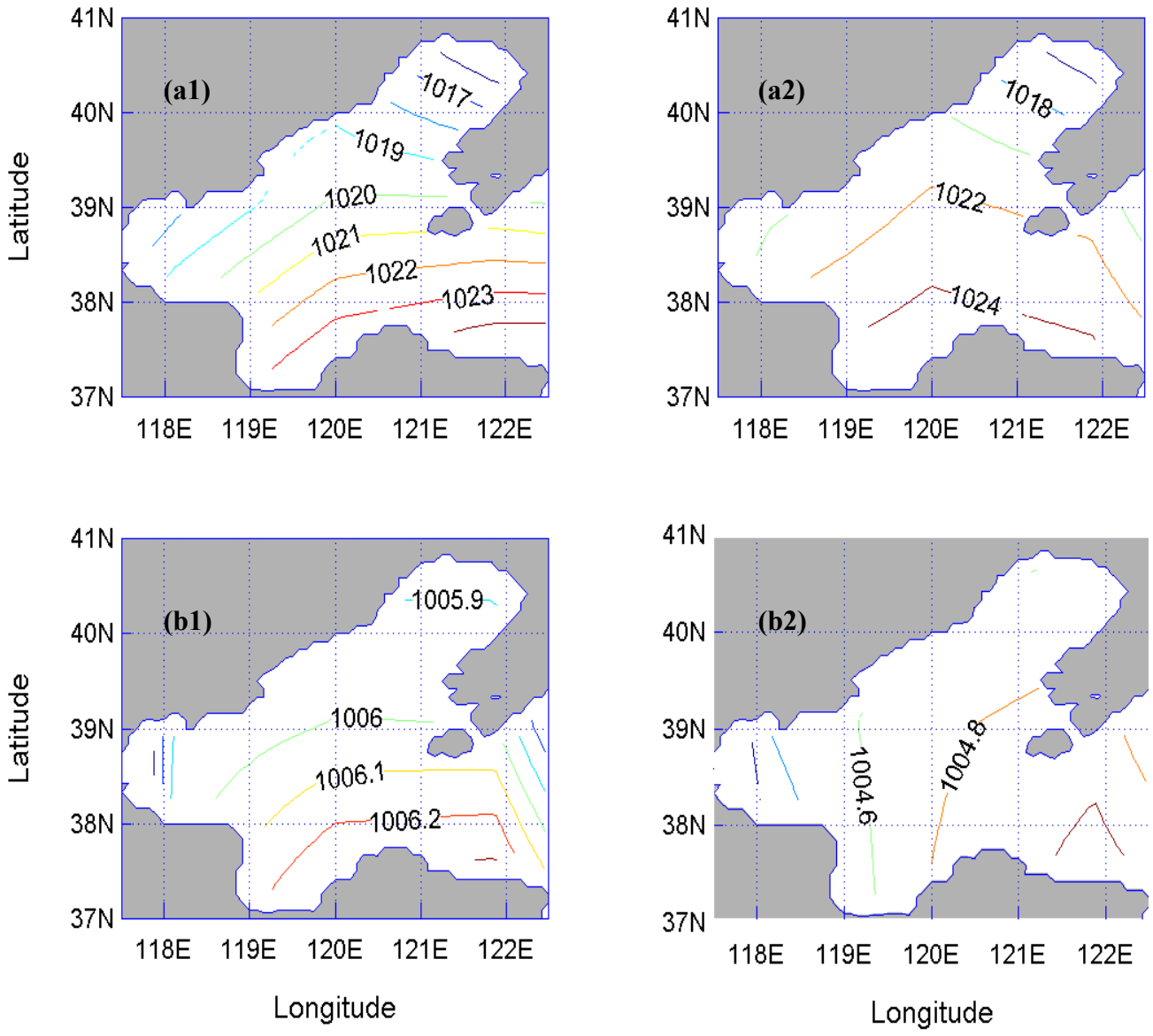

Figure 7. Sea surface pressure (mb) for (a1) January 15, 2000 at 2 a.m. L.T., (a2) January 15, 2000 at 2 p.m. L.T., (b1) July 15, 2000 at 2 a.m. L.T., and (b2) July 15, 2000 at 2 p.m. L.T..

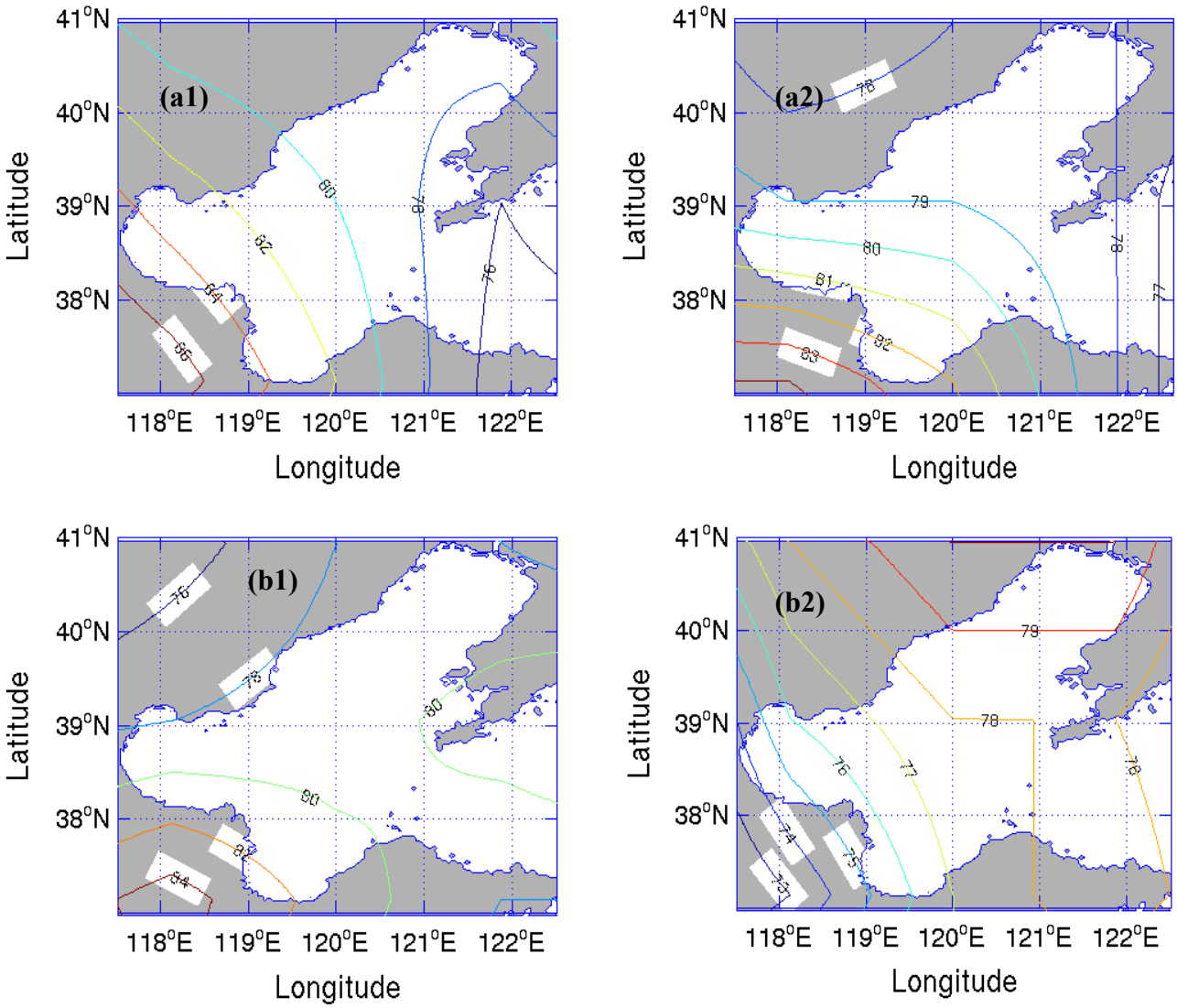

Figure 8. Relative humidity (%) over Bohai Sea for (a1) January 15, 2000 at 2 a.m. L.T., (a2) January 15, 2000 at 2 p.m. L.T., (b1) July 15, 2000 at 2 a.m. L.T., and (b2) July 15, 2000 at 2 p.m. L.T..

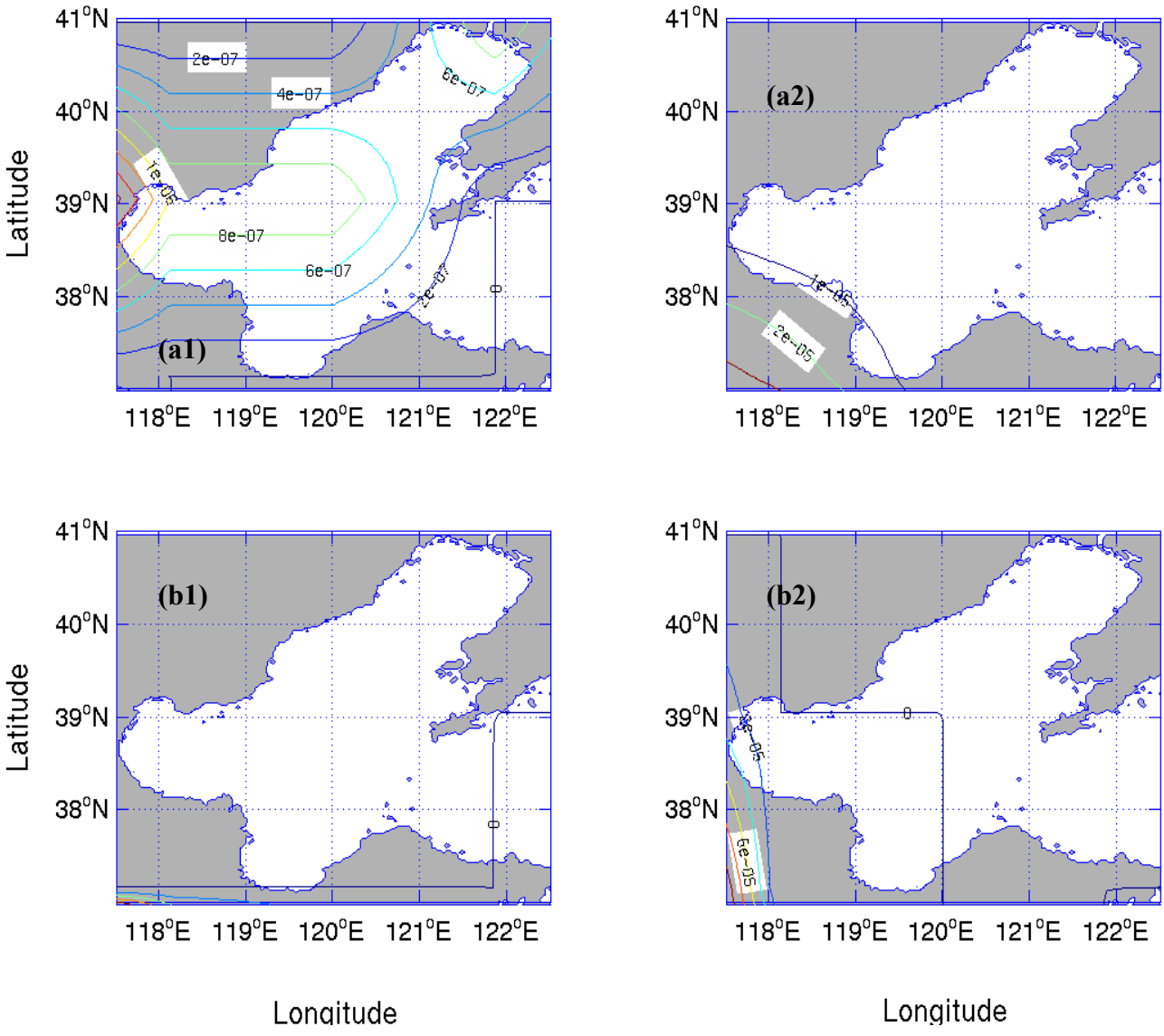

Figure 9. Precipitation rate (kg m^{-2} s^{-1}) over Bohai Sea for (a1) January 15, 2000 at 2 a.m. L.T., (a2) January 15, 2000 at 2 p.m. L.T., (b1) July 15, 2000 at 2 a.m. L.T., and (b2) July 15, 2000 at 2 p.m. L.T..

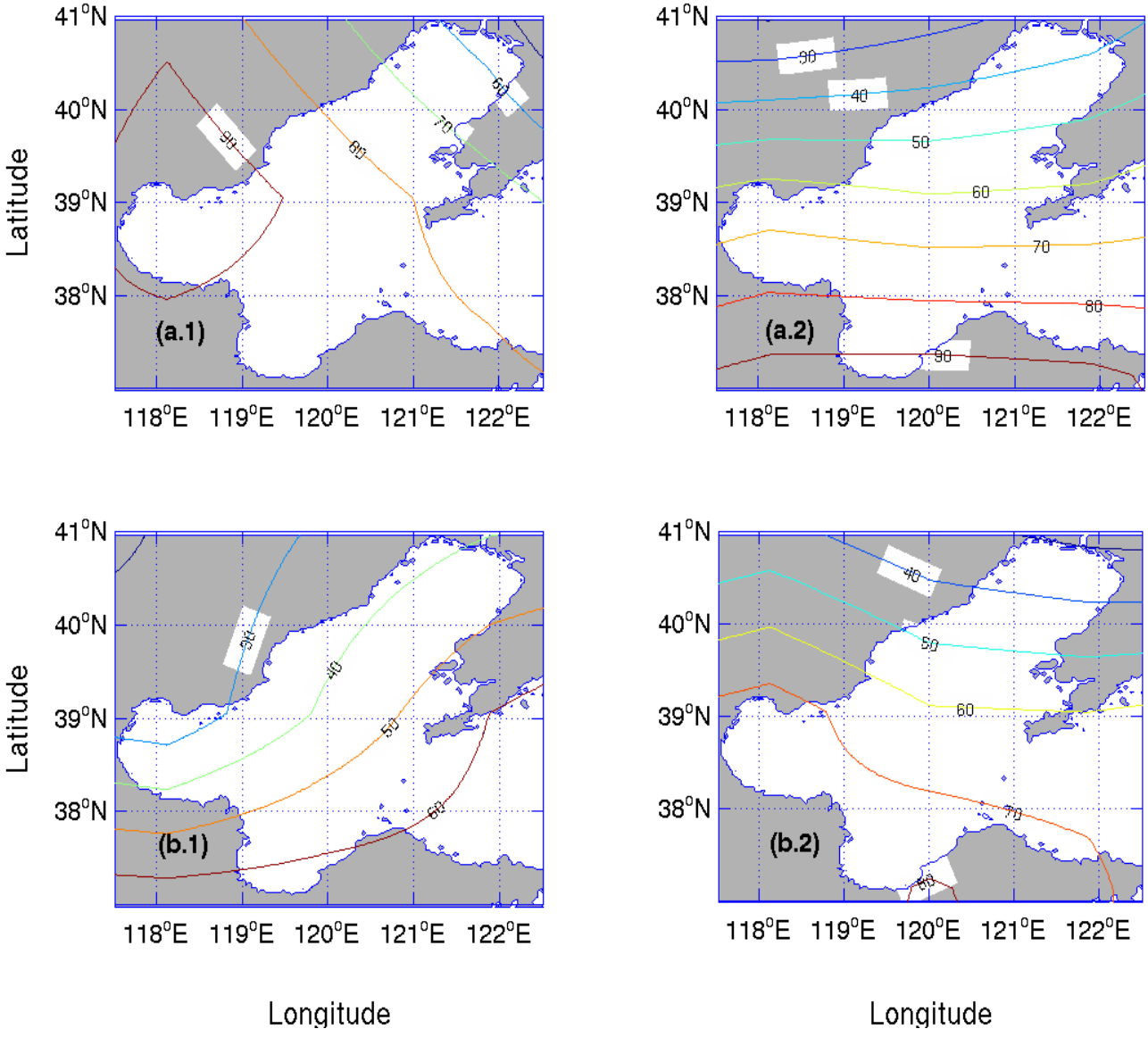

Figure 10. Cloudiness (%) over Bohai Sea for (a1) January 15, 2000 at 2 a.m. L.T., (a2) January 15, 2000 at 2 p.m. L.T., (b1) July 15, 2000 at 2 a.m. L.T., and (b2) July 15, 2000 at 2 p.m. L.T..

III. EXPERIMENTAL DESIGN

Four numerical experiments were conducted to analyze the physical processes controlling the BS circulation and thermohaline structure. All simulations were run for the same period, between 0000Z January 1st and 0000Z December 31st 2000. They all applied the same initial and lateral open boundary conditions, resultant from the end of the spin-up phase. The spin-up phase consisted in a 6-month simulation from 0000Z July 1st 1999, which was enough time to reach the quasi-steady state.

Sensitivity analyses are performed to determine the influence of the tides, winds and surface fluxes. The control run (Run-1) used the lateral open boundary conditions, complete meteorological data, k-ε turbulence scheme, and tidal forcing. To simplify the study, no river runoff was used in the simulations. The "no fluxes" simulation (Run-2) did not account for surface heat and salt fluxes. In the "no wind" run (Run-3), the only difference noted from the control run is that the wind was not taken into account. Finally, the "no tide" experiment (Run-4) did not consider the effect of the tidal harmonic components applied at the lateral open boundary. The contribution of each of the forcing mechanisms in the region is determined by selecting four months equally spaced for the appropriate analyses: January, April, July and October, 2000. Horizontal fields and vertical cross-sections are presented to examine the effect of the forcing mechanisms. Chapters VI to VII present the analyses of these experiments.

To study the difference between the "*k*-ε" and "*k*-*l*" turbulence closure schemes, the model was run again with the "*k*-*l*" turbulence closure schemes for January and July (Run-5) with everything else the same as the control run. The hourly turbulence kinetic energy (TKE) for the entire domain is obtained from Run-1 and Run-5. Comparison between the two leads to the difference of the two schemes. Details of this experiment are provided in Chapter VIII.

THIS PAGE INTENTIONALLY LEFT BLANK

IV. CONTROL RUN

A. CIRCULATION

The simulated daily-mean circulation on January 15, April 15, July 15, and October 15, 2000) are selected to represent the seasonal variability of the velocity field. On January 15, 2000, the velocity is mostly south- and southeastward. There is an anticyclonic circulation in the Liaodong Gulf (Figure 11a). In the northern Bohai Strait, the flow is strong and westward, but then curves counterclockwise and the southern part becomes a southeastward flow, which is responsible for an outflow in the southern part of the Bohai Strait. On April 15, 2000, the dominant direction in the southern part of the Bohai Sea is eastward. At the Liaodong Gulf, the current flows northward, but with a cyclonic tendency. In the middle of the central basin, the circulation is counterclockwise. The northern Bohai Strait still presents a westward flow and then turns northward along the east BS coast (Figure 11b). On July 15, 2000, the currents are mostly northeastward. At the Liaodong Gulf, the circulation is cyclonic (Figure 11c). At the Bohai Strait, the current assumes eastward direction. On October 15, 2000, the velocity shifts again to be south- and southeastward. In the northern Bohai Strait, a westward current is still present. In the Bohai Gulf, the currents are weak. At the head of Liaodong Gulf, the circulation is clockwise. At the middle of the central basin, the velocities are southeastward, with a cyclonic motion and flow to the southern part of the Bohai Strait (Figure 11d).

At 20 m depth and at the bottom, the circulation pattern still has a strong seasonal variability which is opposite to the wind direction (Figures 12 and 13). For example, the currents are mostly northeastward on January 15, 2000 (northeast winds in winter), and southwestward on July 15, 2000 (southwest wind in summer). The sub-surface circulation in January and July is represented by a compensating current due to the surface velocity at the central basin and at the Liaodong Gulf. This is consistent with the studies of Zhao and Shi (1994).

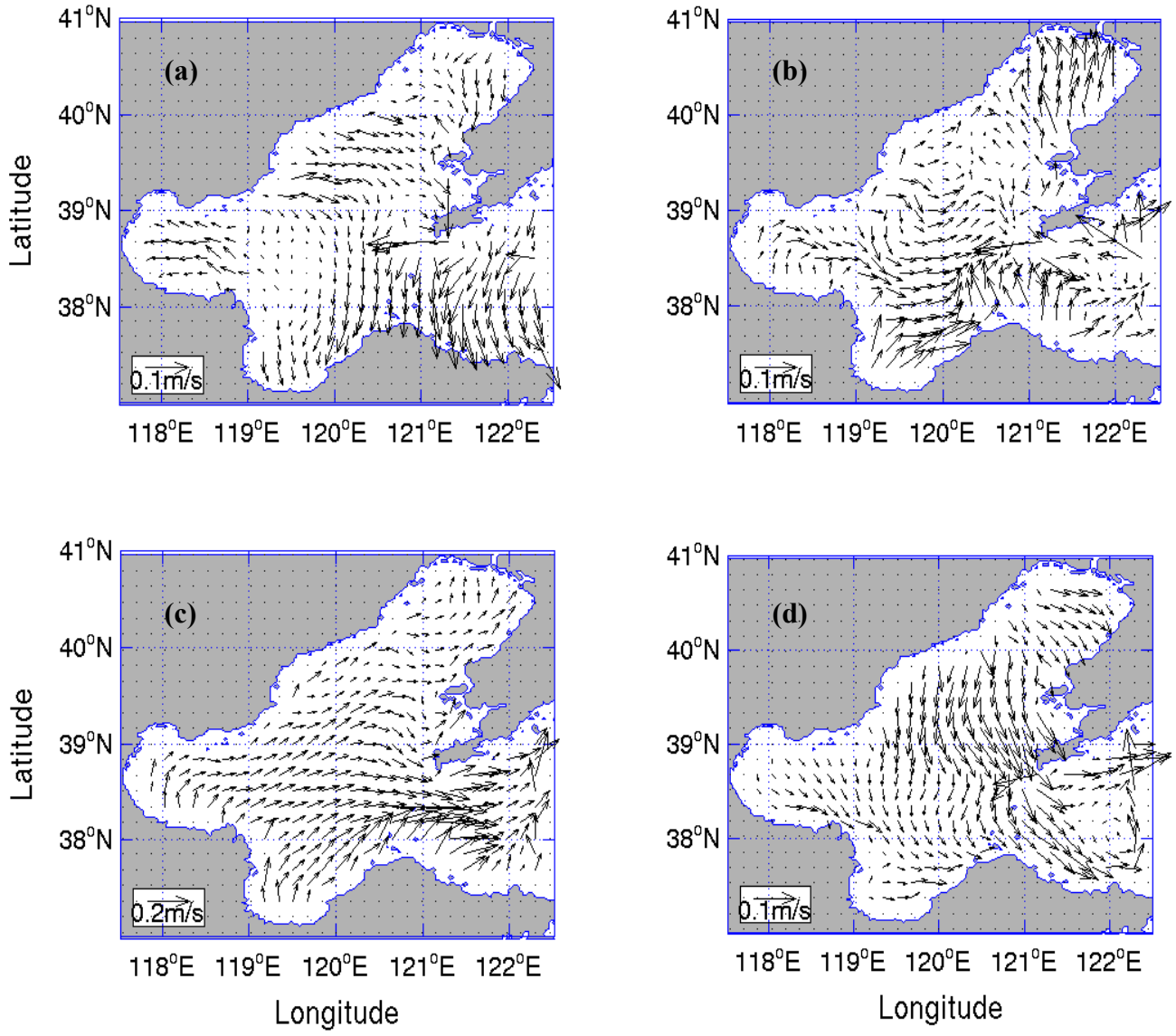

Figure 11. Simulated horizontal velocity field at the Surface on (a) January 15, (b) April 15, (c) July 15 and (d) October 15, 2000.

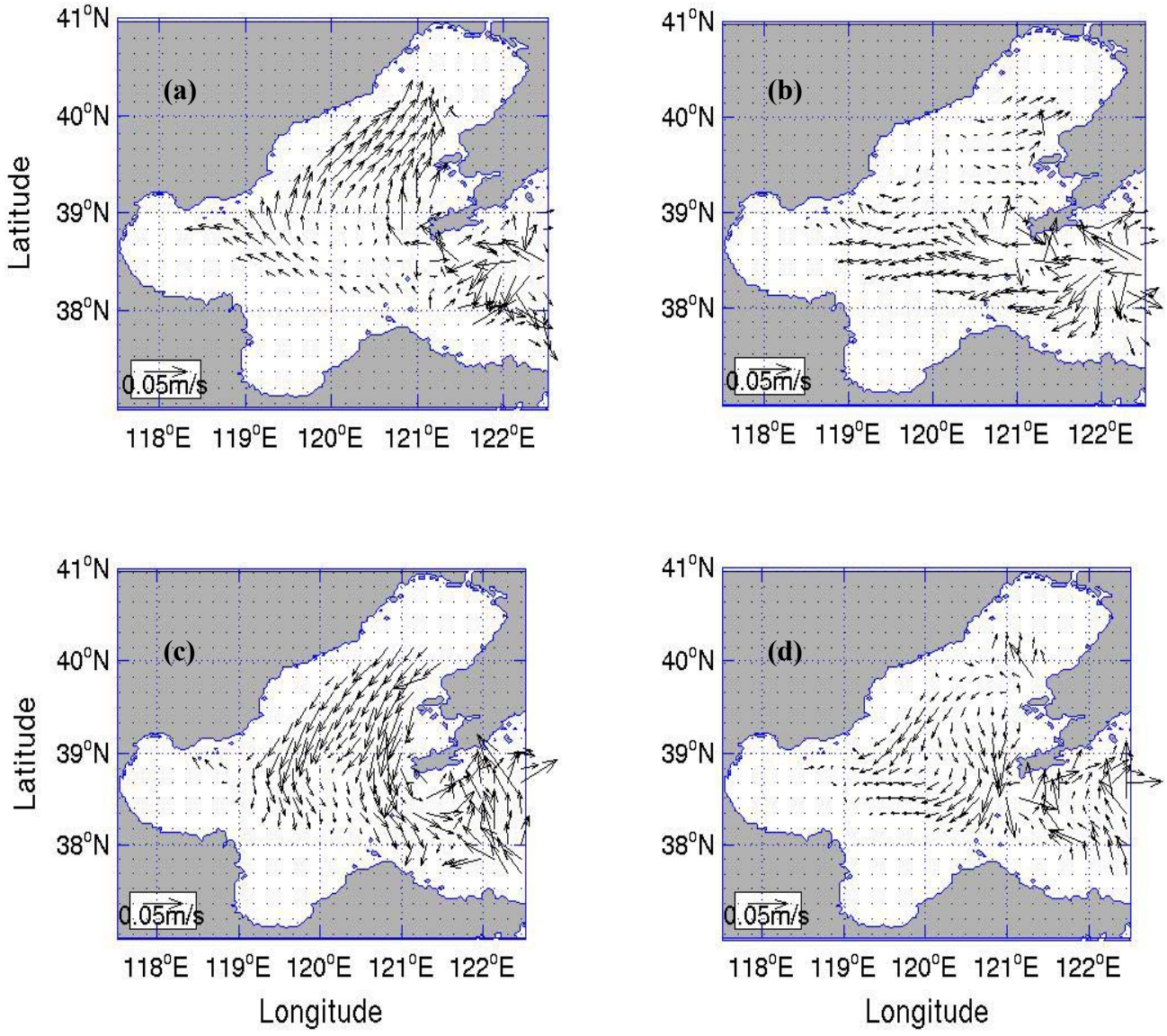

Figure 12. Simulated horizontal velocity field at 20 m depth for (a) January 15, (b) April 15, (c) July 15 and (d) October 15, 2000.

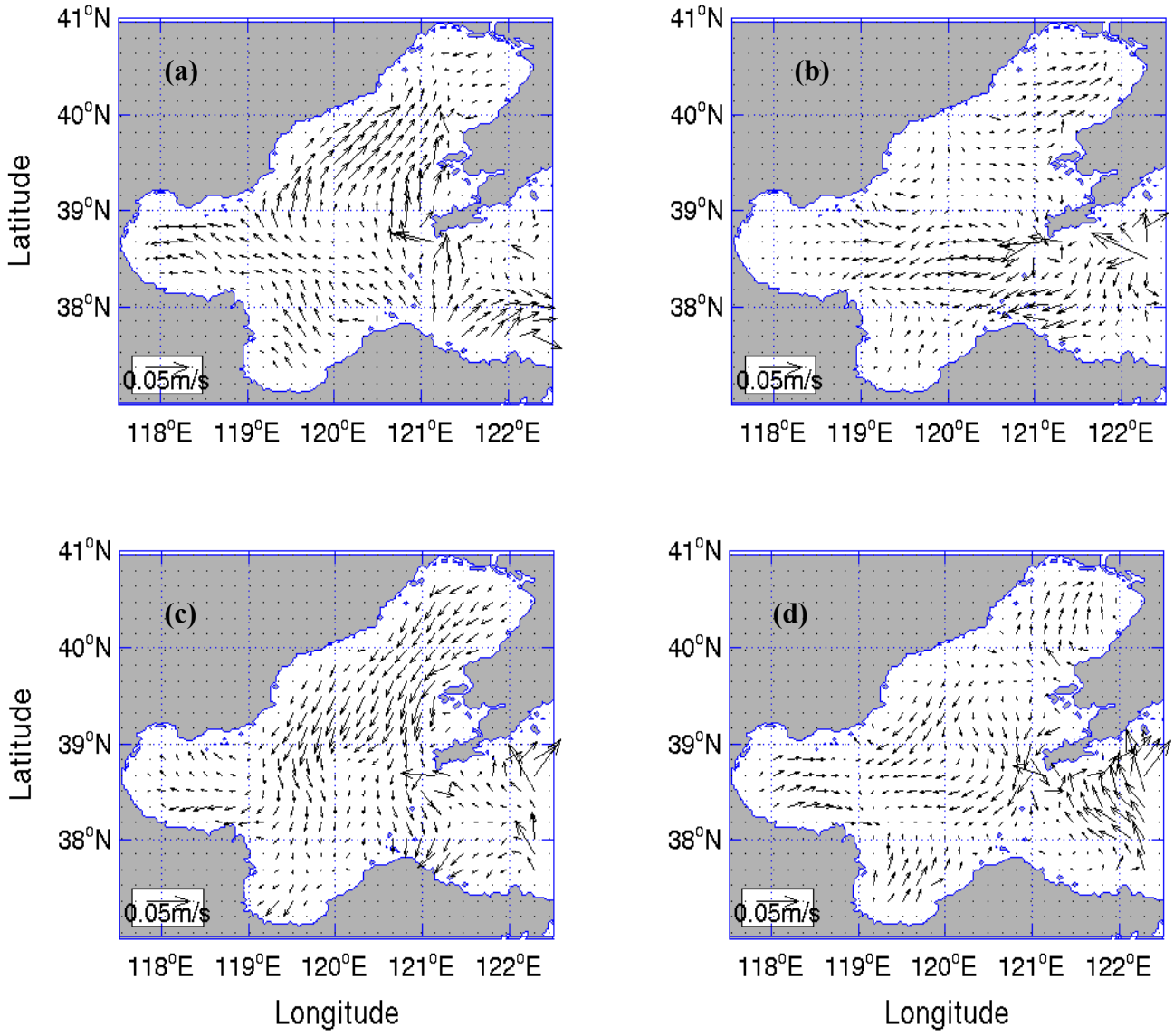

Figure 13. Simulated horizontal velocity field at the bottom on (a) January 15, (b) April 15, (c) July 15, and (d) October 15, 2000.

B. TEMPERATURE FIELD

The simulated temperature field (Figures 14, 16 and 18) shows a strong warm water intrusion from the Yellow Sea through the northern Bohai Strait and tends to flow northward along the eastern coast of the Liaodong Gulf. This tongue can be relatively warm or cold depending on the season.

On January 15, 2000, the sea surface temperature field (Figure 14a) illustrates cold waters in the shallow regions, represented by the Gulfs and the southern Bohai Strait. The deep-water region on the northern Bohai Strait presents the warmer region. The entrances of the Liaodong Gulf and Bohai Gulf also have warm water but have values lower than the Bohai Strait. Near 39°N-120°W, there is a small region with a relative low temperature compared with the surroundings (below 0.5°-1°C). The winter monsoon occurs during this month so cold regions are expected to be found near the coast and in shallow regions. These features of the sea surface temperature are consistent with the observations (Figure 15a). The mid-depth (Figure 16a) and the bottom (Figure 18a) horizontal temperature plots indicate almost the same structure of the sea surface temperature (SST), which is also seen in the observational data (Figures 17a and 19a).

On April 15, 2000, the horizontal temperature field shows that on the deep-water region the temperature decreases about 1.5°C and at the head of the Gulfs the temperature increases by approximately 5°C (Figure 14b), which is also agreeable with the observation (Figure 15b). Compared to January 15, 2000, there is an indication that the shallow regions absorbed some heat flux and the deeper areas released its energy. Some of this energy in the form of heat was probably diverted to the shallow waters. The mid-depth (Figure 16b) and the bottom (Figure 18b) temperature profiles are very similar to the SST field. The simulated fields qualitatively agree with the observations (Figures 17b and 19b).

The entire BS warms up rapidly during the summer monsoon season. On July 15, 2000, high temperatures (~26^{o}C at the surface) are found in the shallow-water regions and low temperatures (~22^{o}C at the surface) are found in the deep-water regions and in the Bohai Strait. The central basin is cooler compared to the surroundings (Figure 14c). The simulated characteristics agree well with the observations (Figure 15c). At the mid-

depth (Figure 16c) and on the bottom (Figure 18c), the temperature contours appear to be very different from the surface. The warmer regions are still at the head of the Gulfs, but there is a colder water mass coming from the YS with temperatures lower than 16°C and associated with the North Yellow Sea Bottom Cold Water (Su and Weng, 1994). These features can also be found in the observational data (Figures 15c, 17c, and 19c).

On October 15, 2000, the entire BS basin cools from the summer. However, at the Bohai Gulf entrance there is a high temperature tongue of ~19°C. The middle of the central basin becomes relatively cold compared with the surroundings. The mid-depth (Figure 16d) and the bottom (Figure 18d) horizontal temperature fields describe almost the same structure as the sea surface temperature (Figure 14d).

Since the seasonal variation of the BS water masses is detected from the horizontal distributions (Figures 14-16), it is reasonable to ask what is the seasonal variation in the vertical thermal structure. To answer this question, we plot zonal (38°35.52'N, Figure 17) and meridional (121°01.5'E, Figure 18) thermal cross-sections. A single-layer structure (i.e., vertically uniform temperature from surface to bottom) is found from January 15 (Figures 17a and 18a), April 15 (Figures 17b and 18b), and October 15, 2000 (Figures 17d and 18d). This single-layer structure means a very deep mixed-layer extending from the surface to bottom. On the other hand, July 15's cross-sections (Figures 17c and 18c) indicate a multi-layer structure (i.e., mixed-layer, thermocline, and deep layer) with a shallow surface mixed-layer. Such a strong seasonal variation in vertical thermal structure is caused by a strong surface cooling in winter and a strong surface warming in summer.

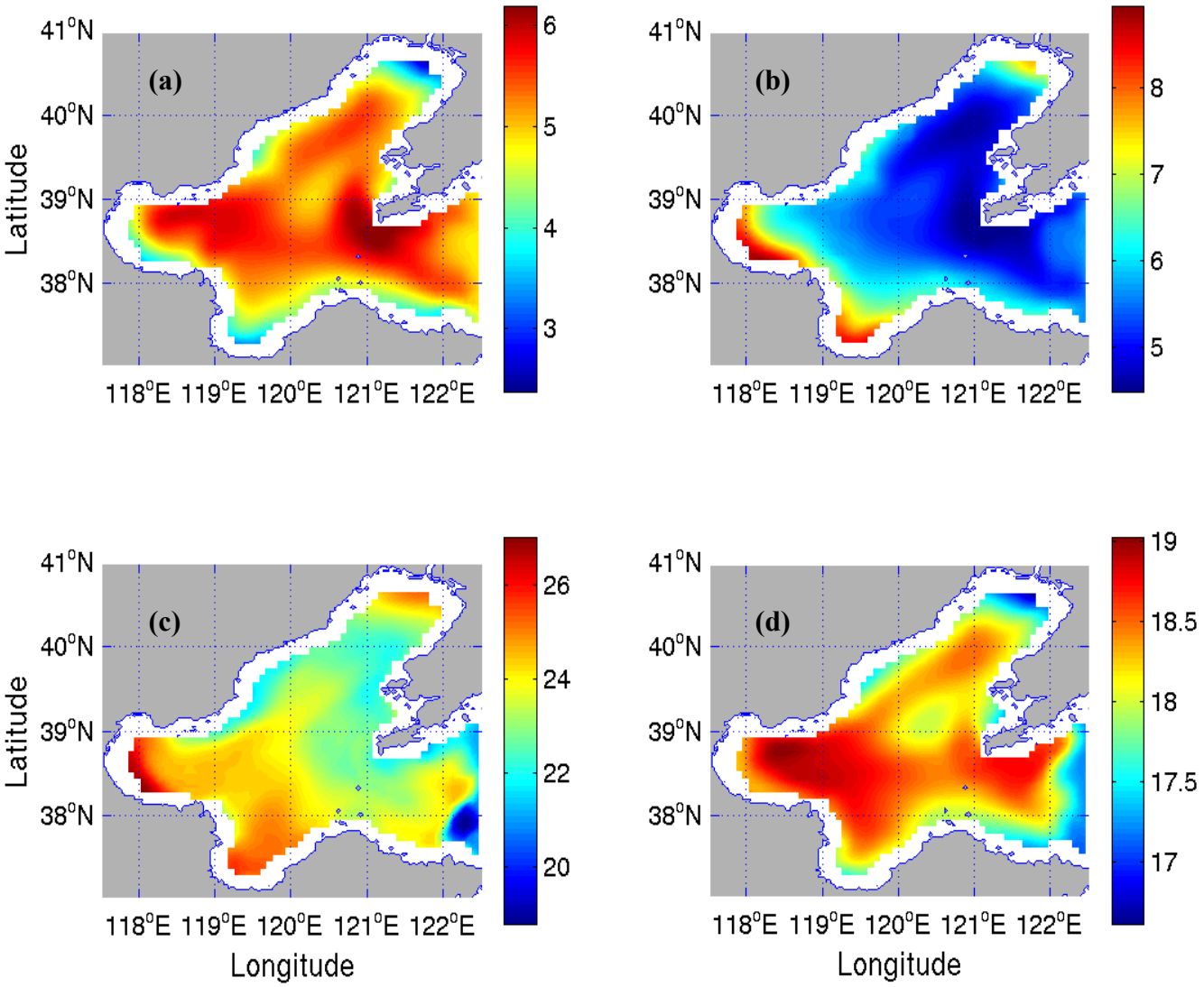

Figure 14. **Simulated sea surface temperature (°C) on (a) January 15, (b) April 15, (c) July 15 and (d) October 15, 2000.**

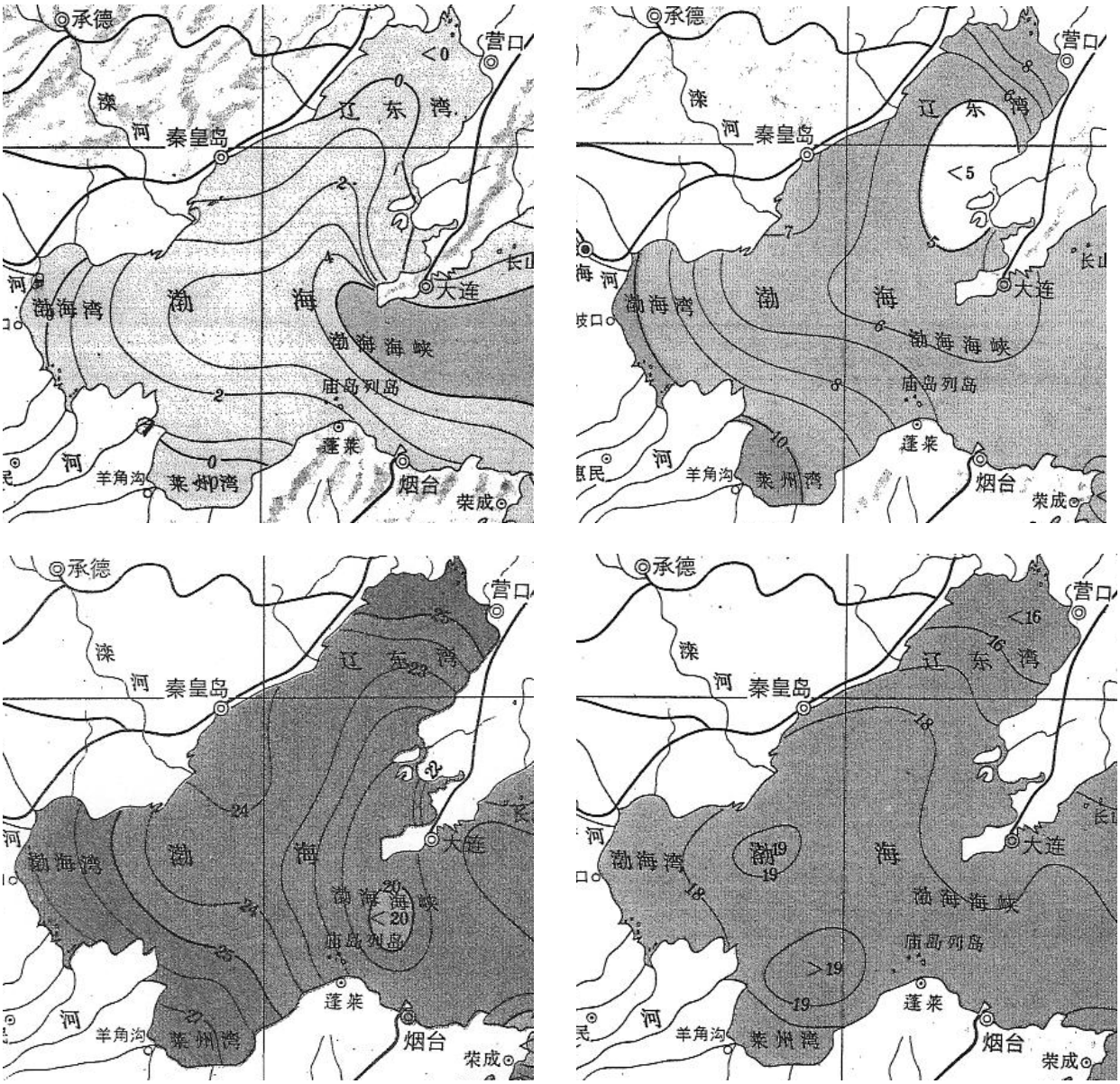

Figure 15. Sea surface temperature atlas from State Oceanic and Administration of China (1992) for January (upper left), April (upper right), July (lower left) and October (lower right).

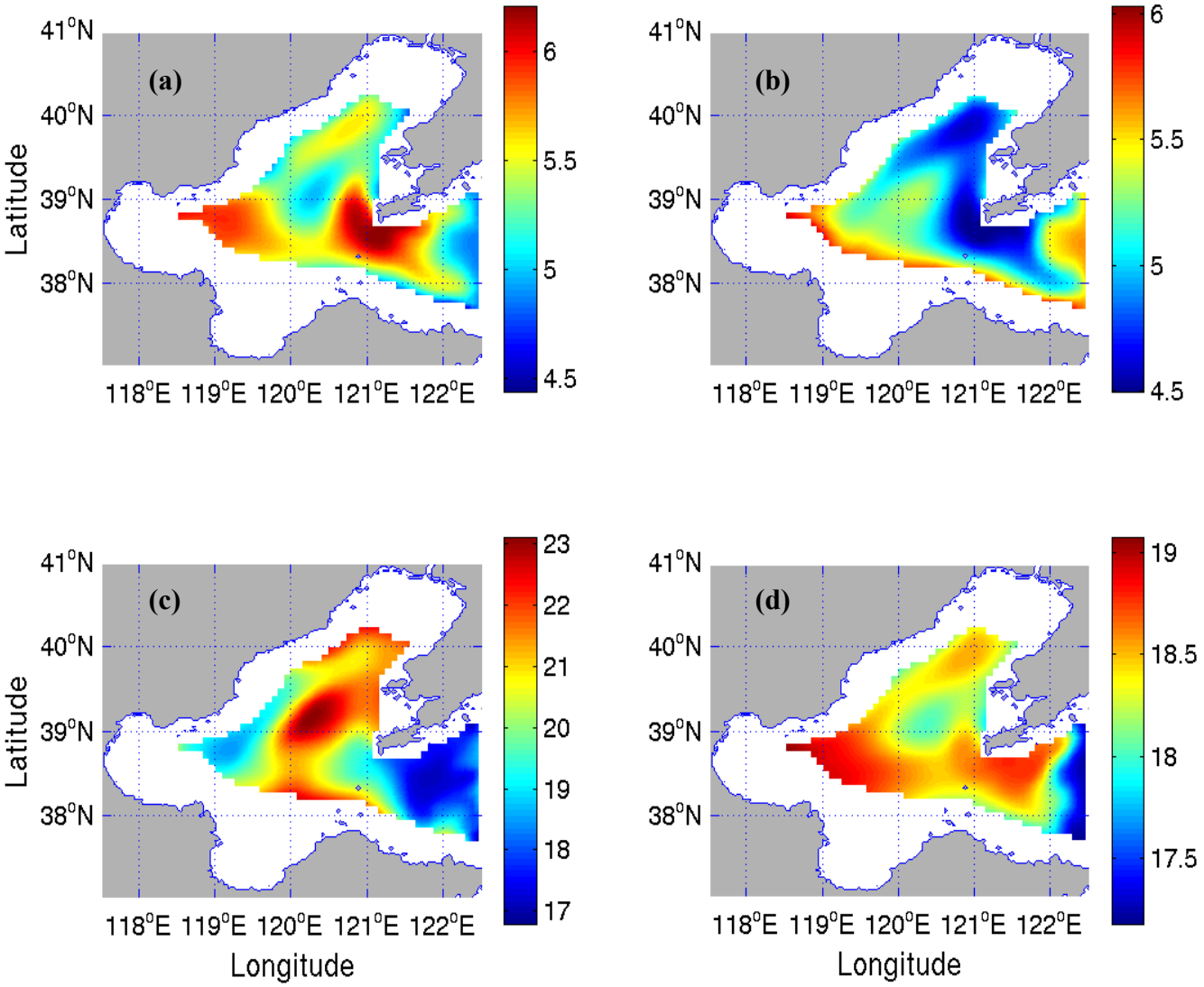

Figure 16. **Simulated temperature (^{0}C) field at 20 m depth on (a) January 15, (b) April 15, (c) July 15 and (d) October 15, 2000.**

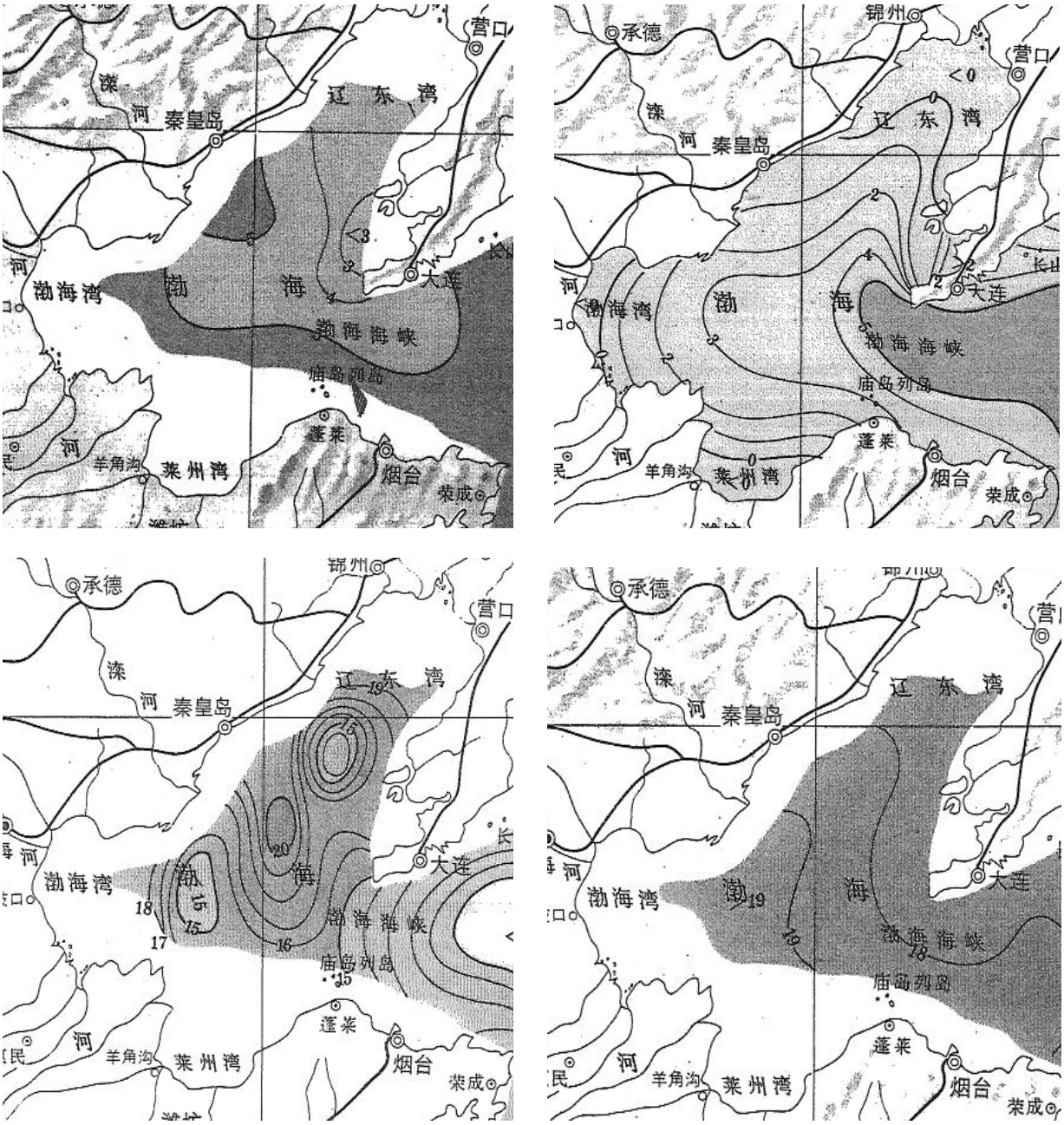

Figure 17. Temperature atlas at 20 m depth from State Oceanic and Administration of China (1992) for January (upper left), April (upper right), July (lower left) and October (lower right).

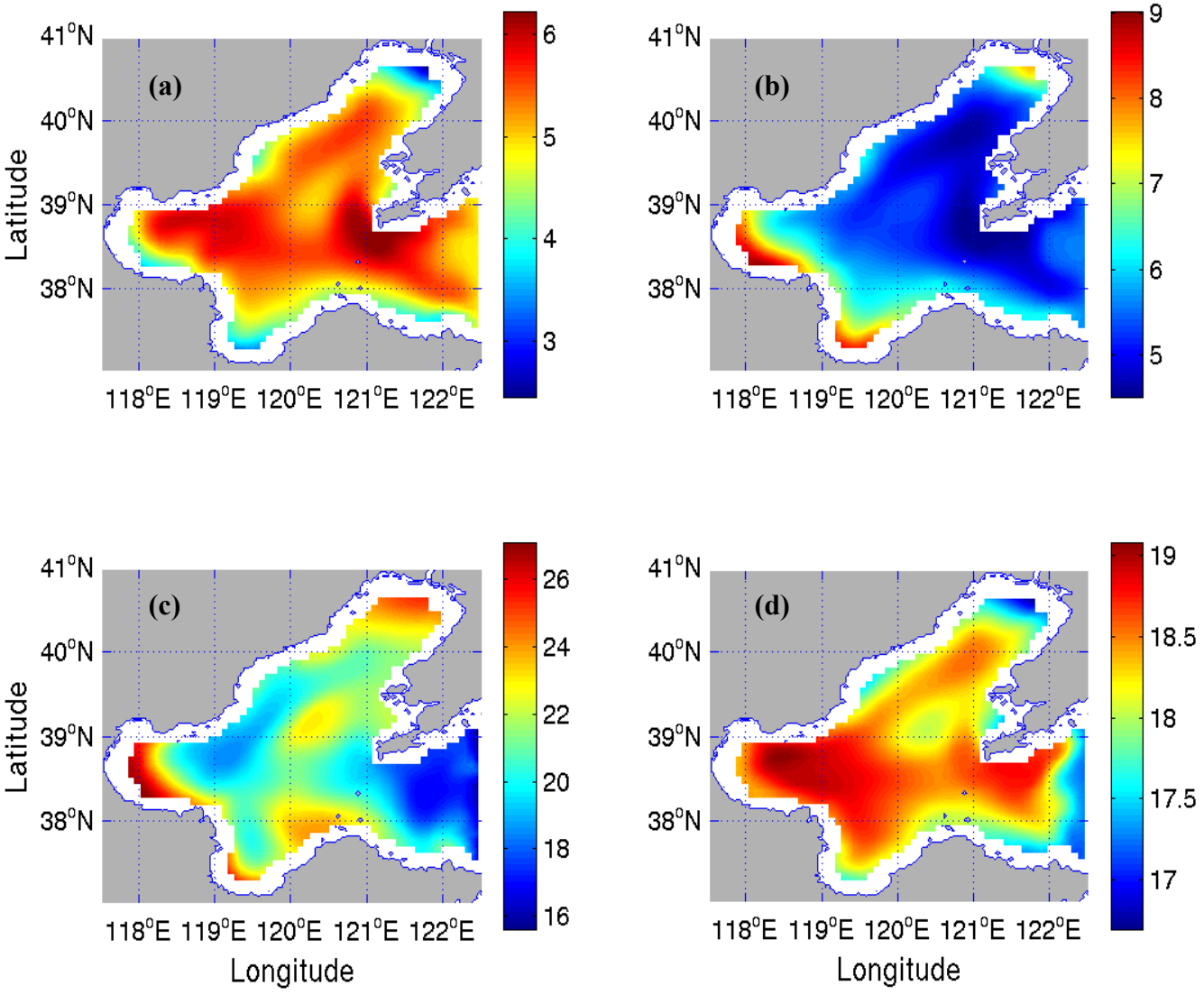

Figure 18. **Simulated temperature (°C) field at the bottom on (a) January 15, (b) April 15, (c) July 15 and (d) October 15, 2000.**

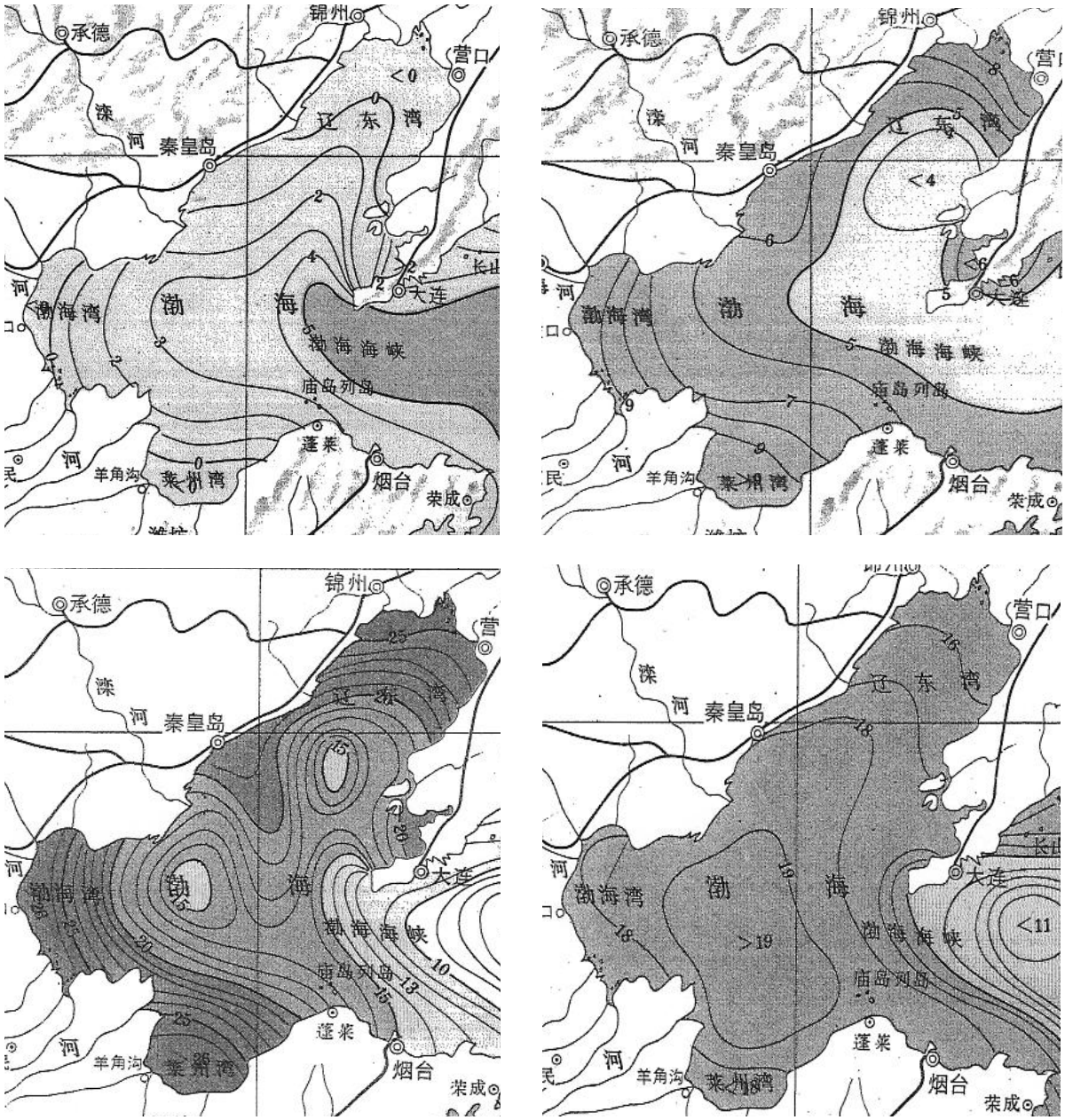

Figure 19. Bottom temperature atlas from State Oceanic and Administration of China (1992) for January (upper left), April (upper right), July (lower left) and October (lower right).

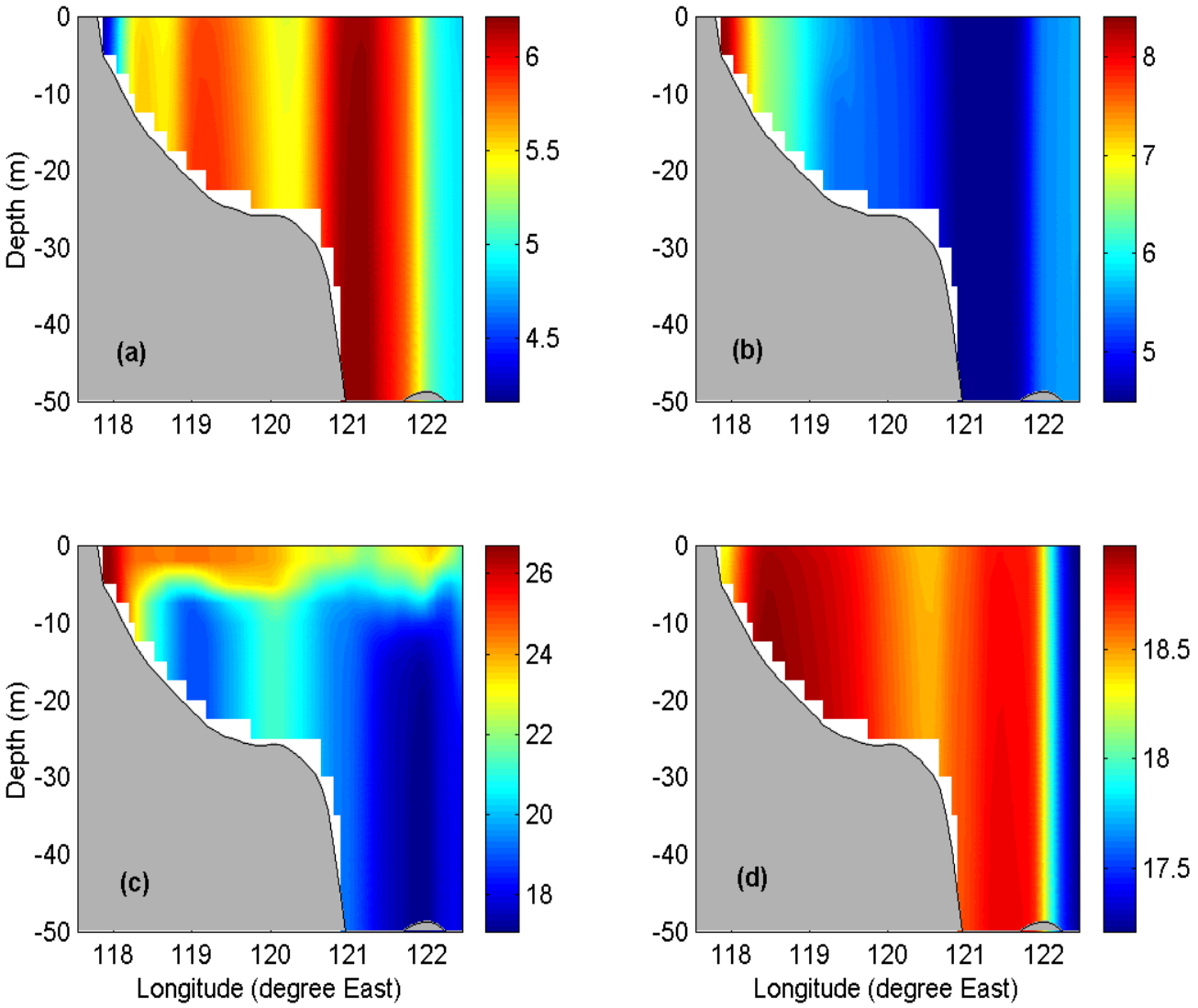

Figure 20. Simulated zonal (38°35.52'N) temperature (°C) cross-sections on (a) January 15, (b) April 15, (c) July 15 and (d) October 15, 2000.

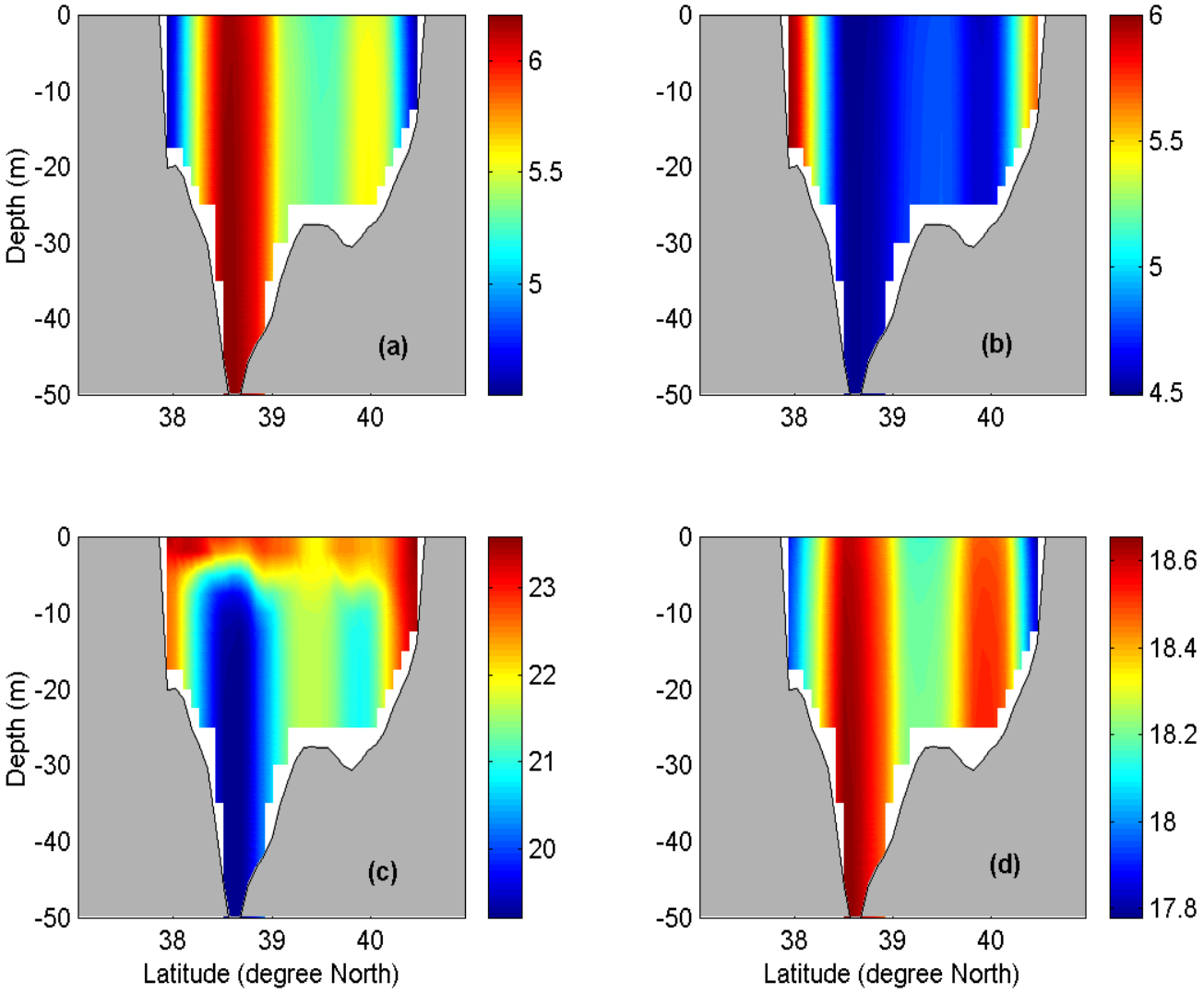

Figure 21. Simulated meridional (121°01.5'E) temperature (^{o}C) cross-sections on (a) January 15, (b) April 15, (c) July 15 and (d) October 15, 2000.

C. SALINITY FIELD

The simulated salinity field (Figures 22, 24 and 25) shows a strong water intrusion from the Yellow Sea through the northern Bohai Strait and tends to flow northward along the eastern coast of the Liaodong Gulf. This tongue is relatively salty, and makes the central BS basin is saltier than the northern (Liaodong Gulf) and southern (Bohai Gulf, Laizhou Bay) BS. Such a simulated pattern agrees well with available observations (Figure 22) and observed (Figure 23). However, the model surface salinity fields generally over predicts in Bohai Gulf and Laizhou Bay. This may be caused by the exclusion of the river runoff of the Huanghe River in the current simulation. The region to the east of the Bohai Strait appears to be less affected due to the presence of the lateral boundary.

At the surface, a less salty region is simulated during the winter monsoon (January 15, 2000) between Bohai Gulf and Laizhou Bay, and Liaodong Gulf, that agrees with observations (Figure 23). The central BS basin and the Bohai Strait are dominated by saltier water (Figure 22a). On April 15, 2000, the saltier region expands and enhances. The Huanghe River estuary and the Liaodong Gulf still present smaller values. The eastern boundary has not changed much from January 15, 2000 (Figure 22b). During the summer monsoon (July 15, 2000), the salinity slightly reduces in the whole BS basin and the delta of the Huanghe River is simulated as a low salinity area (Figure 22c). On October 15, 2000, the heads of Laizhou Bay, Liaodong Gulf and Bohai Gulf are saltier. The eastern boundary region is simulated as a low salinity area (Figure 22d).

At mid-depth (20 m), the simulated salinity fields on January 15, 2000 (Figure 24a) and April 15, 2000 (Figure 24b) are found almost the same as the surface plots (Figures 22a and b). On July 15, 2000 (Figure 24c), the southern low salinity area expands toward the central basin. On October 15, 2000, the region east to the Bohai Strait is less saline and is connected to the less saline water in the southern BS (Figure 24d).

At the bottom, the simulated salinity fields on January 15, 2000 (Figure 25a), April 15, 2000 (Figure 25b), and October 15, 2000 (Figure 25d) are found almost the same as the surface plots (Figures 22a, b and d). On July 15, 2000, the simulated salinity

pattern (Figure 25c) is similar to that at the mid-depth (Figure 24c) but different from that at the surface (Figure 22d).

The zonal and meridional cross-sections of the simulated salinity (Figures 26 and 27) show a vertical uniform structure on January 15, April 15, and October 15, 2000, and a multi-layer structure on July 15, 2000. The salinity on July 15, 2000 is strongly stratified near the surface. In central basin, the simulated salinity in the surface layer is saltier than the deeper layer. Below the salinity maximum, there exists a salinity minimum layer.

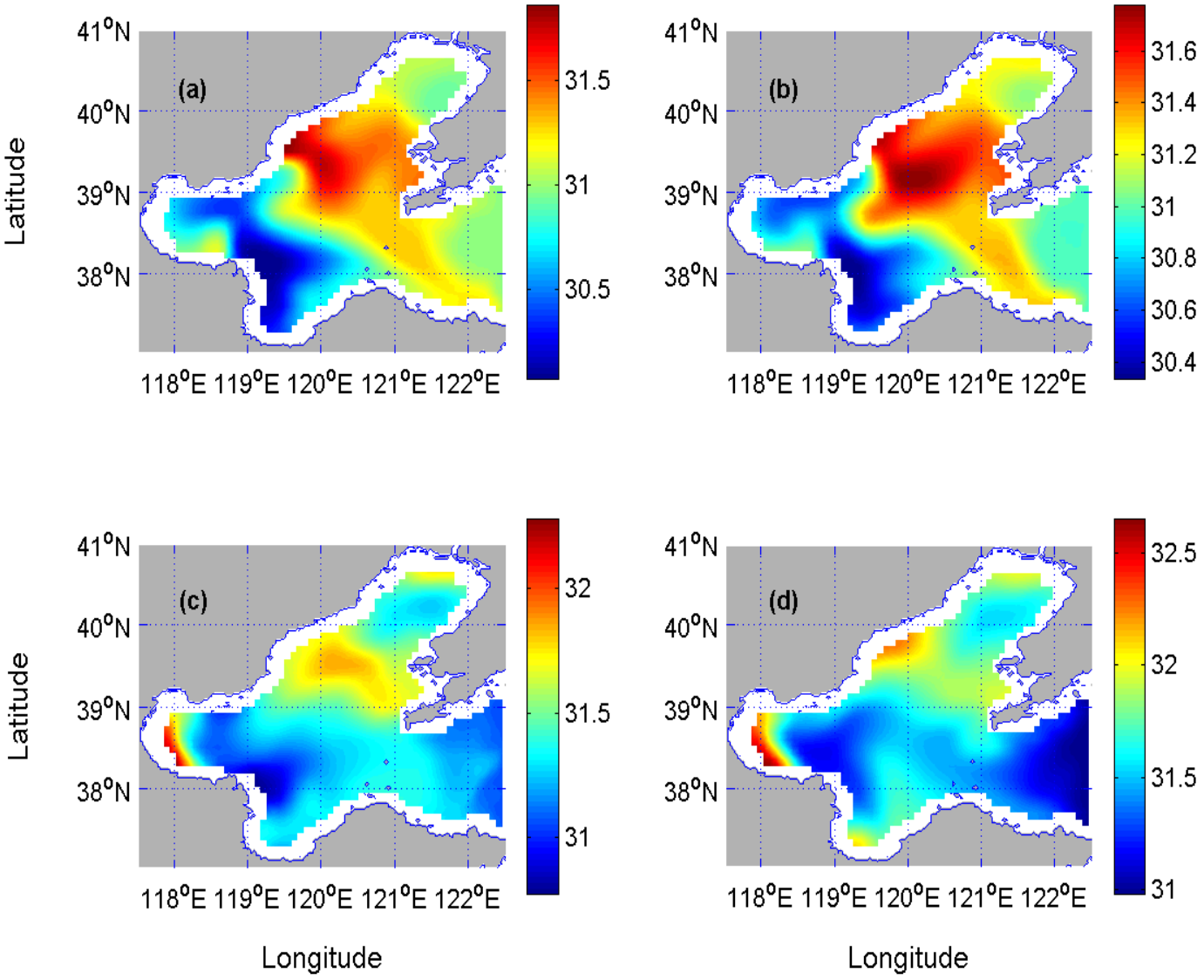

Figure 22. Simulated horizontal salinity (psu) field at the surface on (a) January 15, (b) April 15, (c) July 15 and (d) October 15, 2000.

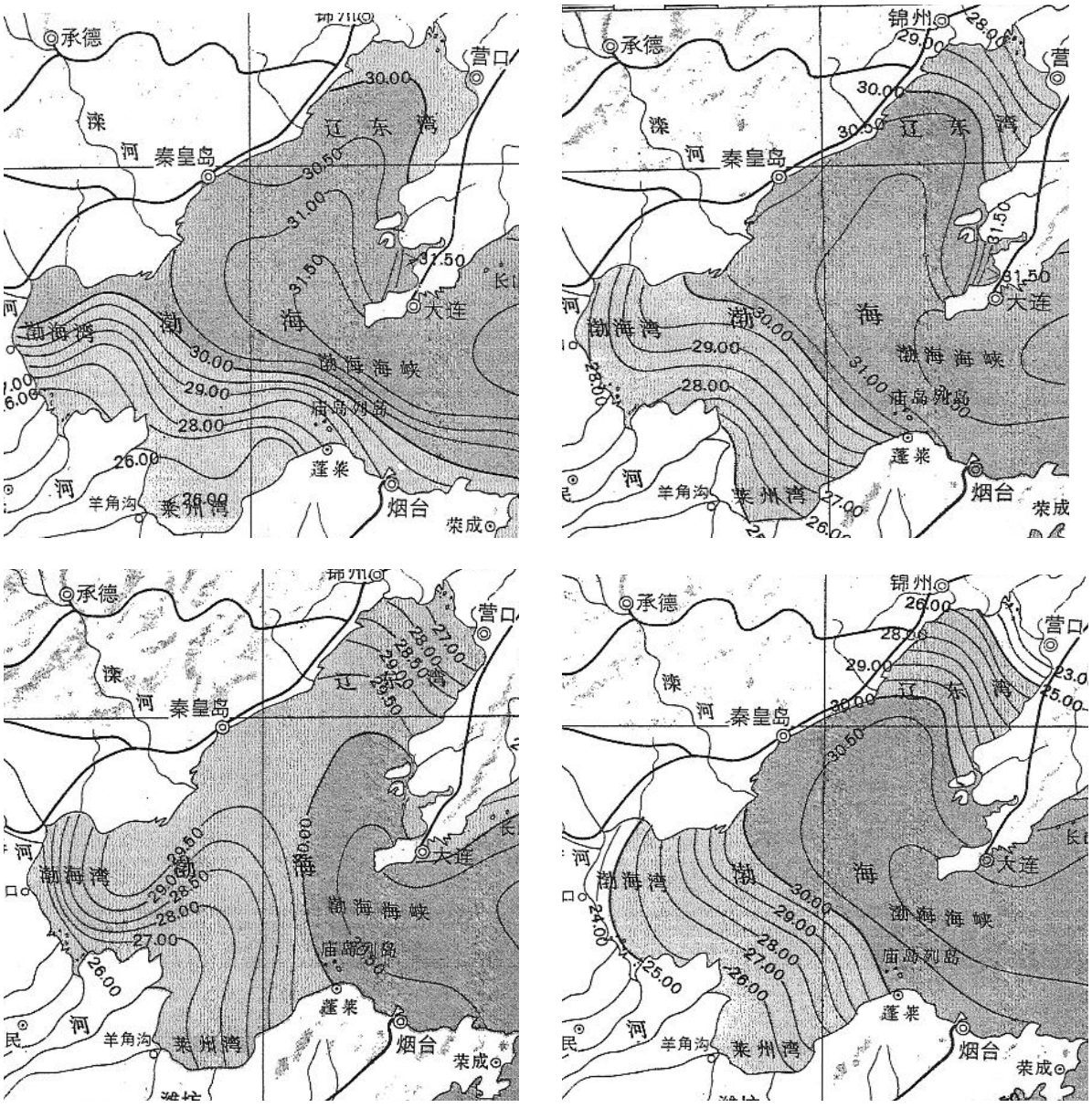

Figure 23. Sea surface salinity atlas from State Oceanic and Administration of China (1992) for January (upper left), April (upper right), July (lower left) and October (lower right).

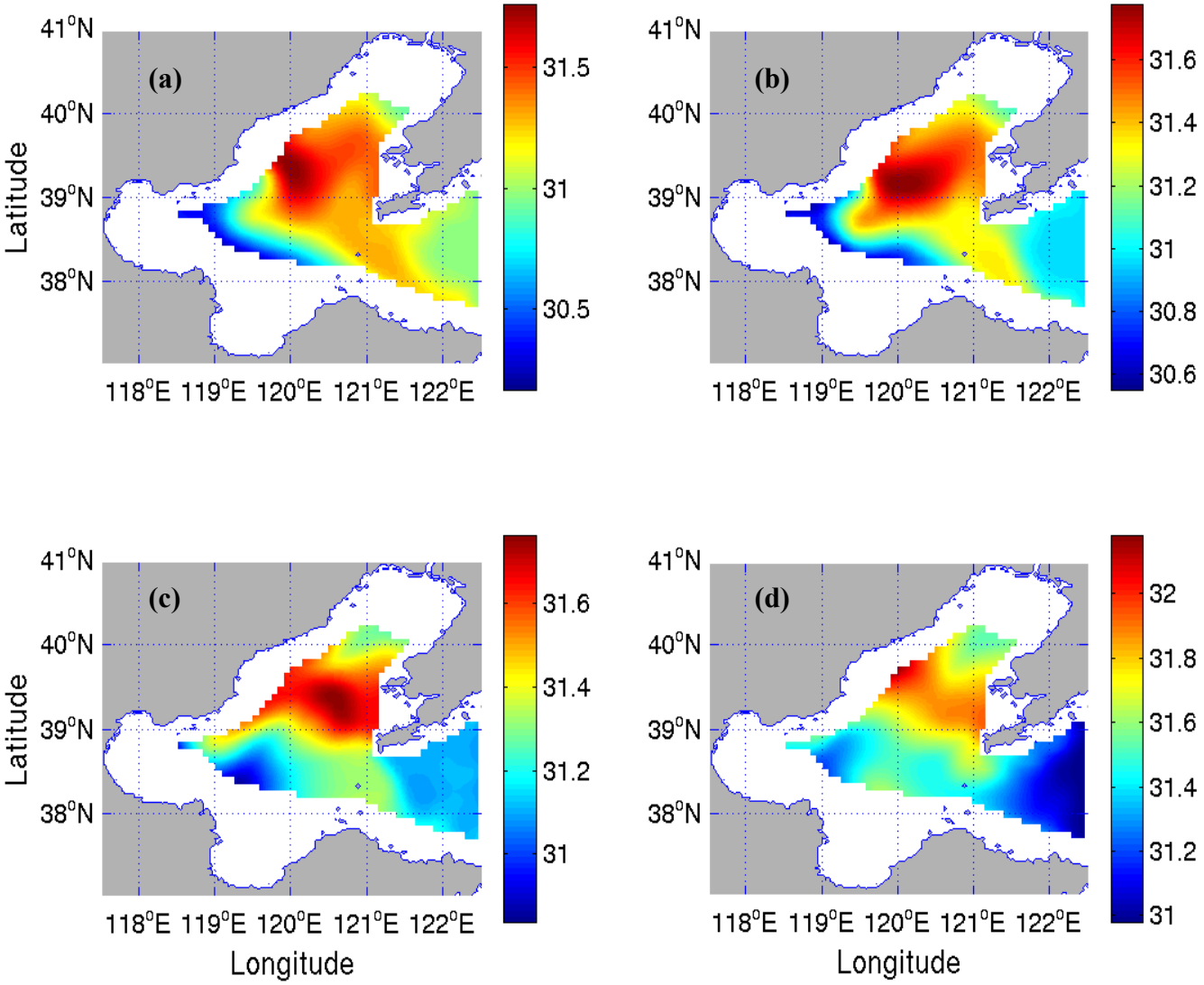

Figure 24. Simulated horizontal salinity (psu) field at 20 m depth on (a) January 15, (b) April 15, (c) July 15 and (d) October 15, 2000.

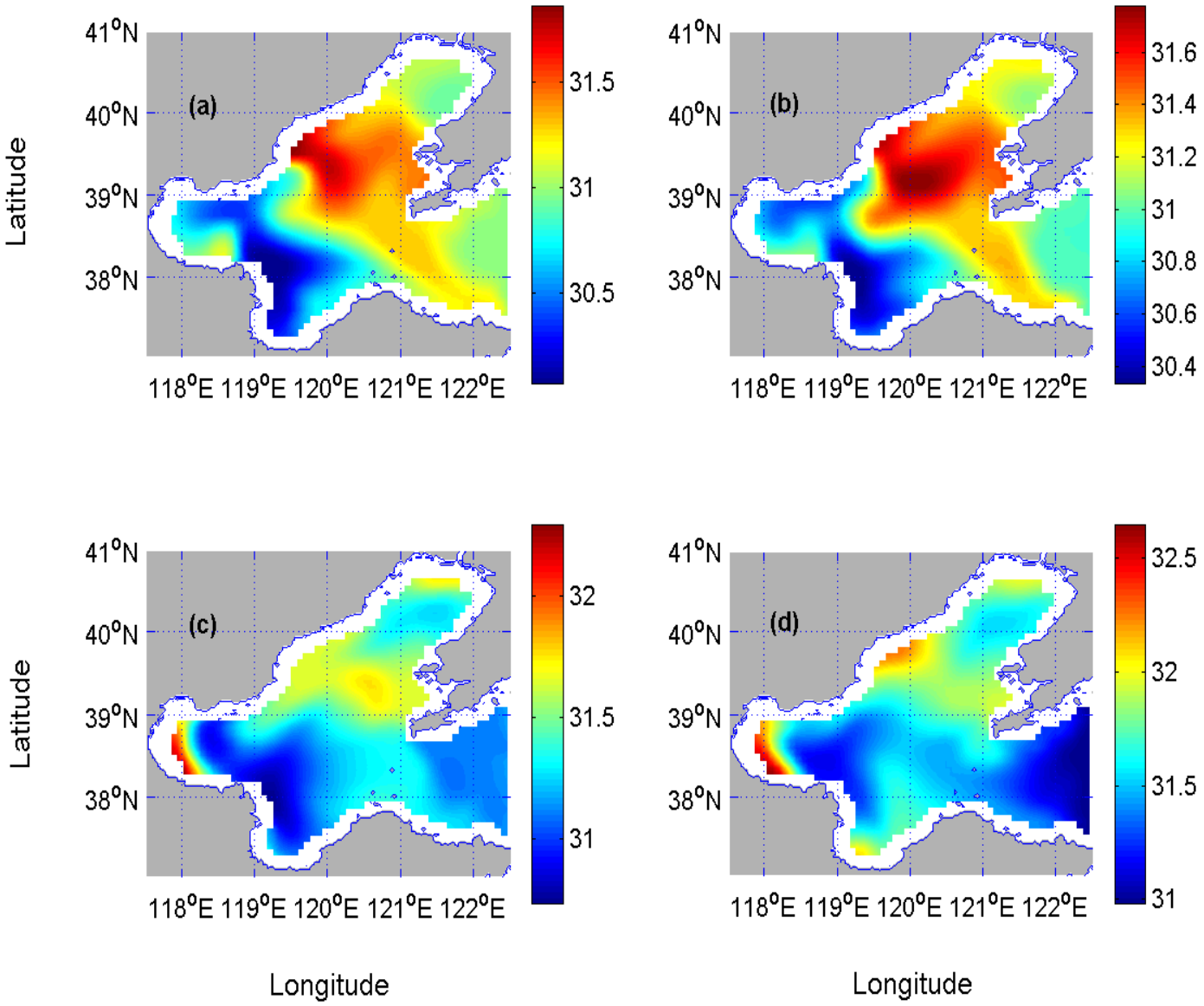

Figure 25. Simulated horizontal salinity (psu) field at the bottom on (a) January 15, (b) April 15, (c) July 15 and (d) October 15, 2000.

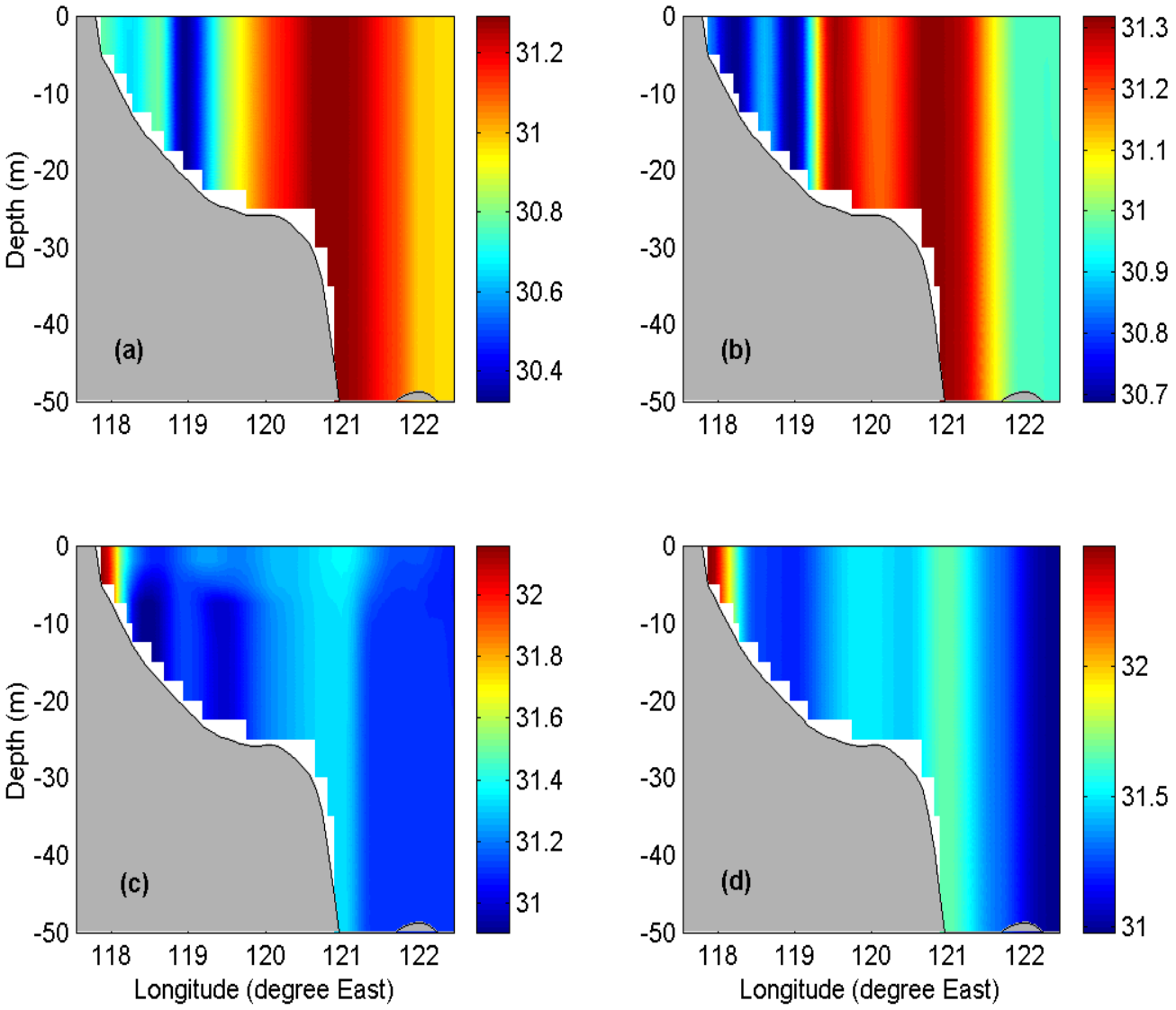

Figure 26. Simulated zonal salinity (psu) cross-sections along 38°35.52'N on (a) January 15, (b) April 15, (c) July 15 and (d) October 15, 2000.

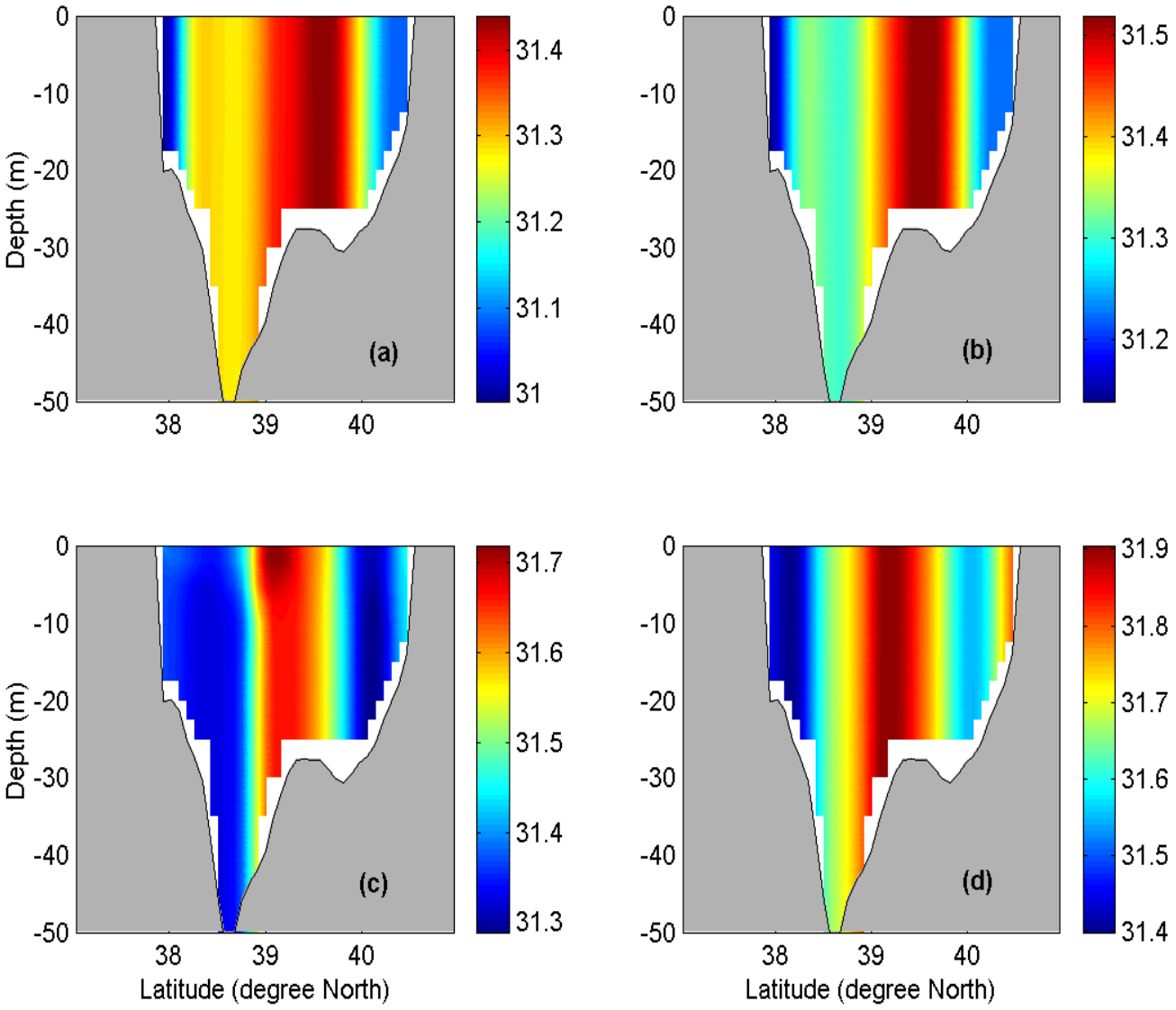

Figure 27. Simulated meridional salinity (psu) cross-sections along 121°01.5'E on (a) January 15, (b) April 15, (c) July 15 and (d) October 15, 2000.

THIS PAGE INTENTIONALLY LEFT BLANK

V. EFFECTS OF SURFACE THERMOHALINE FLUXES

In the first sensitivity study, the surface thermohaline flux terms (heat and moisture fluxes) were removed. Otherwise, the same parameters as the control run were used. The difference (Run-1 minus Run-2) of the model output (velocity, temperature, and salinity) indicates the surface flux effect.

A. EFFECTS ON CIRCULATION

The simulated velocity difference fields (Figures 28-30) show the effects of the surface heat and salt fluxes on the circulation of the BS. A comparison between Figures 28-30 and Figures 11-13 leads to identification of the surface thermohaline forcing effect. If the directions of the velocity vectors are nearly the same in Figures 28-30, as in Figures 11-13, for the corresponding depths and seasons, the surface thermohaline fluxes enhance the circulation. If the directions of the velocity vectors are opposite in Figure 28-30 as in Figures 11-13 for the corresponding depths and seasons, the surface thermohaline fluxes weaken the circulation. Thus, the effects of the surface thermohaline fluxes on the circulation are identified as follows. In the winter (January), the surface thermohaline fluxes weaken the circulation from the surface to bottom. The weakening of the circulation at the surface, however, is minimal due to small values of the velocity difference. In the spring (April), the surface thermohaline fluxes enhance the surface circulation, and the mid-depth and bottom circulation in the southern BS, and weaken the bottom circulation in the northern BS. In the summer (July), the surface thermohaline fluxes enhance the circulation from the surface to the bottom. In the fall (October), the surface thermohaline fluxes slightly weaken the circulation from the surface to the bottom.

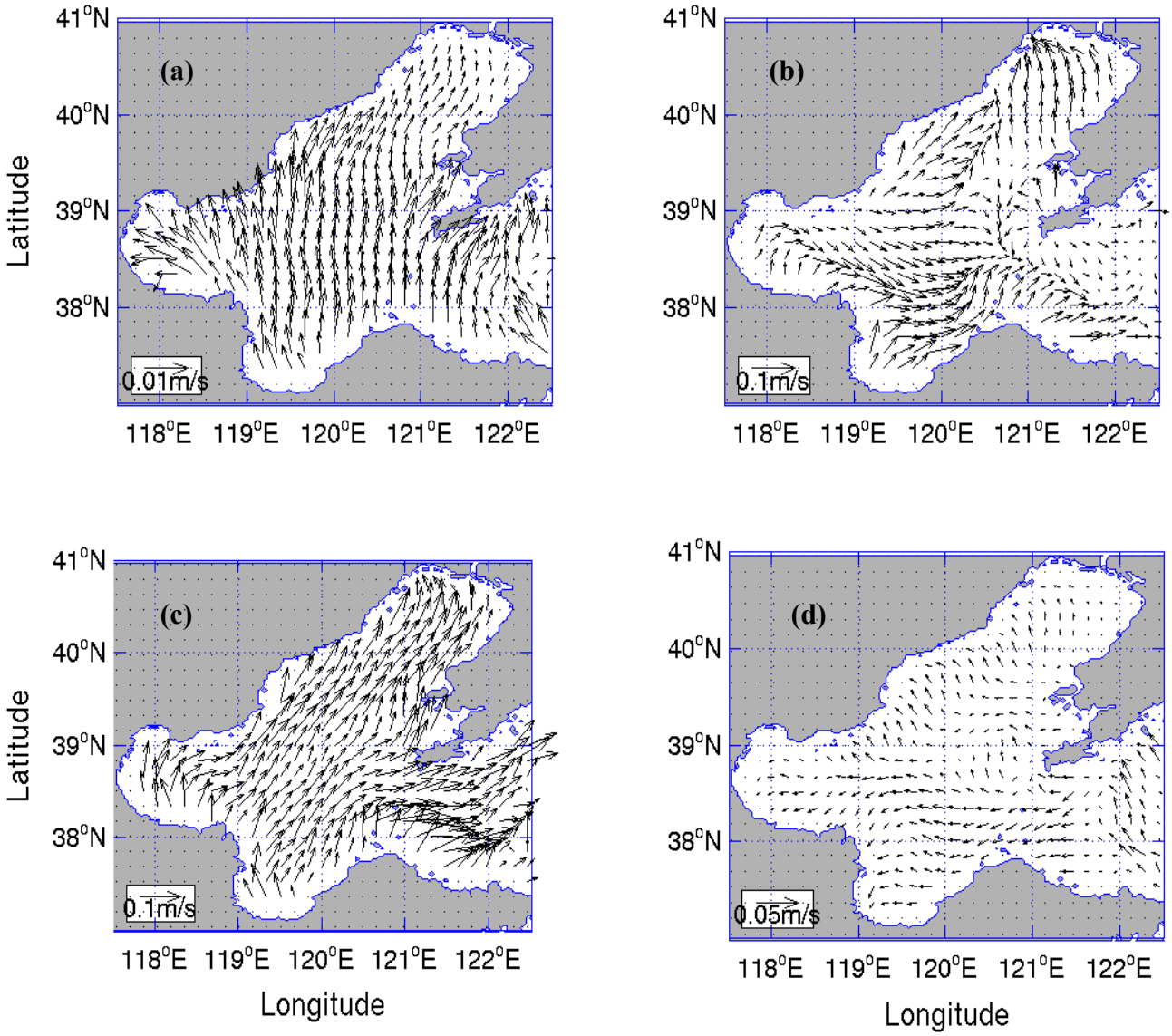

Figure 28. Velocity difference (Run-1 minus Run-2) on the surface on (a) January 15, (b) April 15, (c) July 15 and (d) October 15, 2000.

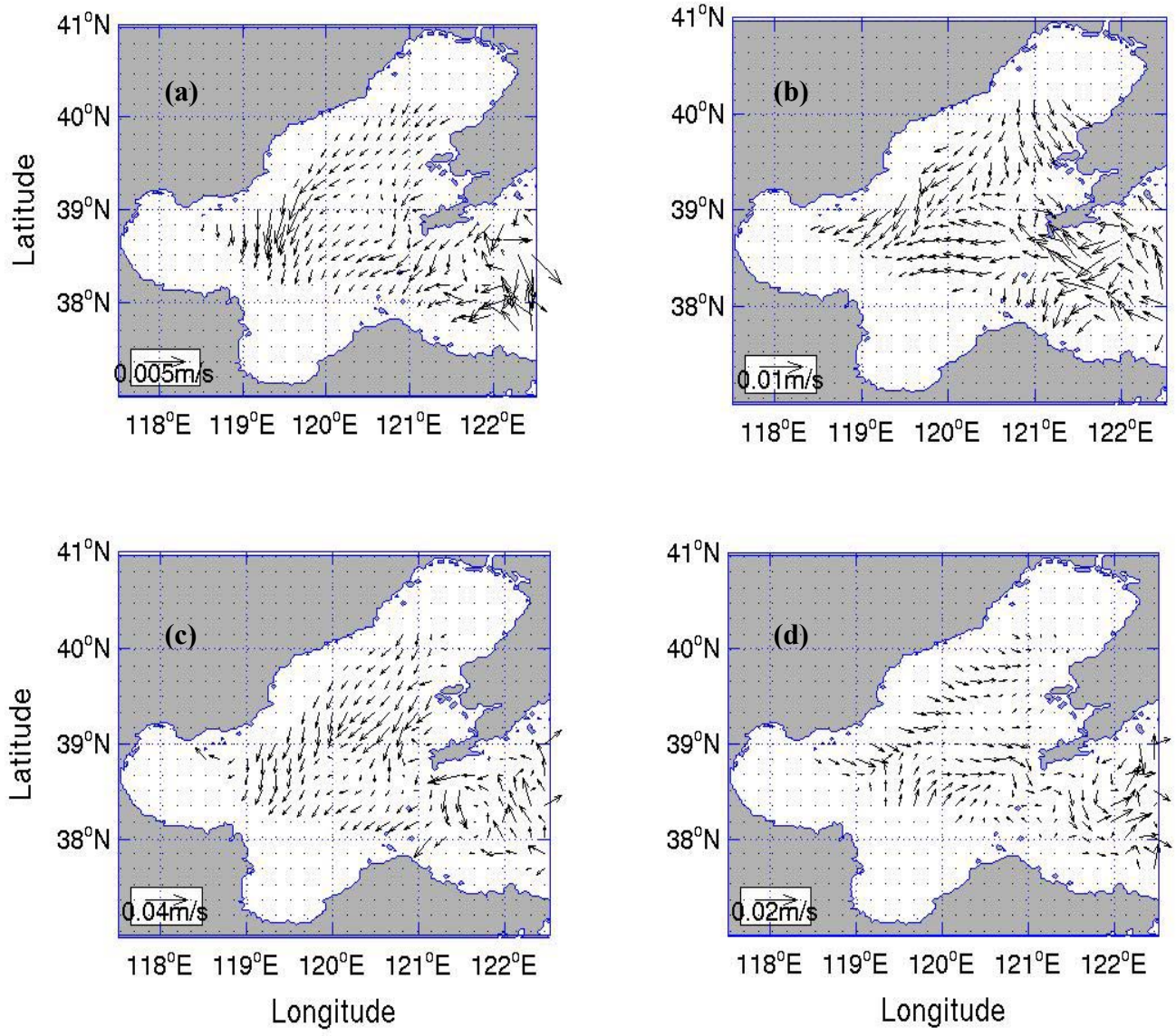

Figure 29. Velocity difference (Run-1 minus Run-2) at 20 m depth on (a) January 15, (b) April 15, (c) July 15 and (d) October 15, 2000.

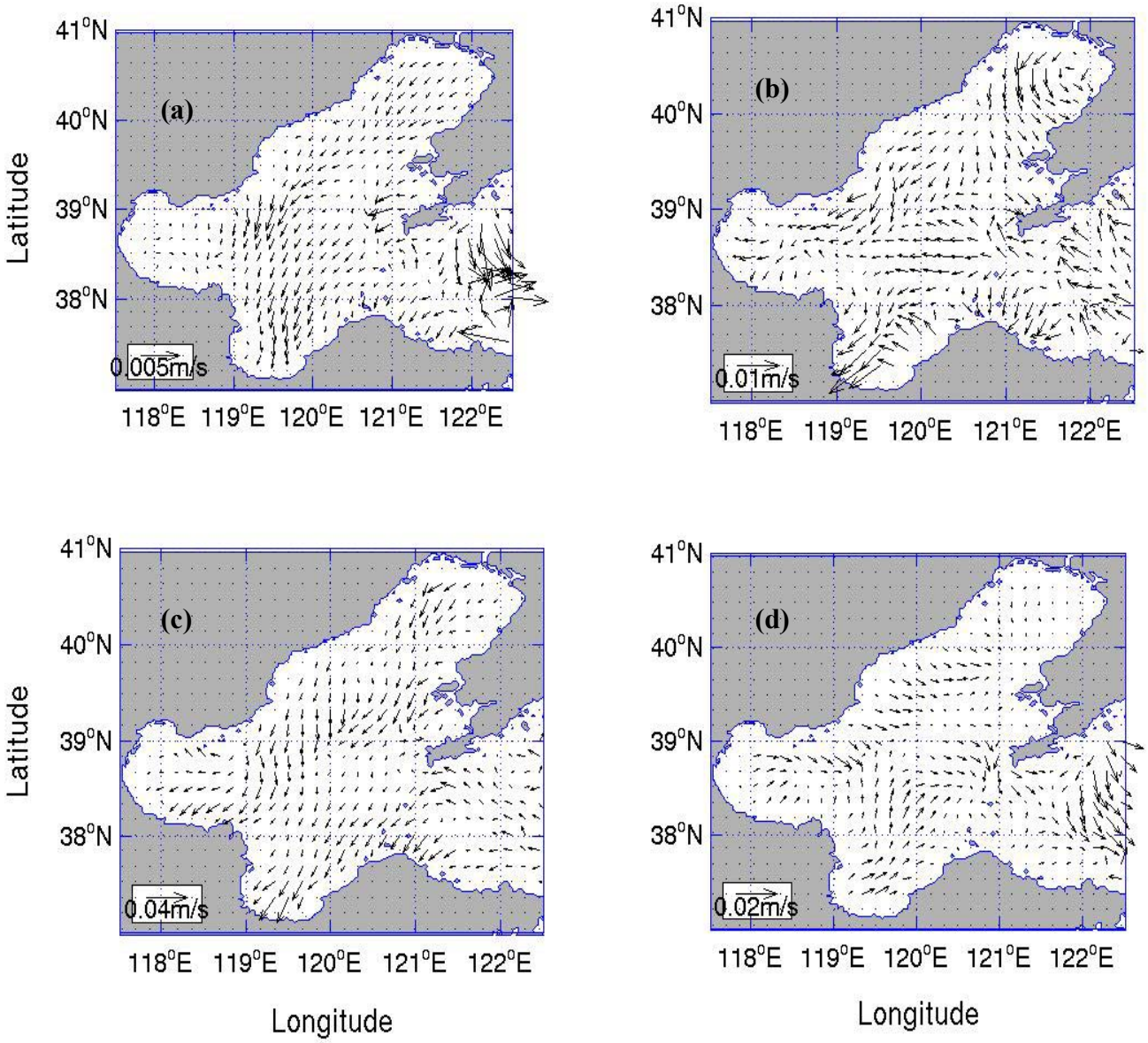

Figure 30. Velocity difference (Run-1 minus Run-2) at the bottom on (a) January 15, (b) April 15, (c) July 15 and (d) October 15, 2000.

B. EFFECTS ON TEMPERATURE

The major effect of the surface thermohaline fluxes is to cool (warm) the BS in the winter (summer) for the whole water column (Figures 31-33) since the temperature difference (ΔT) is negative (positive) all over the BS basin in the winter (summer). This effect becomes stronger at the gulfs and at the Laizhou Bay due to the shallow depth, and quite weak near the eastern boundary in Bohai Strait. There is not much difference in ΔT values at the surface, mid-depth (20 m), and bottom on January 15, April 15 and October 15, 2000. Nevertheless, there is evident difference in ΔT values at the surface, mid-depth (20 m), and bottom on July 15, 2000. For example, the temperature difference reaches –3^{o}C on 15 January 2000 and 7^{o}C on 15 July 2000 in Liaodong Gulf. In the central BS basin, however, the temperature difference is –2^{o}C on 15 January 2000 and 3-4^{o}C on 15 July 2000.

The temporal evolution of ΔT is depicted as follow. On January 15, 2000, ΔT is negative everywhere all over the BS basin with less cooling in deeper than shallower regions of the BS, and with a greater cooling in the central BS (-2^{o}C) than the surroundings (-1~-2^{o}C). On April 15, 2000, ΔT becomes positive everywhere in the BS that indicates warming due to the heat fluxes over the sea surface. The value of ΔT is around 1-2^{o}C in most parts of BS, and reaches 3-4^{o}C in the coastal shallow regions, especially in Liaodong Gulf, Bohai Gulf, and Laizhou Bay. The value of ΔT is below 1°C in the deep-water region from the eastern open boundary to Bohai Strait that indicates a less warming compared to central BS basin. On July 15, 2000, the warming effect enhances. The value of ΔT (all positive) is around 4-6^{o}C in most part of BS, and reaches 7-8^{o}C in the coastal shallow regions, especially in Liaodong Gulf, Bohai Gulf, and Laizhou Bay. The value of ΔT is below 1°C in the deep-water region from the eastern open boundary to Bohai Strait that indicates a less warming compared to central BS basin. On October 15, 2000, the value of ΔT becomes negative in most areas of the BS and positive only near the eastern open boundary.

The vertical dependence of ΔT is represented by zonal (Figure 34) and meridional (Figure 35) cross-sections. In the winter (Figures 34a and 35a), the cooling effect of the surface fluxes is vertically uniform, which is consistent with the cooling by

the surface fluxes of the whole water column. This effect becomes stronger with decreasing depth. At the gulfs and at Laizhou Bay, the cooling effect is greater. On April 15, 2000 (Figures 34b and 35b), the warming effect of the surface fluxes is vertically uniform. The net surface heat flux warms the whole water column. Again, this effect becomes stronger with decreasing depth. At the gulfs and at the Laizhou Bay, the warming effect is greater. In the summer (Figures 34c and 35c), the warming effect is not vertically uniform. This effect is stronger in the surface layer, at the gulfs and at Laizhou Bay. Below the surface layer and away from the gulfs and the Laizhou Bay, the warming effect of the surface fluxes is vertically uniform. On October 15, 2000 (Figures 34d and 35d), away from the open boundary, the cooling effect of the surface fluxes is almost vertically uniform. This effect becomes stronger with the decrease of depth and at the gulfs and at Laizhou Bay.

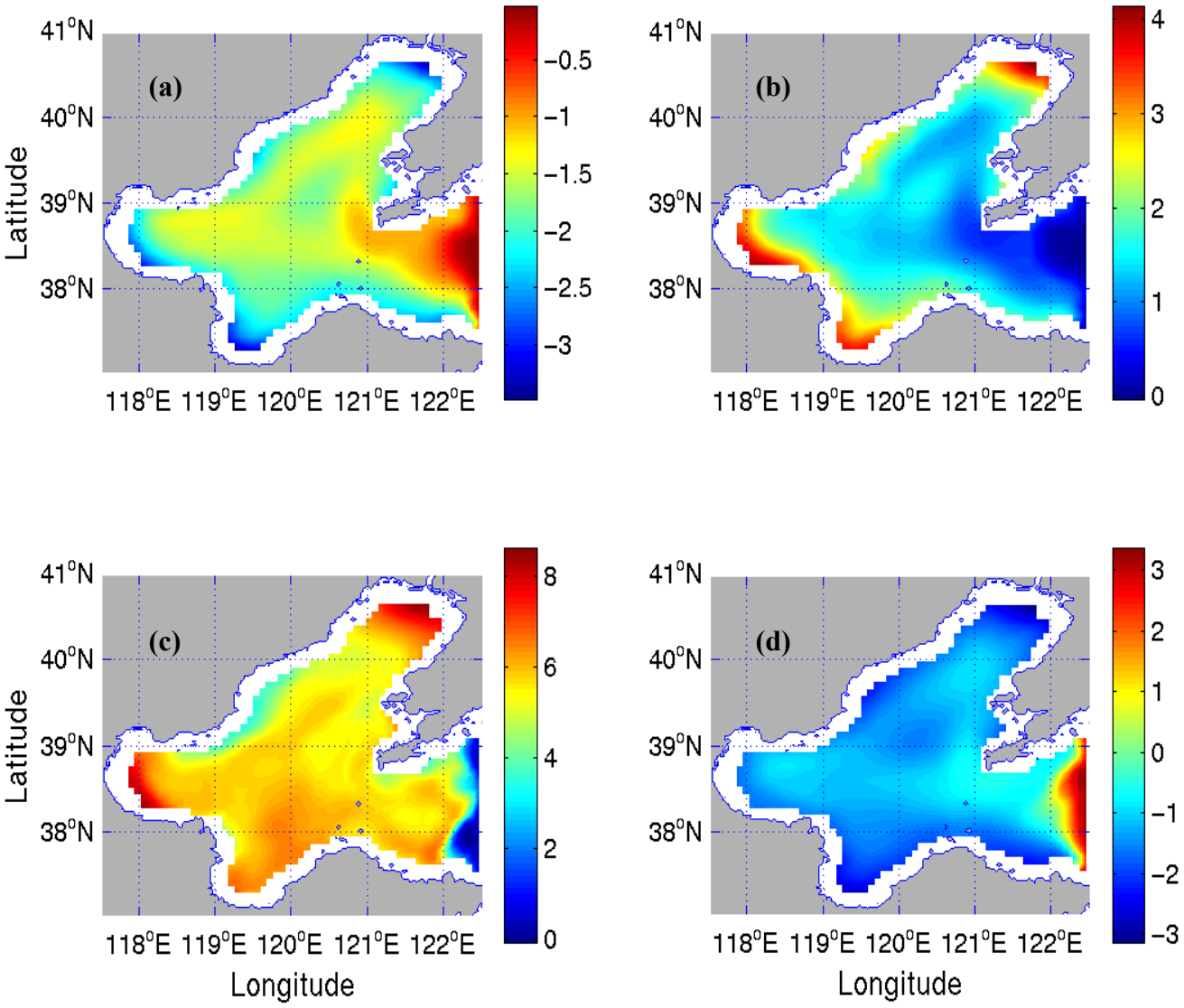

Figure 31. Temperature difference (°C) field (Run-1 minus Run-2) at the surface on (a) January 15, (b) April 15, (c) July 15 and (d) October 15, 2000.

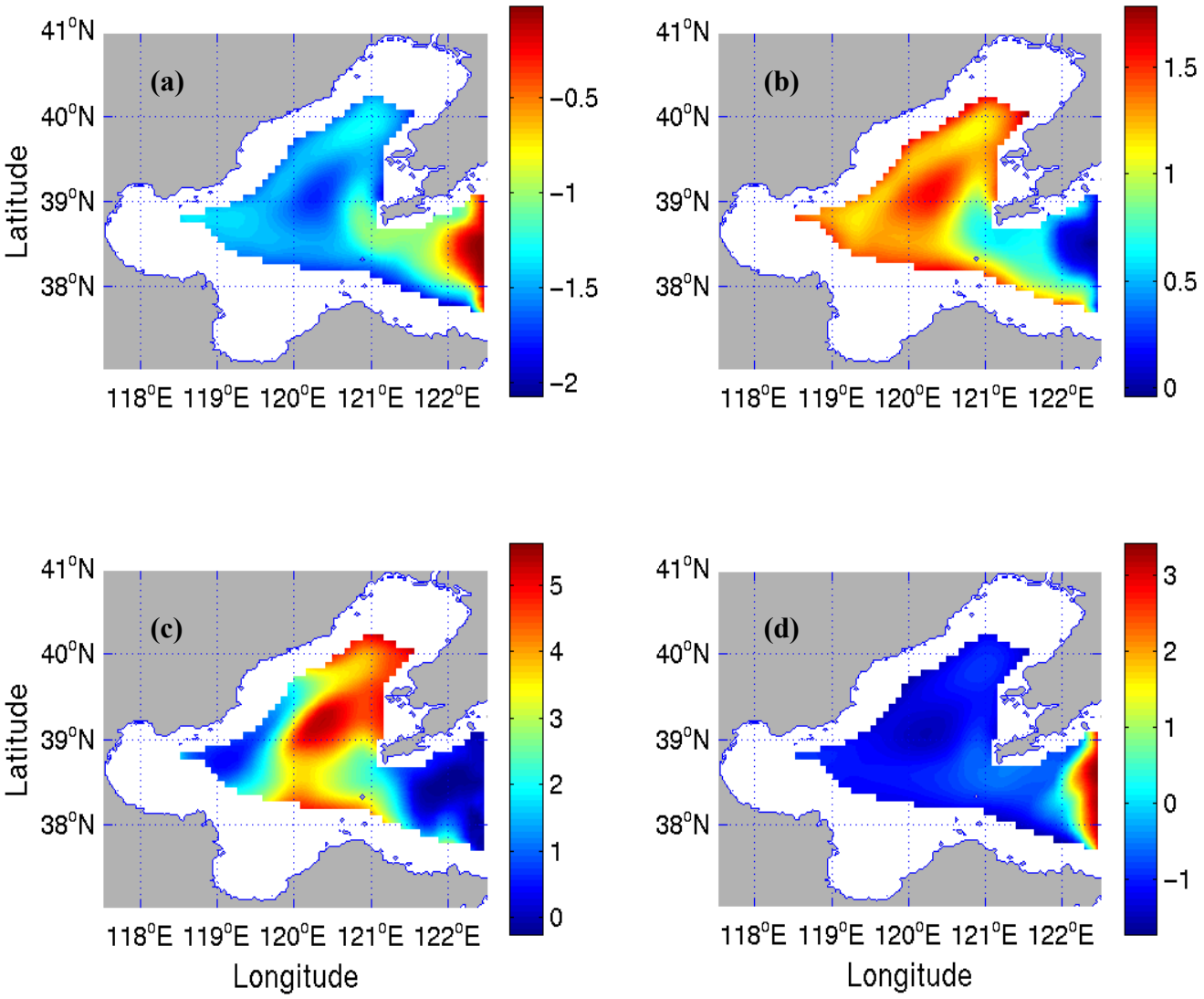

Figure 32. Temperature difference (°C) field (Run-1 minus Run-2) at 20 m depth on (a) January 15, (b) April 15, (c) July 15 and (d) October 15, 2000.

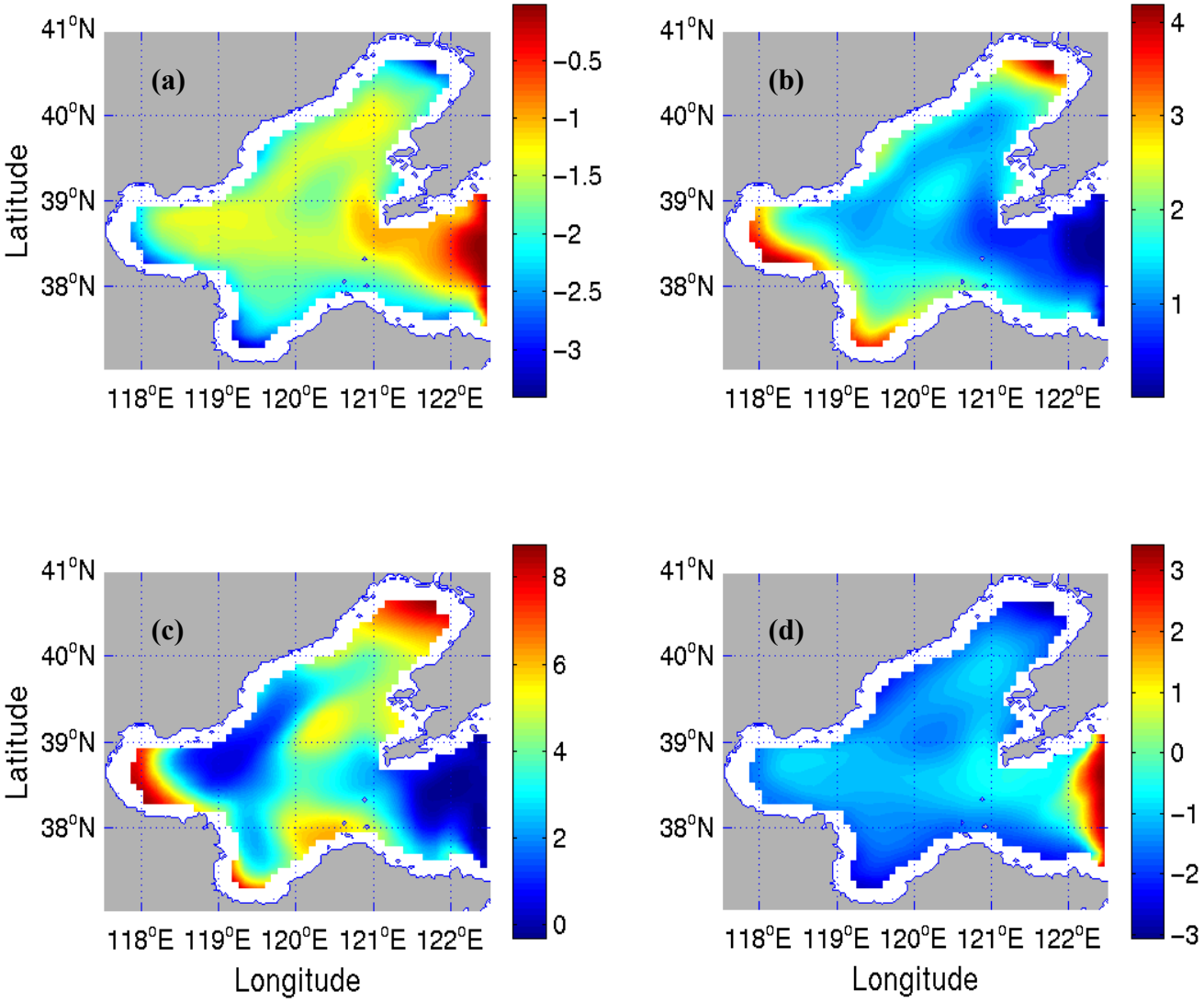

Figure 33. Temperature difference (°C) field (Run-1 minus Run-2) at the bottom on (a) January 15, (b) April 15, (c) July 15 and (d) October 15, 2000.

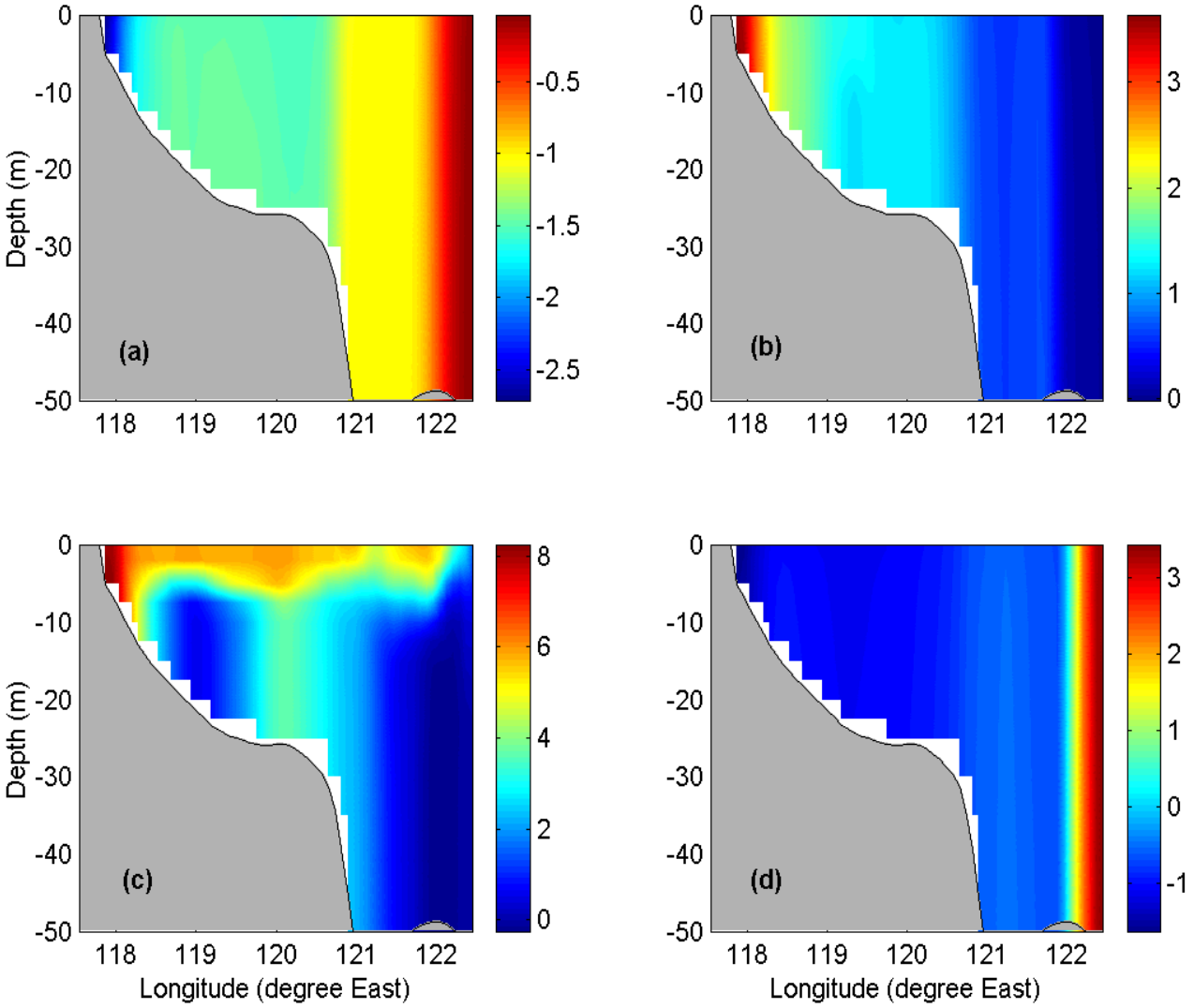

Figure 34. Zonal cross-section of the temperature (^{o}C) difference (Run-1 minus Run-2) along 38°35.52'N on (a) January 15, (b) April 15, (c) July 15 and (d) October 15, 2000.

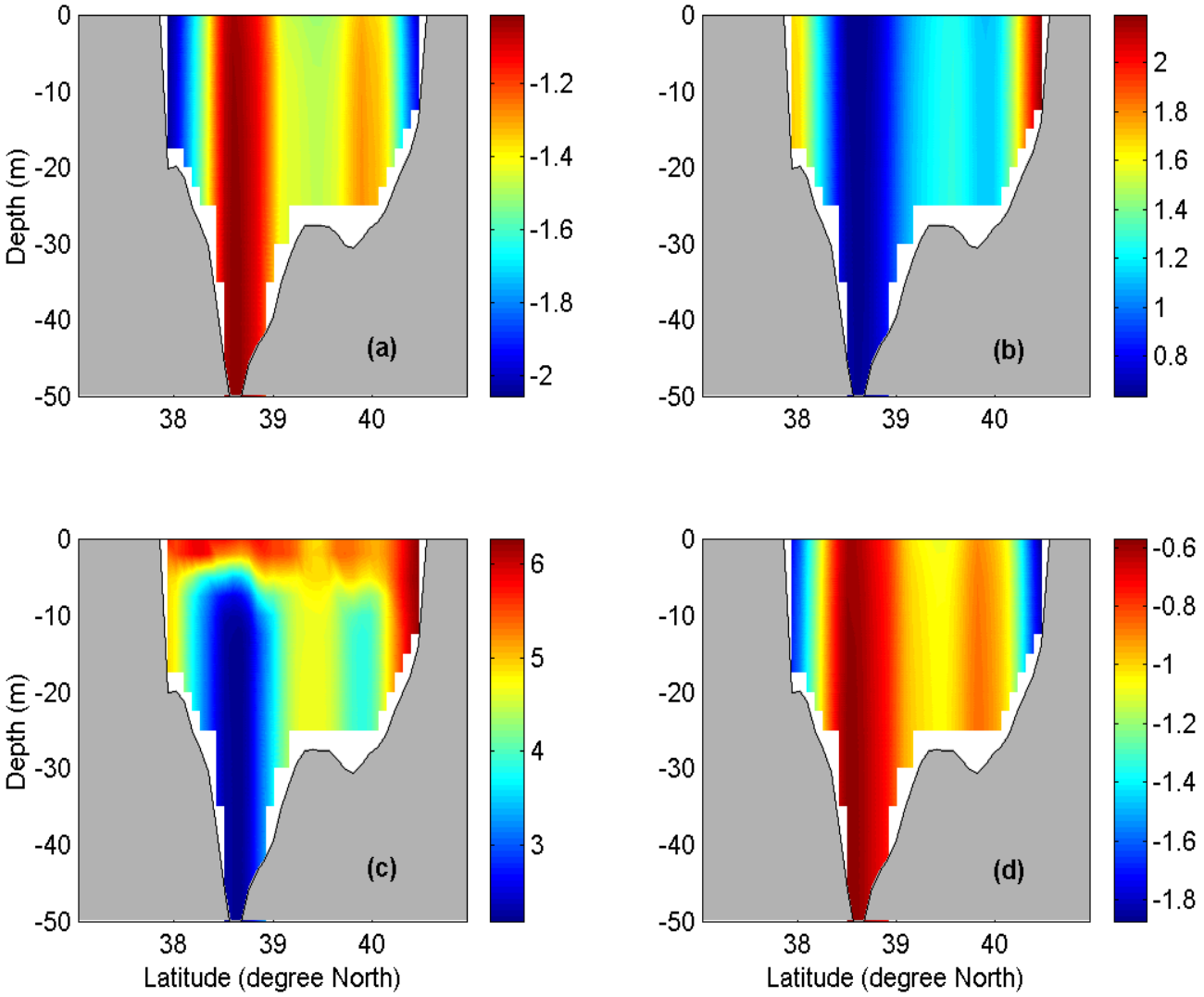

Figure 35. Meridional cross-section of the temperature (^{o}C) difference (Run-1 minus Run-2) along 121°01.5'E on (a) January 15, (b) April 15, (c) July 15 and (d) October 15, 2000.

C. EFFECTS ON SALINITY

The effect of the surface thermohaline fluxes over the salinity field is generally to increase the salinity for almost all the water column (Figures 36-38), since the salinity difference (ΔS) is positive almost all over the basin, except on the bottom at a specific small spot. There is a tendency for the water to be more saline due to the positive salinity difference. The discharge of fresh water from the rivers over the Bohai Sea would balance this tendency. This effect becomes stronger at the gulfs and at Laizhou Bay due to the shallow depth, and quite weak near the eastern boundary in Bohai Strait. There is not much difference in ΔS values at the surface, mid-depth (20 m), and bottom on April 15 and October 15, 2000. There are, however, differences in ΔS values at the surface, mid-depth (20 m), and bottom on January 15 and July 15, 2000.

The temporal evolution of ΔS is described as follows. On January 15, 2000, ΔS is positive everywhere all over the BS basin with smaller values in deeper than shallower regions of the BS. Only on the bottom, there is a small region between the Huanghe river mouth and the Bohai Gulf with negative ΔS values. Laizhou Bay presents the highest differences ΔS (~0.08 psu). On April 15, 2000, ΔS continues positive everywhere in the BS that indicates salinity increases due to the heat fluxes over the sea surface. The value of ΔS is around 0.1-0.25 psu in most part of BS, and reaches 0.55 psu in the coastal shallow regions, especially in Bohai Gulf and in Laizhou Bay. The value of ΔS is below 0.05 psu in the deep-water region from the eastern open boundary to Bohai Strait that indicates a less salinity change compared to central BS basin. On July 15, 2000, the thermohaline effect enhances salinity field. The value of ΔS (still all positive) is around 0.1-0.7 psu in most part of BS, and reaches 1.2-1.7 psu in the coastal shallow regions, especially in Bohai Gulf and in Laizhou Bay. The value of ΔS is below 0.1 psu in the deep-water region from the eastern open boundary to Bohai Strait that indicates a less saline effect compared to central BS basin. On October 15, 2000, the value of ΔS increases even more in most areas of the BS and is less than 0.1 psu only near the eastern open boundary.

The vertical dependence of ΔS is represented by zonal (Figure 39) and meridional (Figure 40) cross-sections. In the winter (Figures 39a and 40a), the effect of salinity increases due to the surface fluxes is not vertically uniform. There is a tendency for this effect to become stronger with the decrease of depth. At the gulfs and at Laizhou Bay, the saline effect is greater. At the surface layer, the water is more saline than at the deeper layer. On April 15, 2000 (Figures 39b and 40b), the surface fluxes effect over the salinity filed is vertically uniform. Again, this effect becomes stronger with the decrease of depth and at the gulfs and at Laizhou Bay the saline effect is greater. In the summer (Figures 39c and 40c), the saline effect is not vertically uniform. This effect is stronger at the gulfs and at Laizhou Bay. Below the surface layer and away from the gulfs and Laizhou Bay, the saline effect of the surface fluxes is vertically uniform. On October 15, 2000 (Figures 39d and 40d), the saline effect of the surface fluxes is vertically uniform. This effect becomes stronger with the decrease of depth and at the gulfs and at Laizhou Bay. At the surface layer, the water is more saline than at the deeper layer.

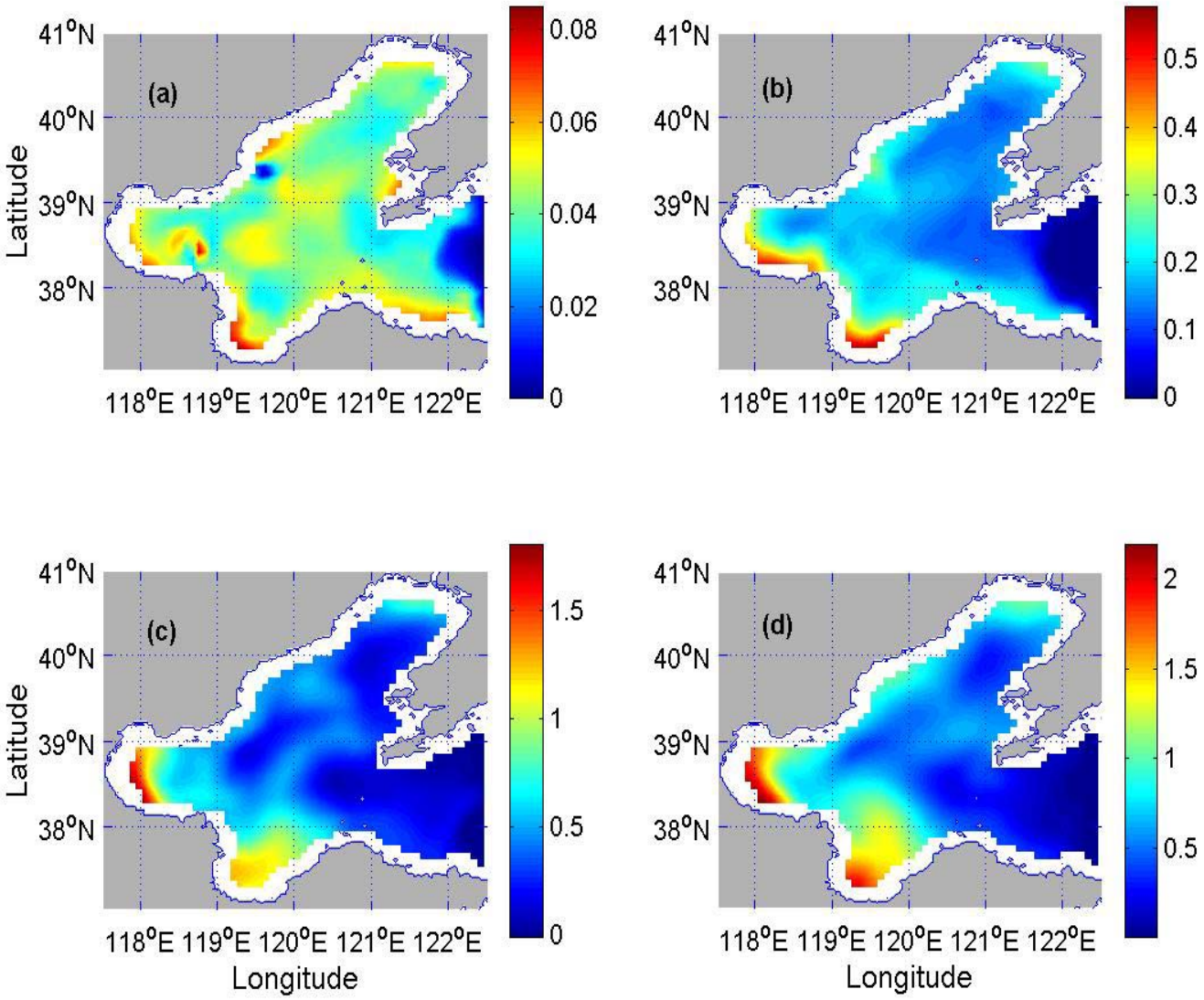

Figure 36. Salinity difference (psu) field (Run-1 minus Run-2) at the surface on (a) January 15, (b) April 15, (c) July 15 and (d) October 15, 2000.

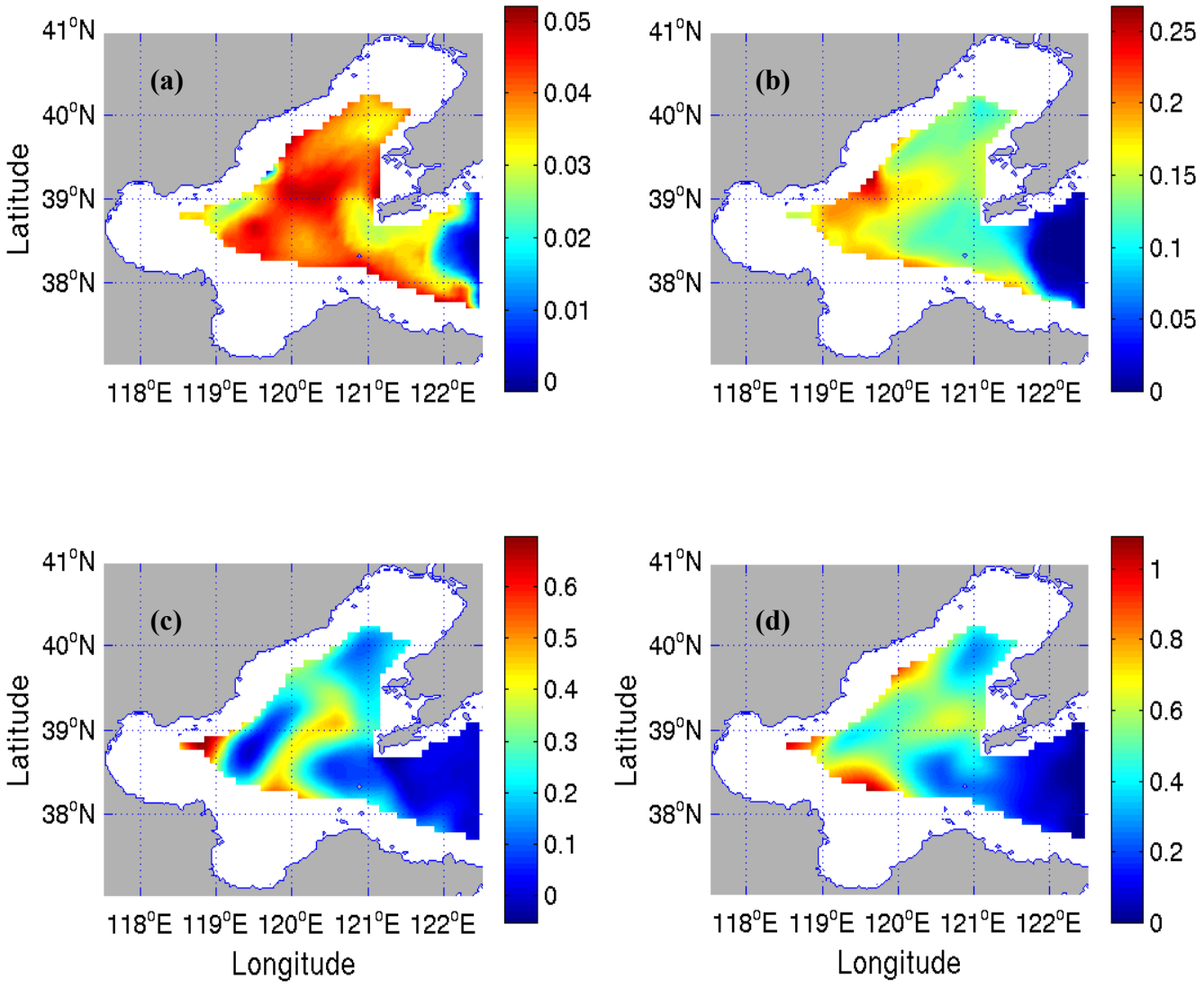

Figure 37. Salinity difference (psu) field (Run-1 minus Run-2) at 20 m depth on (a) January 15, (b) April 15, (c) July 15 and (d) October 15, 2000.

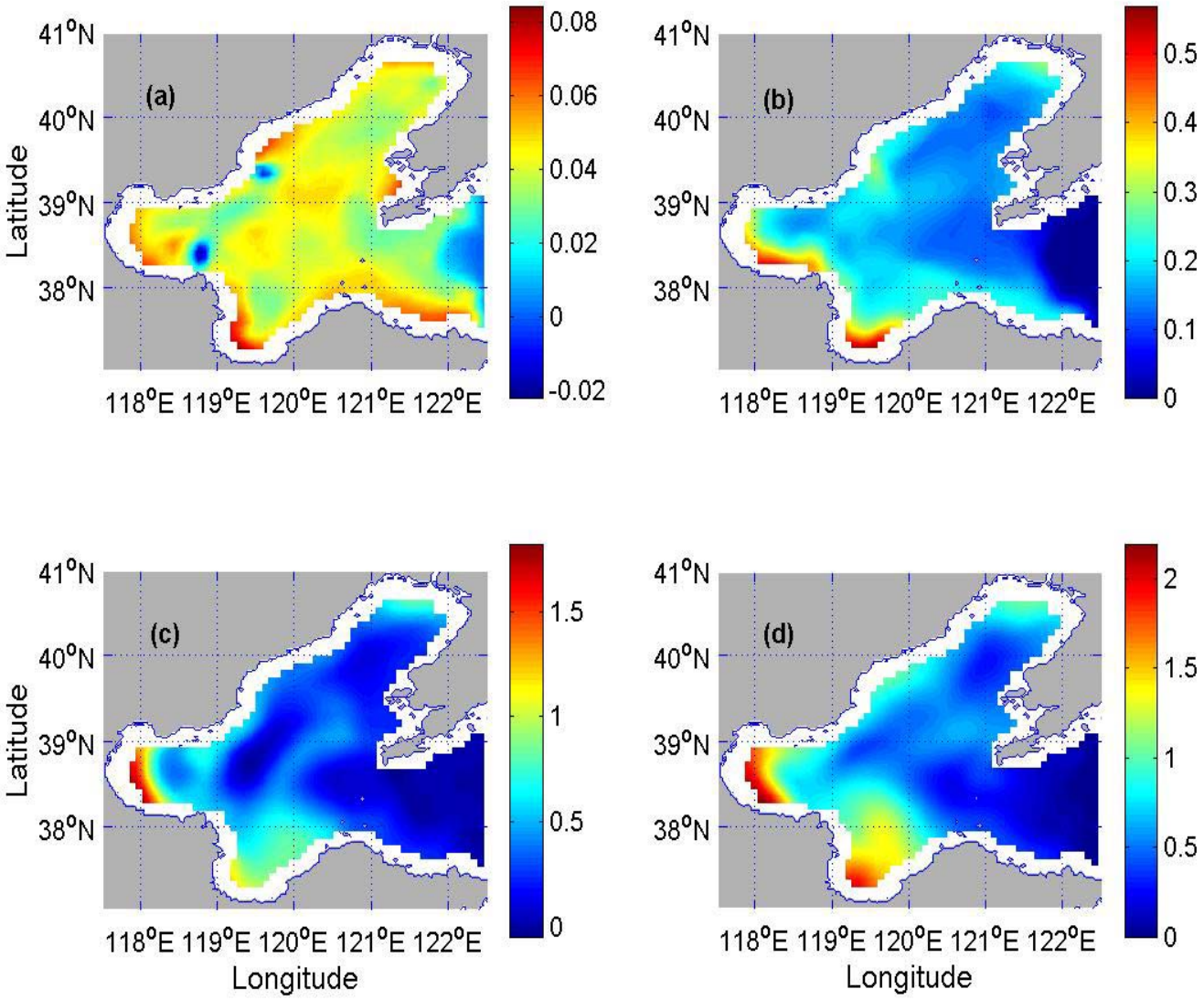

Figure 38. Salinity difference (psu) field (Run-1 minus Run-2) at the bottom on (a) January 15, (b) April 15, (c) July 15 and (d) October 15, 2000.

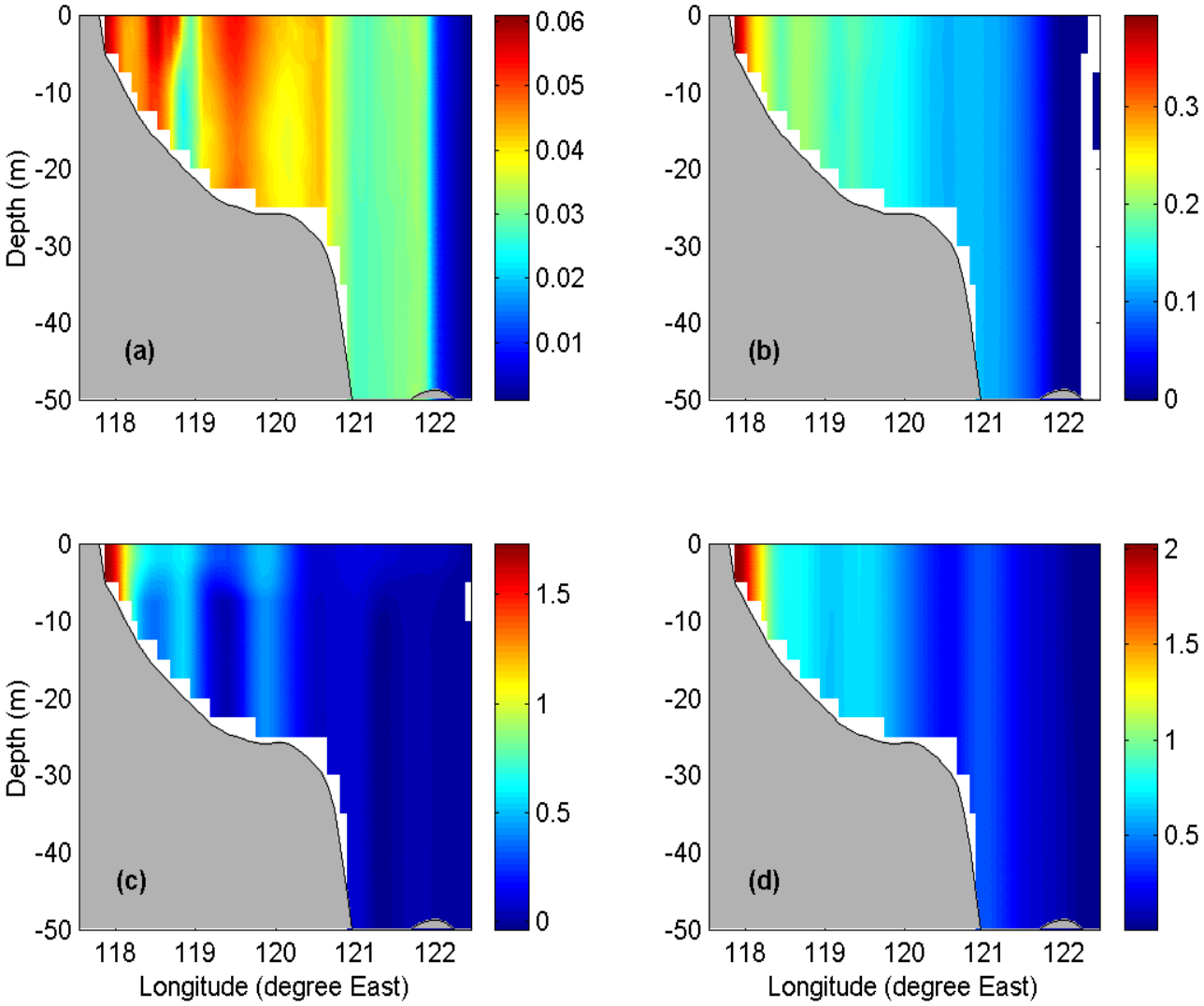

Figure 39. Zonal cross-section of the salinity (psu) difference (Run-1 minus Run-2) along 38°35.52'N on (a) January 15, (b) April 15, (c) July 15 and (d) October 15, 2000.

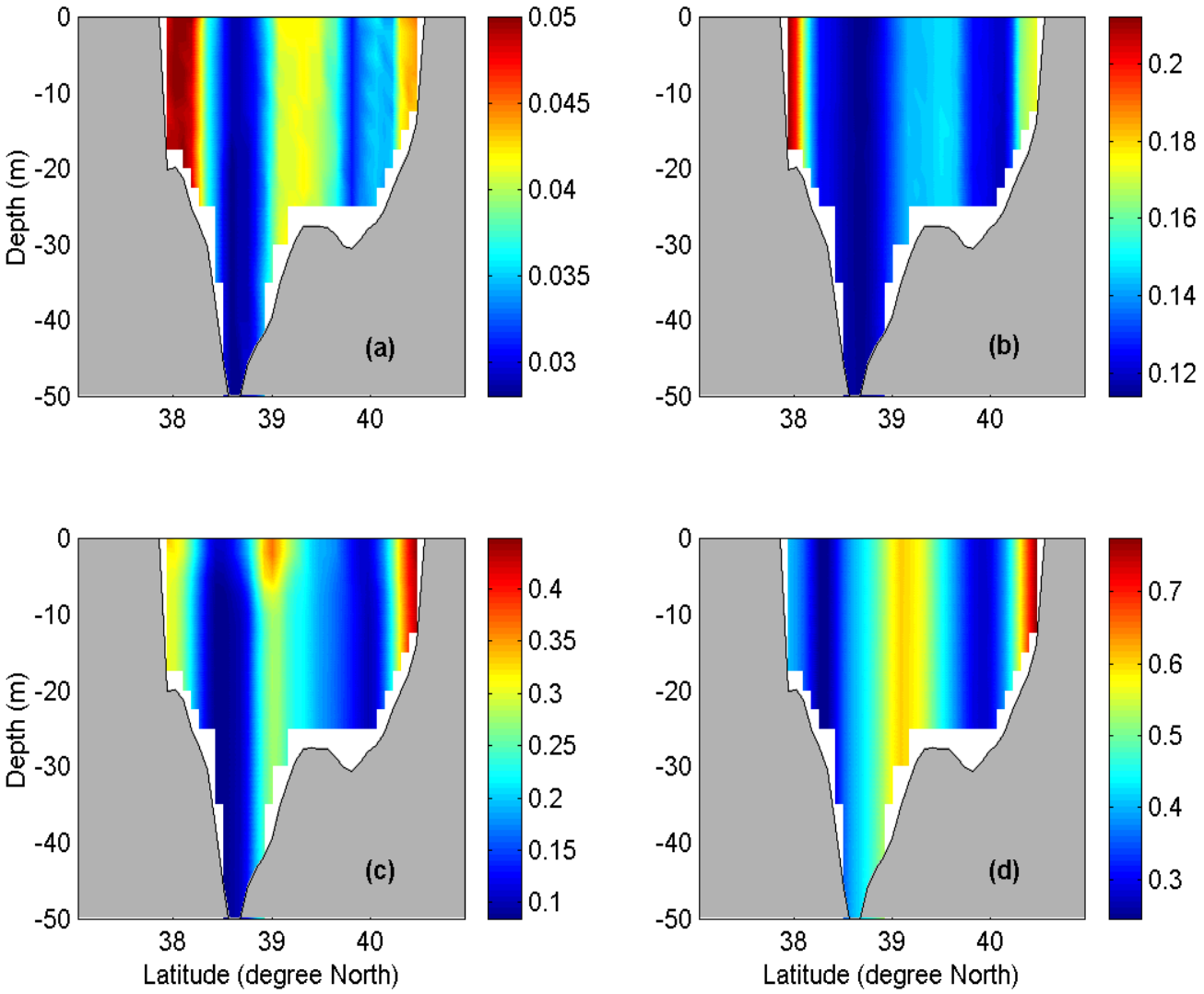

Figure 40. Meridional cross-section of the salinity (psu) difference (Run-1 minus Run-2) along 121°01.5'E on (a) January 15, (b) April 15, (c) July 15 and (d) October 15, 2000.

VI. EFFECTS OF SURFACE WIND STRESS

In the second sensitivity study, the wind effect on the surface stress was removed. Otherwise, the same parameters as the control run were used. The difference (Run-1 minus Run-3) of the model output (velocity, temperature, and salinity) indicates the wind effect.

A. EFFECTS ON CIRCULATION

The simulated velocity difference fields (Figures 41-43) show the effects of the surface stress due to the winds on the circulation of the BS. A comparison between Figures 41-43 and Figures 11-13 leads to identification of the wind forcing effect. If the directions of the velocity vectors are nearly the same in Figure 41-43 as in Figures 11-13 for the corresponding depths and seasons, the wind stress enhances the circulation. If the directions of the velocity vectors are opposite in Figure 41-43 as in Figures 11-13 for the corresponding depths and seasons, the wind stress weakens the circulation. Thus, the effects of the surface stress on the circulation are identified as follows. In the winter (January), the wind stress enhances the circulation from the surface to bottom. The stronger influence is to the east of the Bohai Strait and the velocity differences reach 0.2 m/s. At the Bohai Gulf, the differences are very small. In the spring (April), the surface wind stress enhances the surface circulation, and the mid-depth and bottom circulation in the southern BS, and weakens the bottom circulation at the Liaodong Gulf and at Laizhou Bay. The wind effect is stronger in the west part of BS. In the summer (July), the wind effect enhances the circulation from the surface to the bottom. In the fall (October), the surface wind stress enhances the circulation from the surface to the bottom, except at the Liaodong Gulf and at Laizhou Bay. In these places, the wind stress weakens the circulation at the bottom.

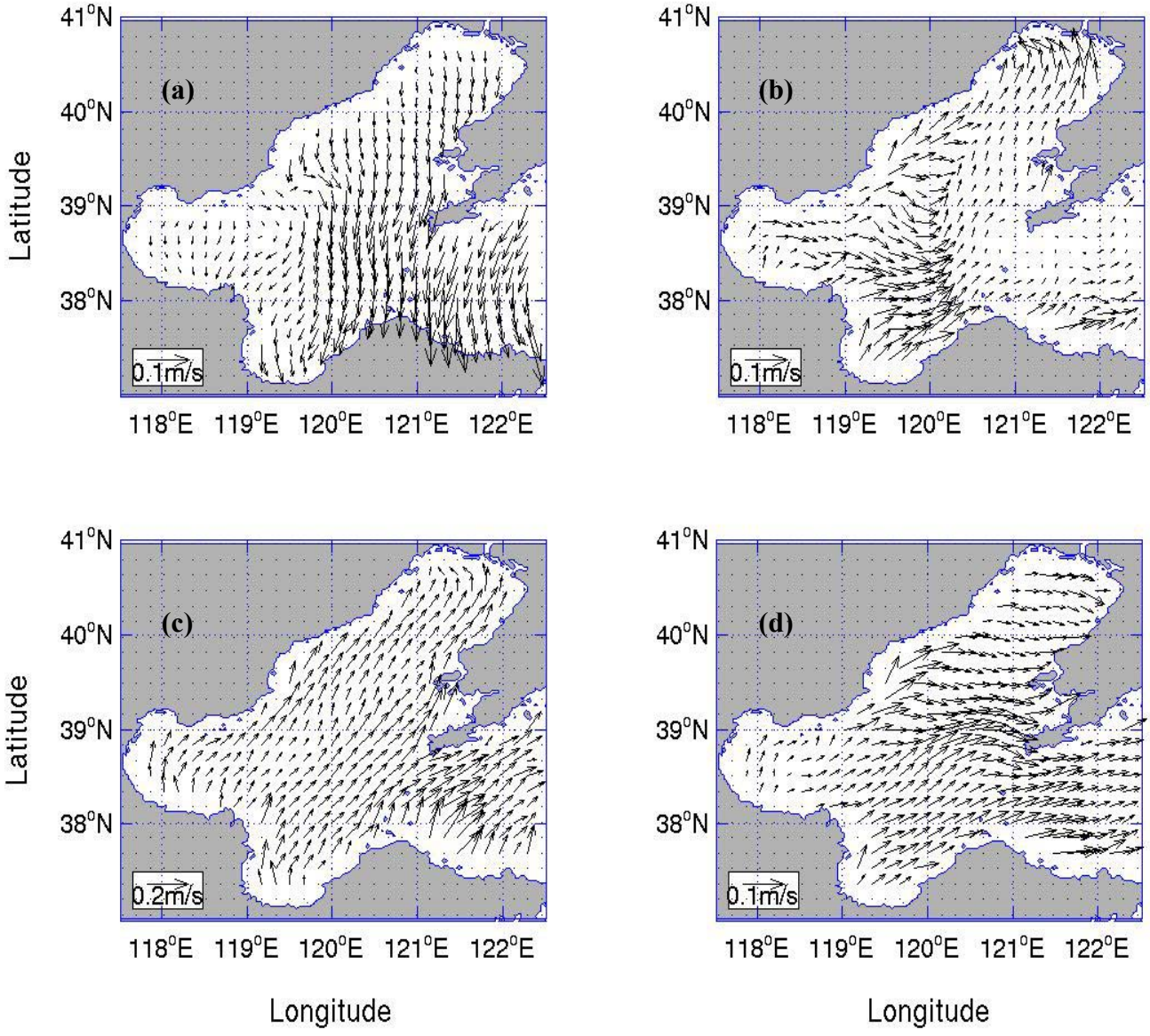

Figure 41. Velocity difference (Run-1 minus Run-3) on the surface on (a) January 15, (b) April 15, (c) July 15 and (d) October 15, 2000.

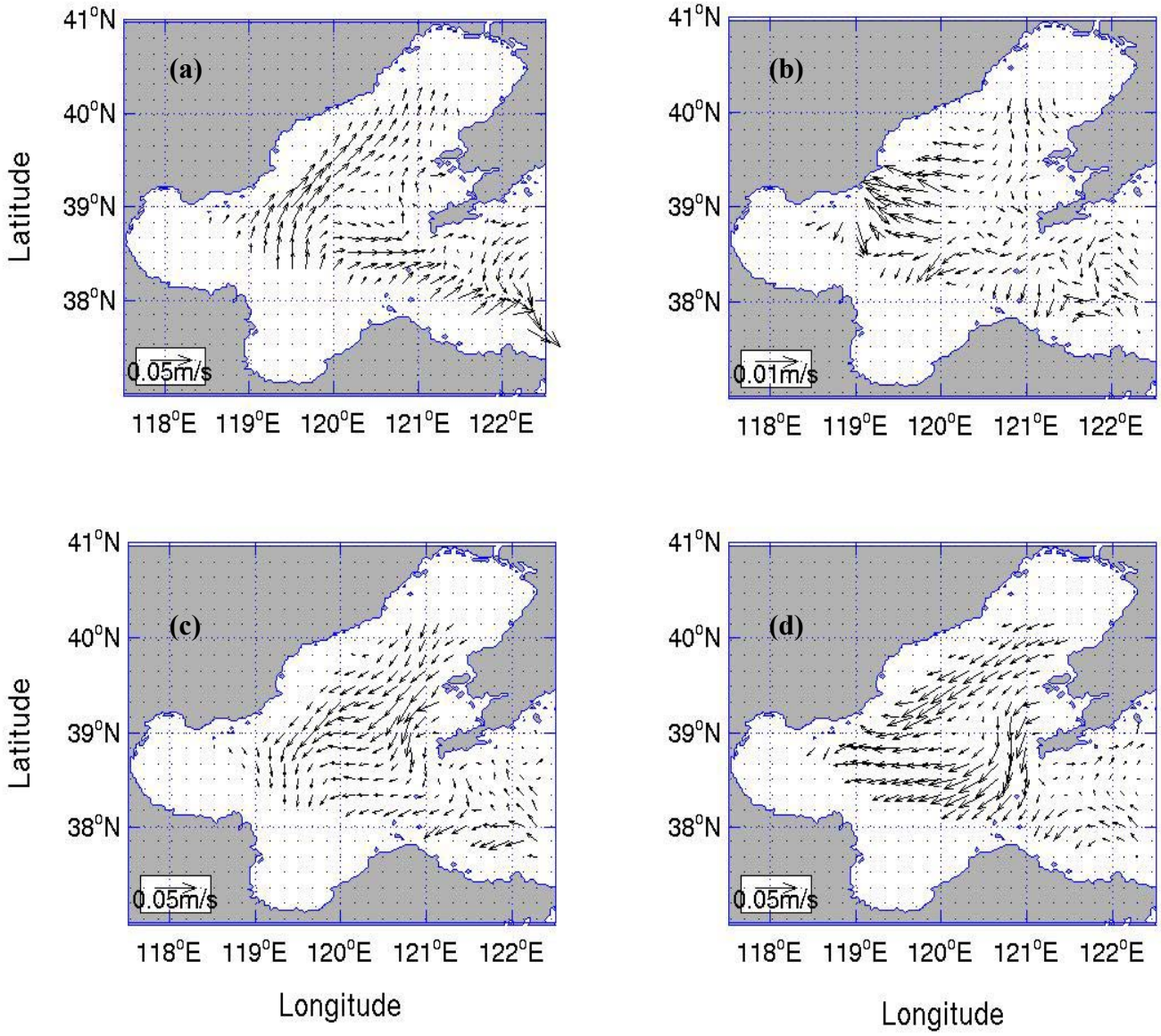

Figure 42. Velocity difference (Run-1 minus Run-3) at 20 m depth on (a) January 15, (b) April 15, (c) July 15 and (d) October 15, 2000.

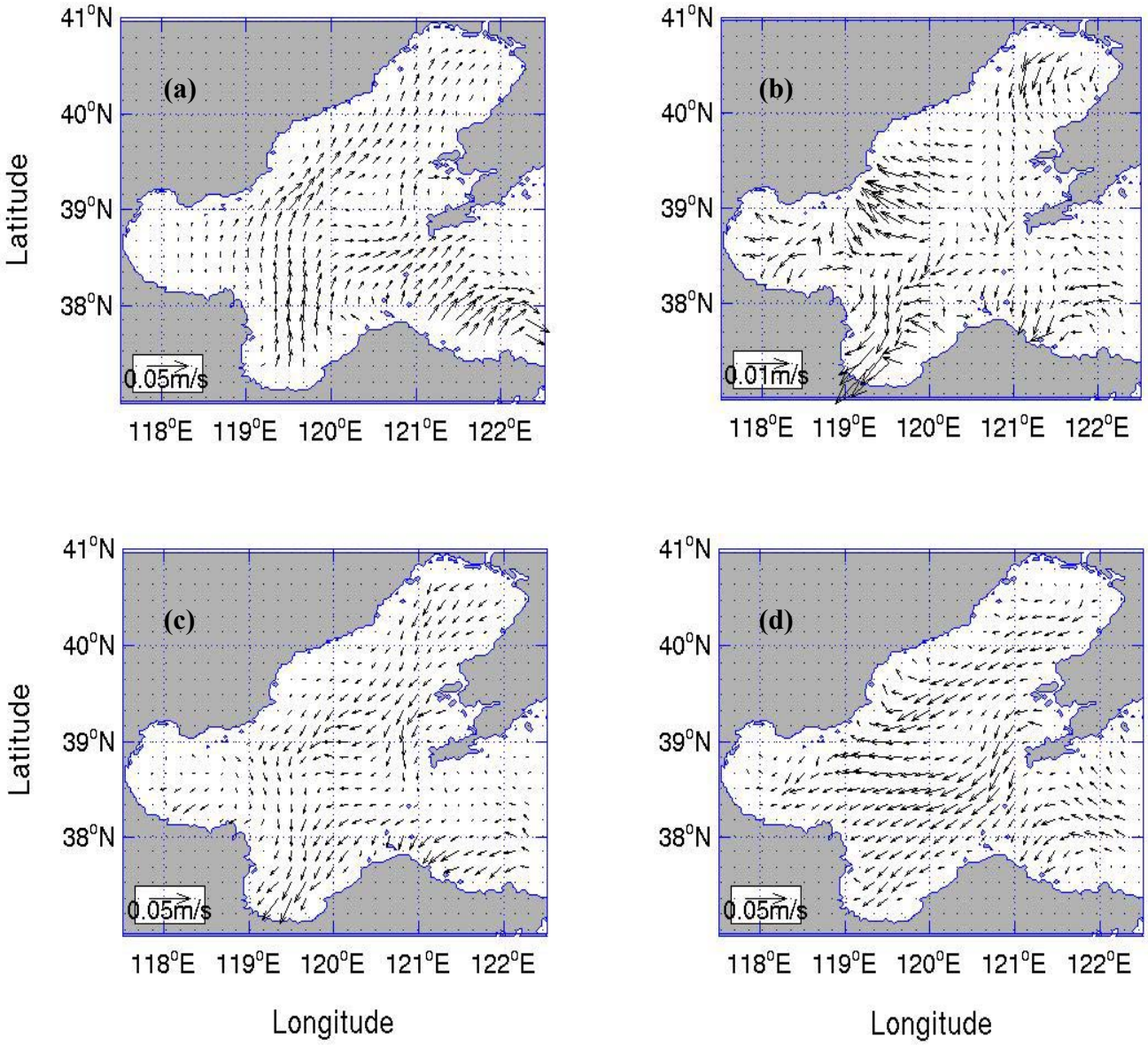

Figure 43. Velocity difference (Run-1 minus Run-3) at the bottom on (a) January 15, (b) April 15, (c) July 15 and (d) October 15, 2000.

B. EFFECTS ON TEMPERATURE

The temperature difference (Run-1 minus Run-3) ΔT represents the warming ($\Delta T > 0$) or cooling ($\Delta T < 0$) effect of the surface wind stress. This effect (Figures 44-46) is not as strong as the effect of the surface heat and moisture fluxes (Figures 31-33). There is not much difference in ΔT values at the surface, mid-depth (20 m), and bottom on January 15 and October 15, 2000. Nevertheless, there are differences in ΔT values at the surface, mid-depth (20 m), and bottom on April 15 and July 15, 2000.

The temporal evolution of ΔT is depicted as follows. On January 15, 2000, ΔT is positive in the central BS basin and negative (in mesoscale) in the surroundings. On April 15, 2000, BS is dominated by weak cooling with three cooling centers [southern Bohai Strait (~ -1.5^{o}C), northern Bohai Gulf (~ -1.7^{o}C), and Laizhou Bay (~ -0.5^{o}C)] and several warming centers (around 0.5^{o}C) at the gulfs. On July 15, 2000, the wind effect warms the head of Liaodong Gulf and Bohai Gulf slightly (ΔT ~ 0.5°C) and cools the deep-water region such as the central basin and western Bohai Strait (ΔT ~ -2^{o}C). On October 15, 2000, the BS is dominated by very small values of ΔT. The mid-depth (Figure 45) and the bottom (Figure 46) horizontal plots have the same structure of the surface plots, except for April and July. In April, Bohai Gulf is warmed at the surface, but is cooled at the mid-depth and the bottom. In July, there are some differences between the surface plots and the mid-depth and bottom fields.

The vertical dependence of ΔT is represented by zonal (Figure 47) and meridional (Figure 48) cross-sections. In the winter (Figures 47a and 48a), the cooling and warming effects of the wind forcing are vertically uniform. This warming effect occurs at the shallow regions. On April 15, 2000 (Figures 47b and 48b), the small warming or cooling effect of the wind stress is in general vertically uniform. The spot near the Bohai Gulf presents cooling effect at the surface and warming effect at the sub-surface. In the summer (Figures 47c and 48c), the warming and cooling effects are not vertically uniform. At the surface, the cooling effect is commonly found. Right below the surface, there is a warming effect of the wind forcing. This season represents the strongest wind effect over the temperature. On October 15, 2000 (Figures 47d and 48d),

the cooling and warming effects are vertically uniform. The wind effect during this season decreases.

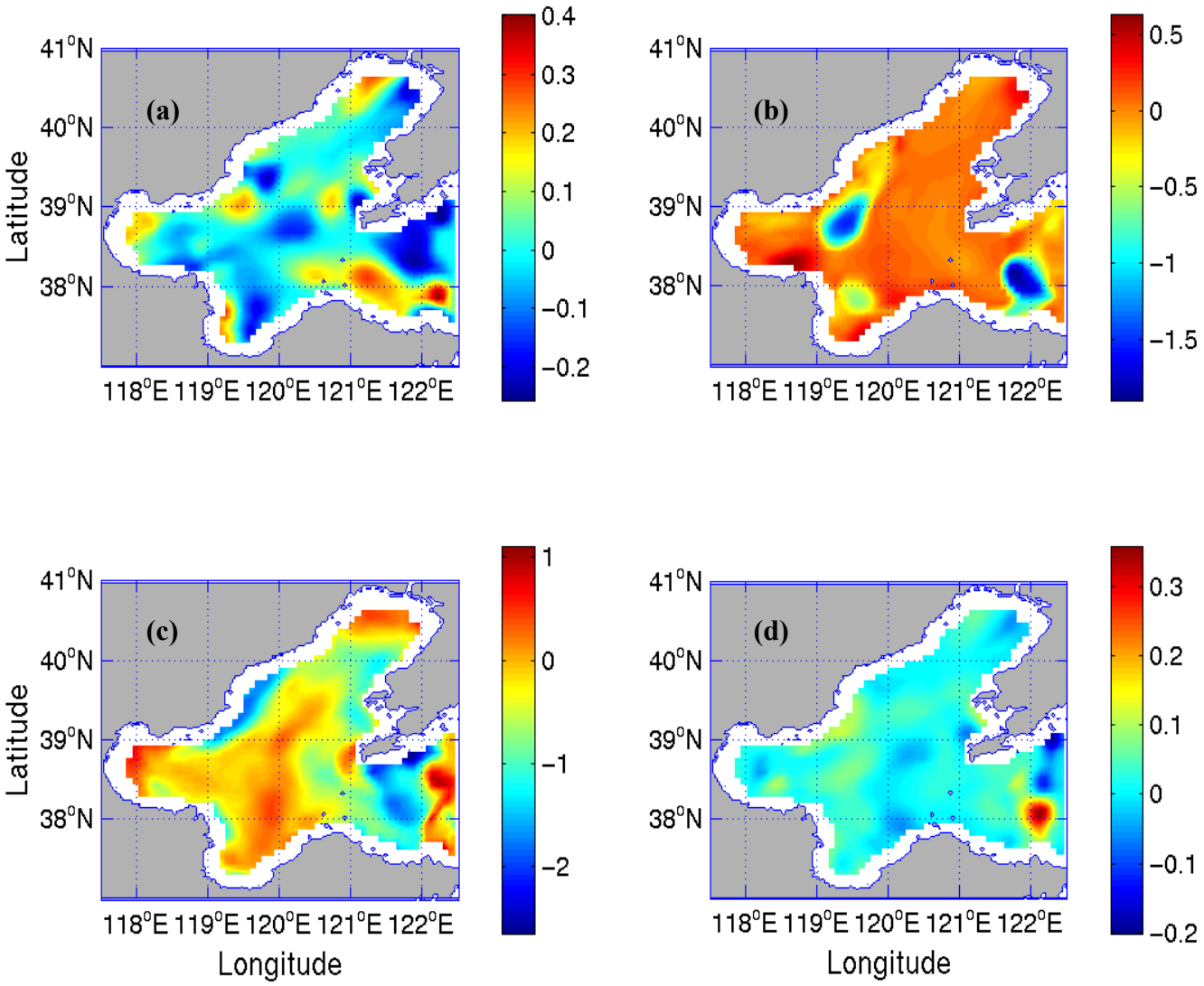

Figure 44. Temperature difference (°C) field (Run-1 minus Run-3) at the surface on (a) January 15, (b) April 15, (c) July 15 and (d) October 15, 2000.

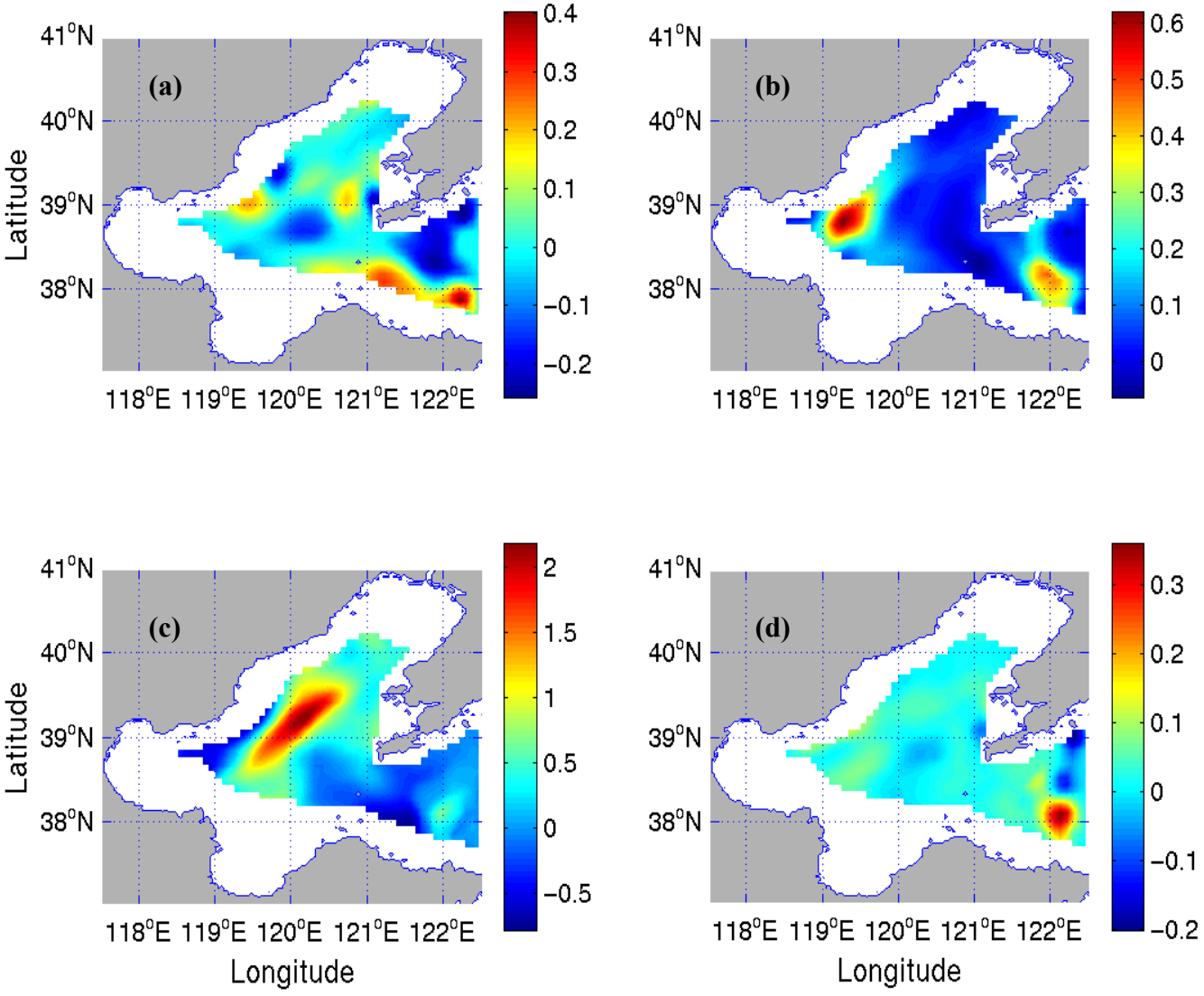

Figure 45. Temperature difference (°C) field (Run-1 minus Run-3) at 20 m depth on (a) January 15, (b) April 15, (c) July 15 and (d) October 15, 2000.

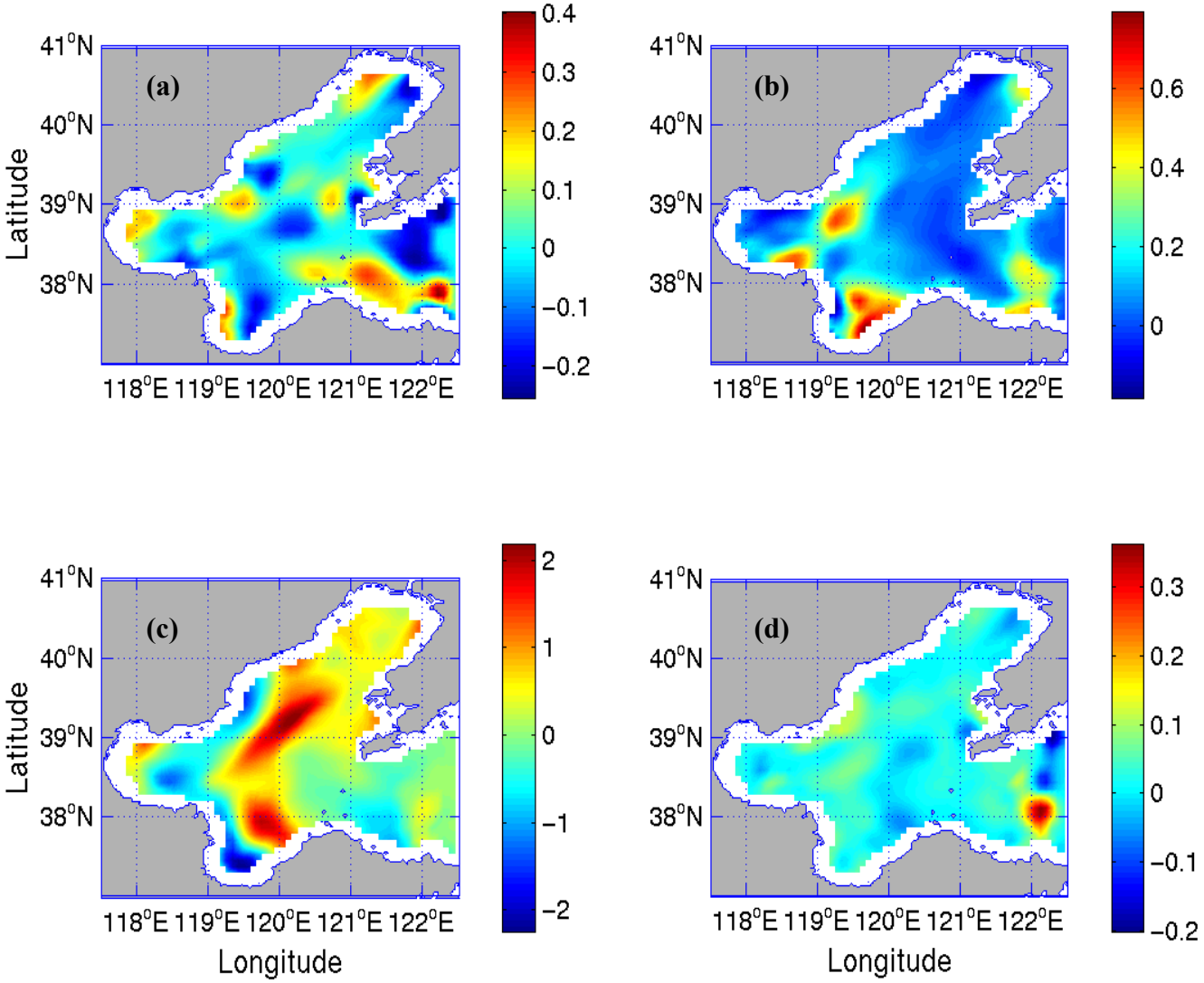

Figure 46. Temperature difference (°C) field (Run-1 minus Run-3) at the bottom on (a) January 15, (b) April 15, (c) July 15 and (d) October 15, 2000.

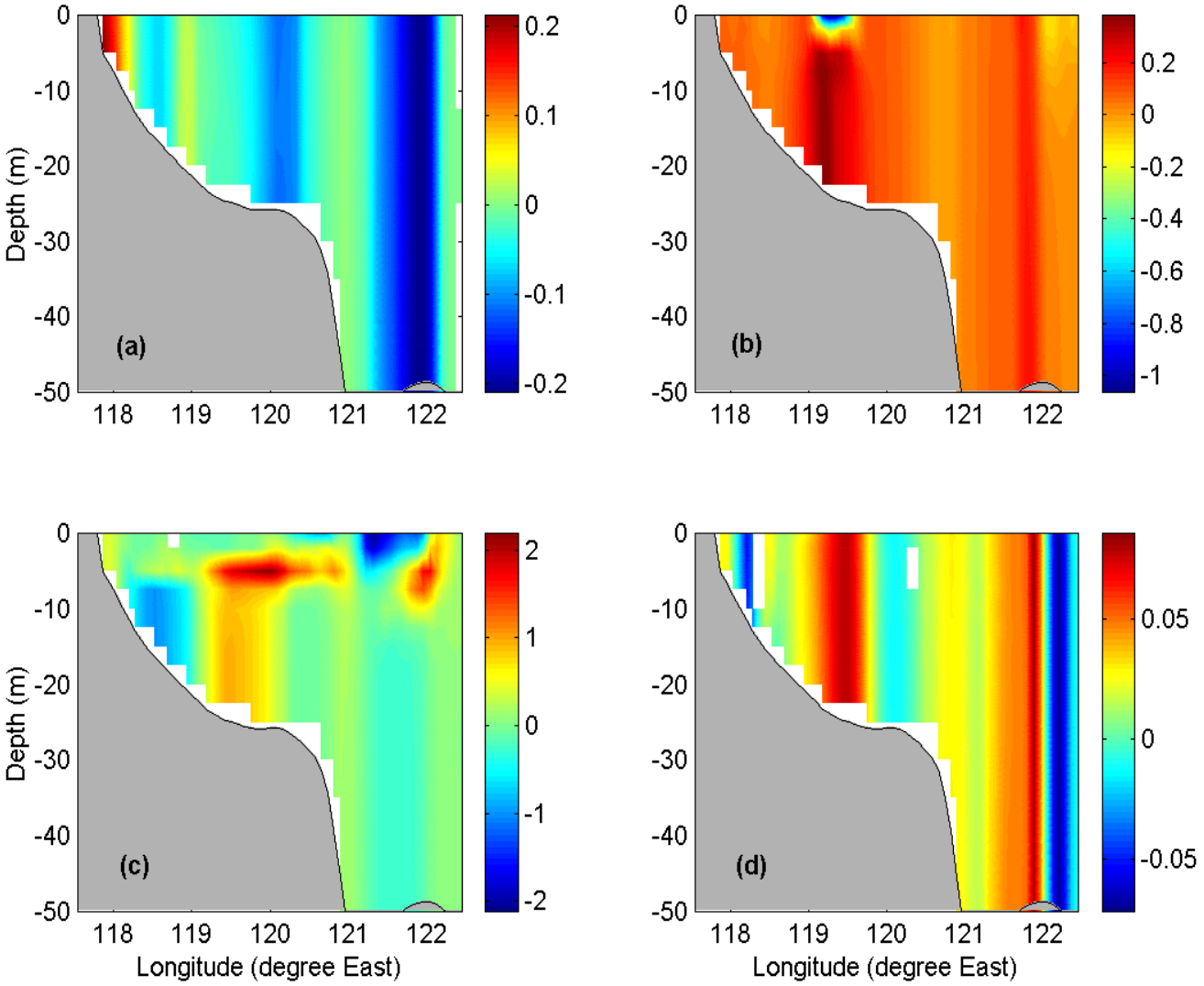

Figure 47. Zonal cross-section of the temperature (^{o}C) difference (Run-1 minus Run-3) along 38°35.52'N on (a) January 15, (b) April 15, (c) July 15 and (d) October 15, 2000.

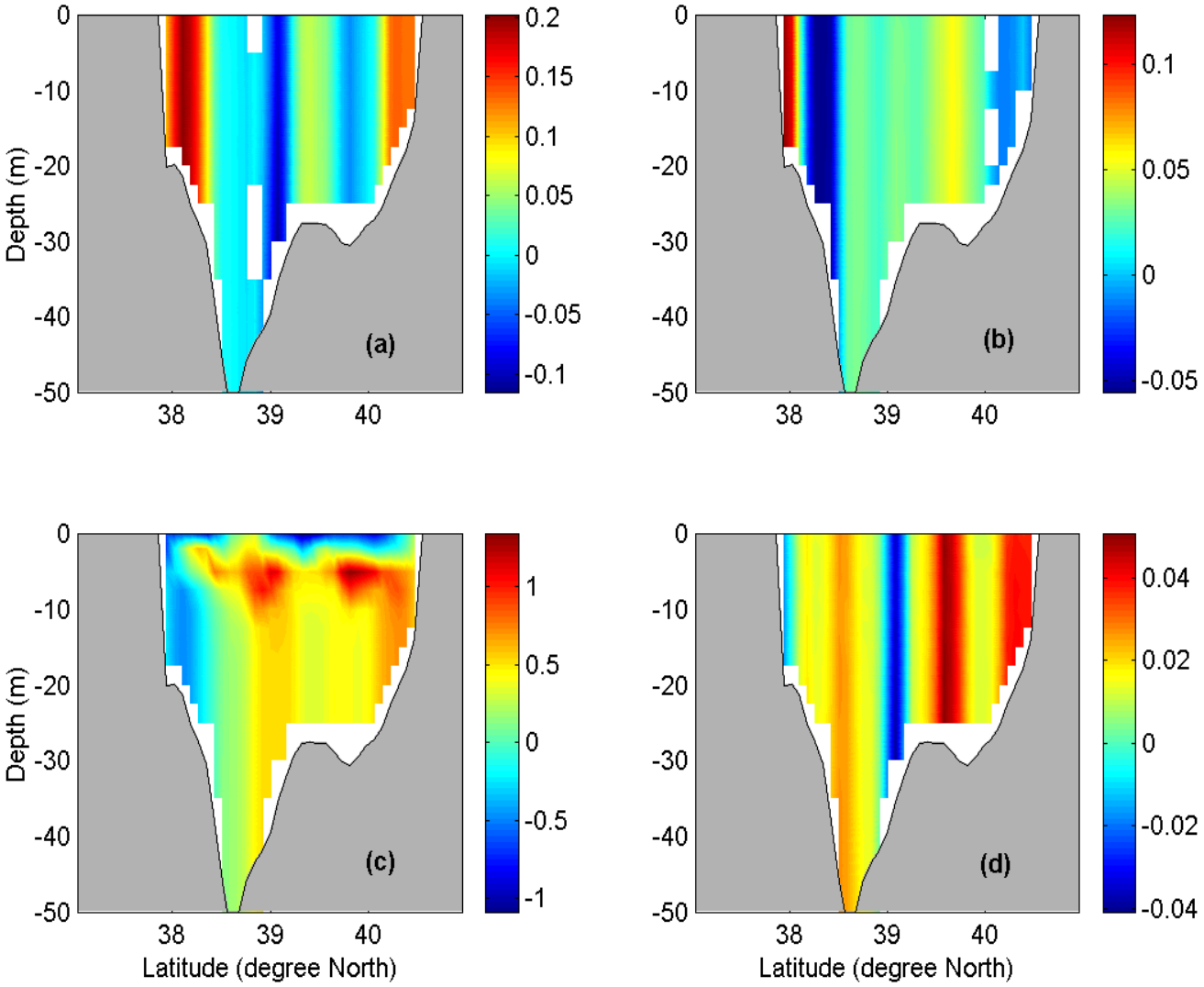

Figure 48. Meridional cross-section of the temperature (^{o}C) difference (Run-1 minus Run-3) along 121°01.5'E on (a) January 15, (b) April 15, (c) July 15 and (d) October 15, 2000.

C. EFFECTS ON SALINITY

The salinity difference (Run-1 minus Run-3) ΔS represents increased salinity ($\Delta S > 0$) or freshening ($\Delta S < 0$) effect of the surface wind stress (Figures 49-51). The salinity difference range increases throughout the year. The effect is quite weak near the eastern boundary in Bohai Strait. There is not much difference in ΔS values at the surface, mid-depth (20 m), and bottom on January 15, April 15 and October 15, 2000. There are, however, differences in ΔS values at the surface, mid-depth (20 m), and bottom on July 15, 2000. The absolute salinity differences are smaller than the differences found in the "non-fluxes" case, which indicates that the wind effect has less influence over the salinity field.

The temporal evolution of ΔS is described as follows. On January 15, 2000, two spots, one less saline of negative values (< -0.2 psu) and other more saline of positive differences (> 0.2 psu), are situated at the central basin. On April 15, 2000, the spot of negative (less saline) values moves to the west coast and spreads out with values around -0.6 psu. The spot with positive differences (more saline) maintains its position, but also spreads out with ΔS about 0.4 psu. At the heads of Bohai Gulf and Laizhou Bay, the water becomes less saline (~ -0.3 psu) due to the wind effect. On July 15, 2000, the wind stress has the effect of producing a less saline tongue at the west coast, spreaded northeast- and southwestward (> -1 psu). Near the open boundary and at the middle of the central basin, the water is saltier due to the wind stress (> 0.2 psu). On October 15, 2000, the absolute ΔS decreases in most part of the BS. The less and more saline regions weaken. At the head of the Bohai Gulf, the wind forcing increases the salinity, while at the head of the Laizhou Bay the wind stress decreases the salinity.

The vertical dependence of ΔS is represented by zonal (Figure 52) and meridional (Figure 53) cross-sections. In the winter (Figures 52a and 53a), the surface wind stress affects (salting or freshening) the whole water column. It salts the central BS (Figure 52a) and Liadong Gulf (Figure 53a) and freshens the surroundings. In the summer (Figures 52c and 53c), the wind effect on salinity is not vertically uniform. At the surface layer, the wind forcing decreases the salinity. The salinity has the tendency to increases with

depth. At the northern part of the Bohai Strait and in the deeper region, the wind effect increases the salinity. On October 15, 2000 (Figures 52d and 53d), the wind effect over the salinity field is vertically uniform. The range of ΔS decreases and the wind effect on salinity weakens.

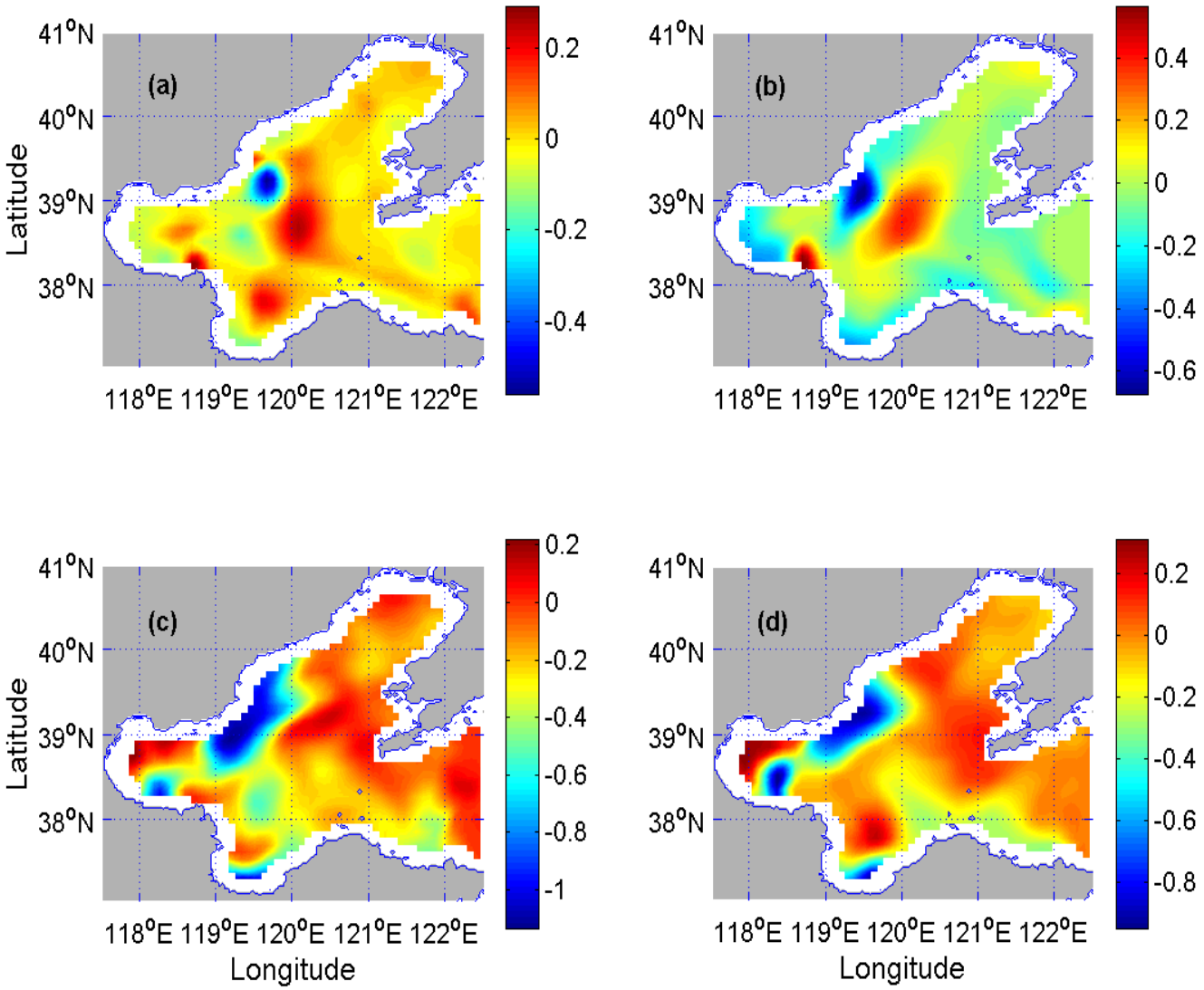

Figure 49. Salinity difference (psu) field (Run-1 minus Run-3) at the surface on (a) January 15, (b) April 15, (c) July 15 and (d) October 15, 2000.

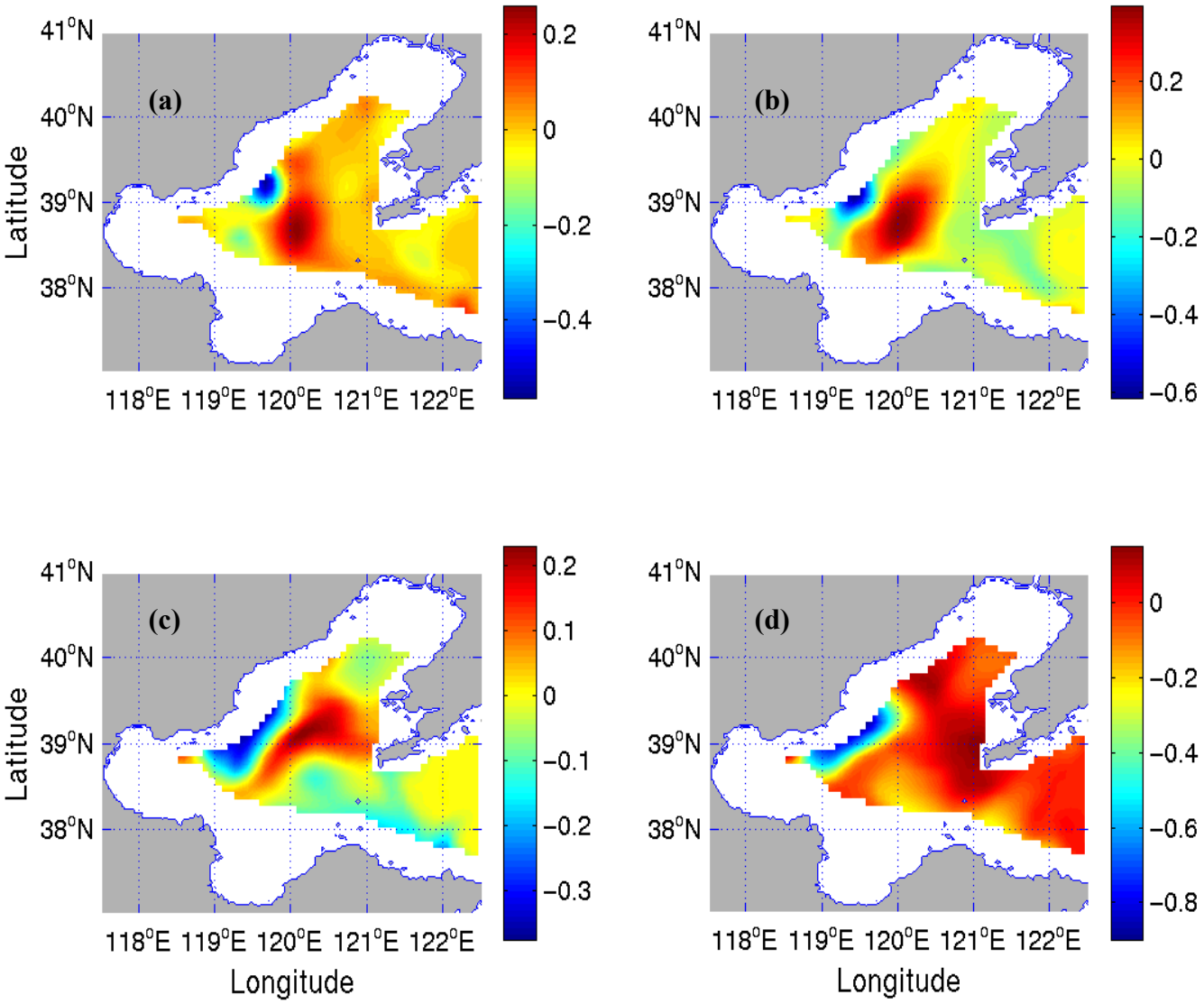

Figure 50. Salinity difference (psu) field (Run-1 minus Run-3) at 20 m depth on (a) January 15, (b) April 15, (c) July 15 and (d) October 15, 2000.

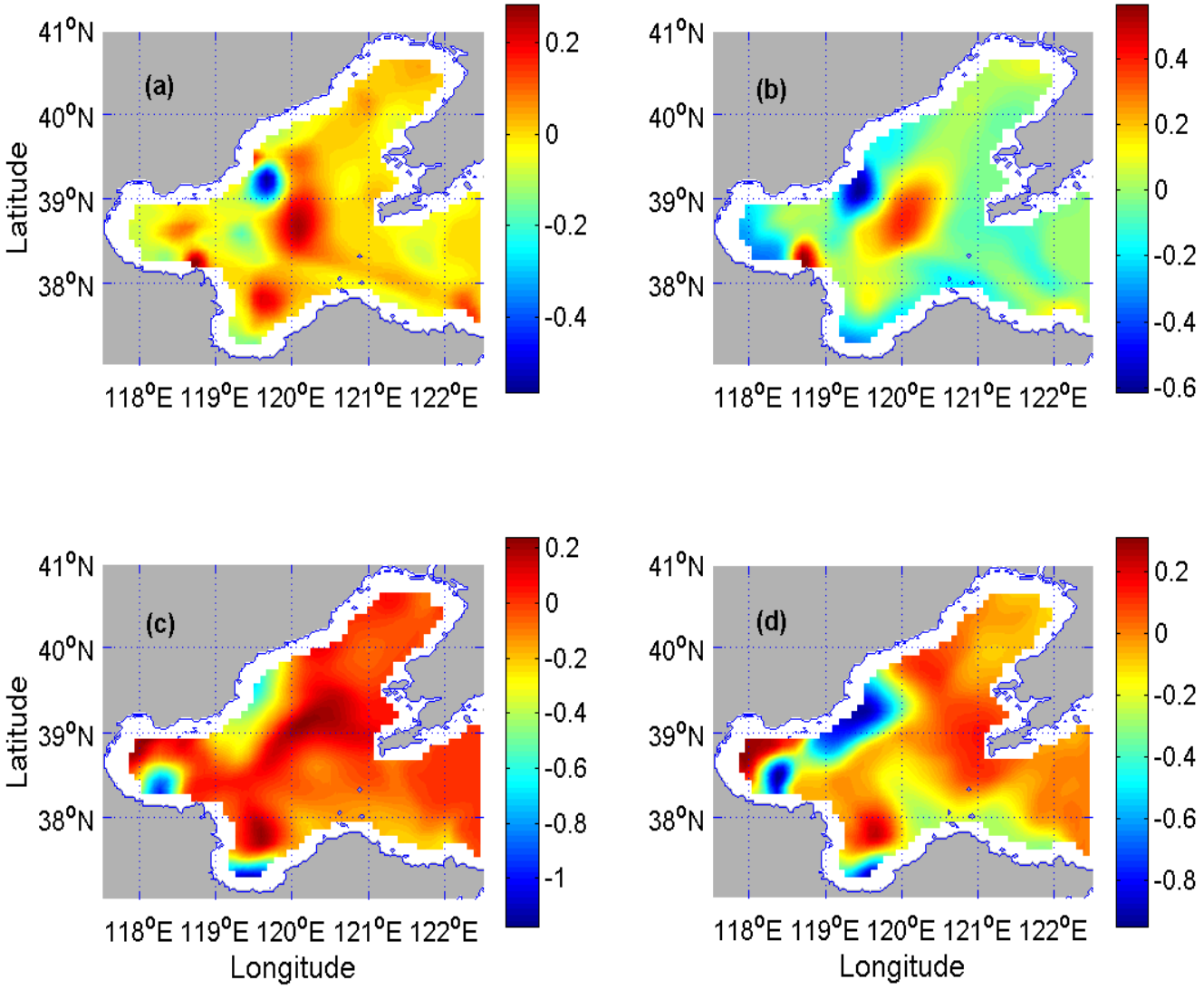

Figure 51. Salinity difference (psu) field (Run-1 minus Run-3) at the bottom on (a) January 15, (b) April 15, (c) July 15 and (d) October 15, 2000.

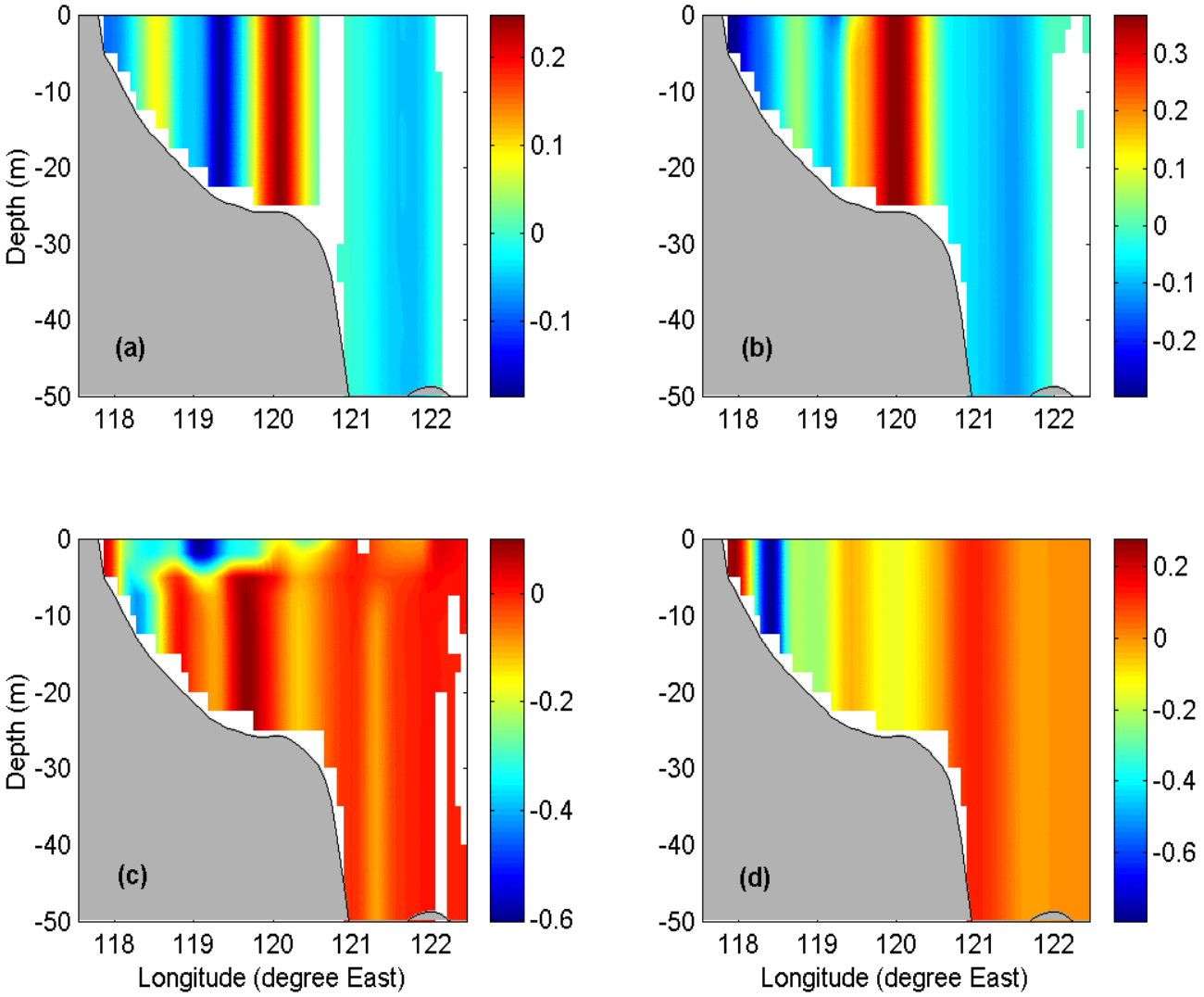

Figure 52. Zonal cross-section of the salinity (psu) difference (Run-1 minus Run-3) along 38°35.52'N on (a) January 15, (b) April 15, (c) July 15 and (d) October 15, 2000.

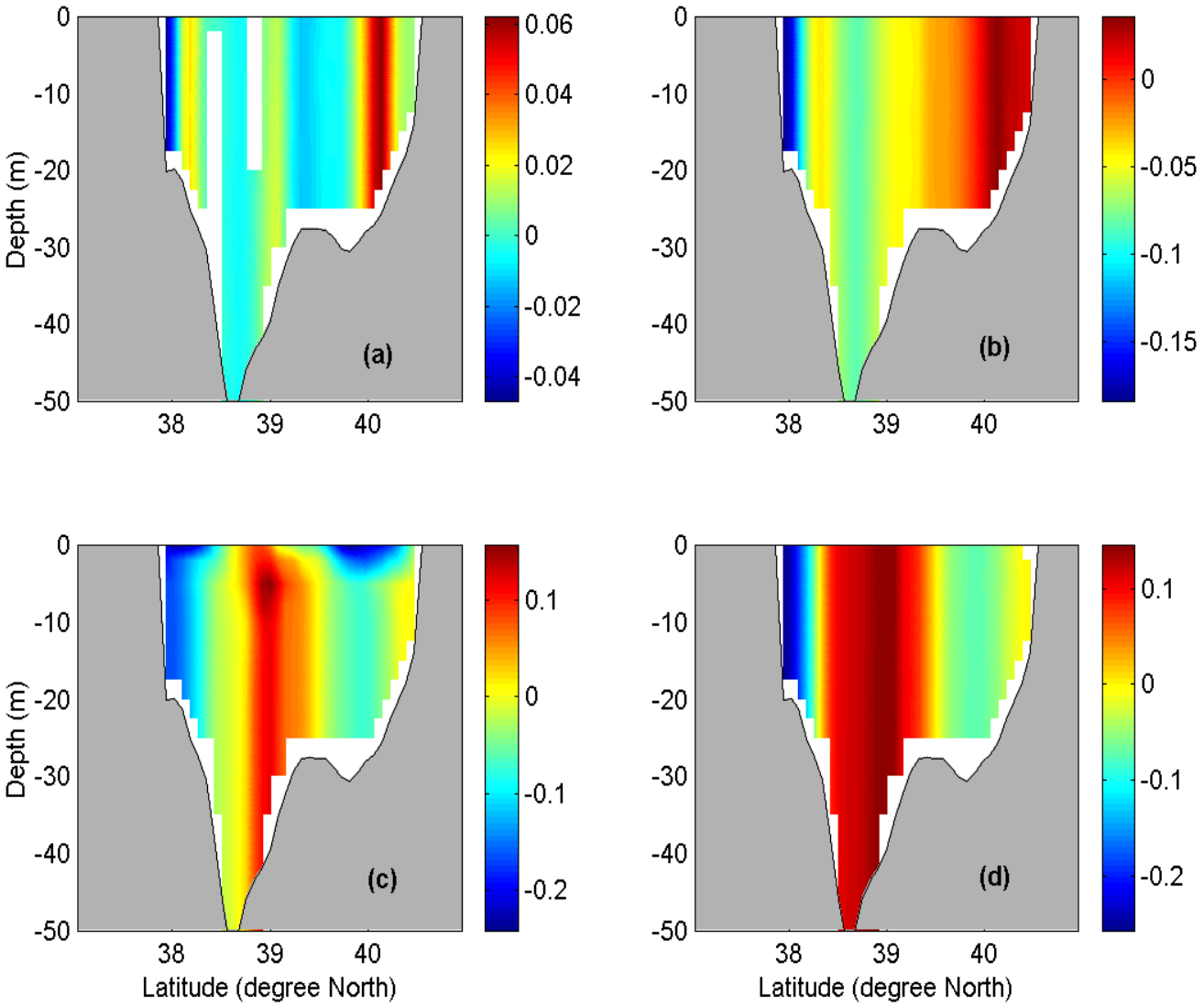

Figure 53. Meridional cross-section of the salinity (psu) difference (Run-1 minus Run-3) along 121°01.5'E on (a) January 15, (b) April 15, (c) July 15 and (d) October 15, 2000.

VII. EFFECTS OF TIDES

In the third sensitivity study, the tidal motion was removed. Otherwise, the same parameters as the control run were used. The difference (Run-1 minus Run-4) of the model output (velocity, temperature, and salinity) indicates the tidal effect.

A. EFFECTS ON CIRCULATION

The simulated velocity difference fields (Figures 54-56) show the effects of tides on the circulation of the BS. A comparison between Figures 54-56 and Figures 11-13 leads to identification of the tidal effect. If the directions of the velocity vectors are nearly the same in Figure 54-56 as in Figures 11-13 for the corresponding depths and seasons, the tidal effect enhances the circulation. If the directions of the velocity vectors are opposite in Figure 54-56 as in Figures 11-13 for the corresponding depths and seasons, the tidal effect weakens the circulation. Thus, the tidal effects on the circulation are identified as follows. Throughout the year, although the tides enhance the currents at the northern part of the Bohai Strait, their effect on the surface currents is much weaker than the wind effect. In the winter (Figures 54a, 55a, and 56a), the tides enhance the surface currents in the central basin, the Bohai Gulf, and the Laizhou Bay, and reduce the anticyclonic eddy in Liaodong Gulf. In the spring (Figures 54b, 55b, and 56b), the tides enhance the surface and mid-depth circulations in the northern BS, and weaken the mid-depth circulation in the southern BS and the bottom circulation. In the summer (Figures 54c, 55c, and 56c), the tides enhance the surface circulation in the southern Bohai Strait and the western part of the central basin, and weaken the circulation in the central basin at the mid-depth and in Liaodong Gulf at the bottom. In the fall (Figures 54d, 55d, and 56d) at the surface, the tides enhance the currents in the central basin and in Laizhou Bay, weaken the currents in Liaodong Gulf, and less affect the currents in the southern part of BS. At the bottom, the tides enhance the circulation in Liaodong Gulf, in Laizhou Bay and at the west coast of BS.

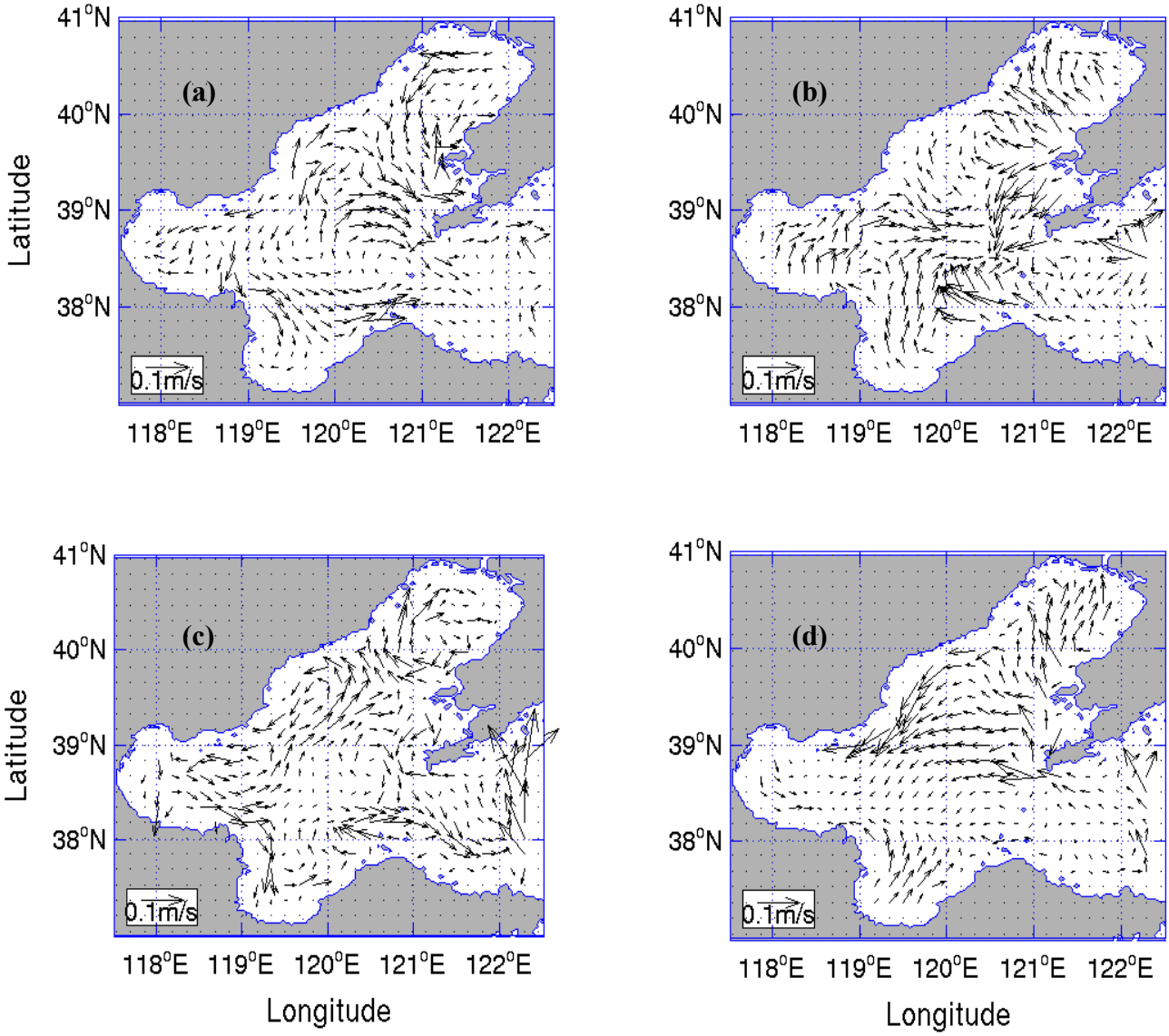

Figure 54. Velocity difference (Run-1 minus Run-4) at the surface on (a) January 15, (b) April 15, (c) July 15 and (d) October 15, 2000.

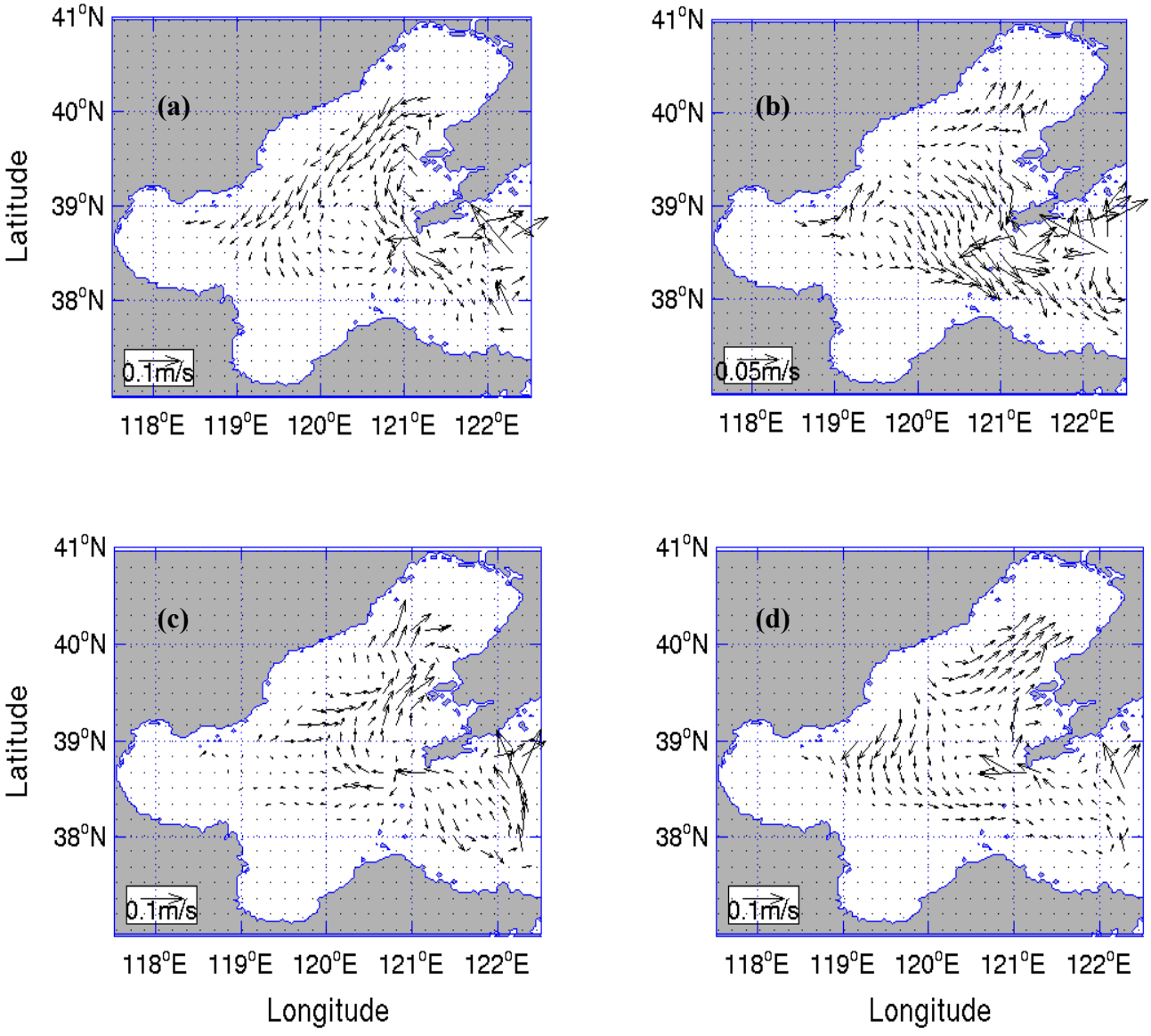

Figure 55. Velocity difference (Run-1 minus Run-4) at 20 m depth on (a) January 15, (b) April 15, (c) July 15 and (d) October 15, 2000.

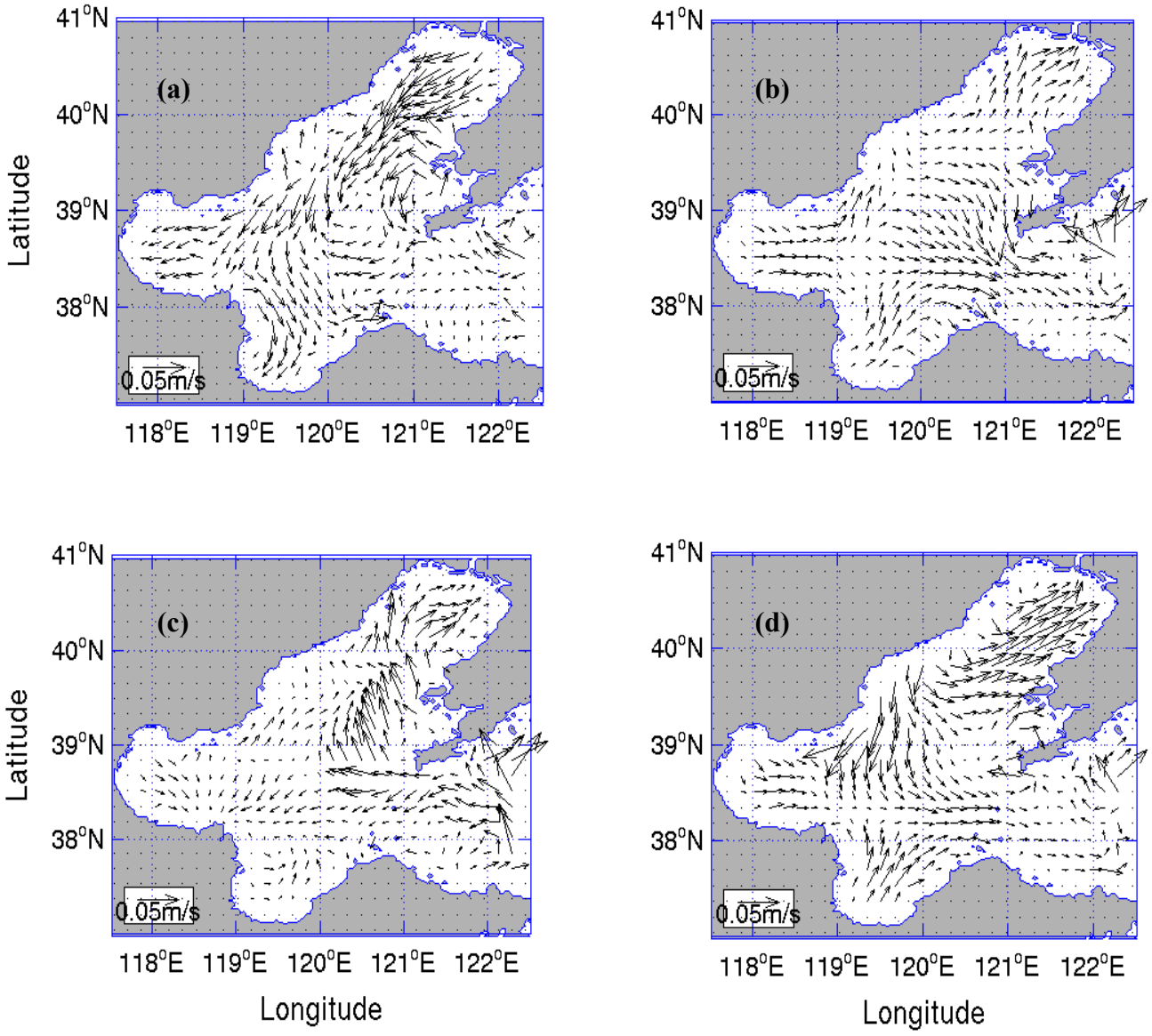

Figure 56. Velocity difference (Run-1 minus Run-4) at the bottom on (a) January 15, (b) April 15, (c) July 15 and (d) October 15, 2000.

B. EFFECTS ON TEMPERATURE

The major effect of the tides is to cool (warm) the BS in the winter (summer) for the whole water column (Figures 57-59) since the temperature difference (ΔT) is negative (positive) over the entire BS basin in the winter (summer). This effect becomes stronger at the gulfs and at Laizhou Bay due to the shallow depth, and quite weak near the eastern boundary in Bohai Strait. There is not much difference in the ΔT values at the surface, mid-depth (20 m), and bottom on October 15, 2000. Nevertheless, there is evident differences in ΔT values at the surface, mid-depth (20 m), and bottom on January 15, April 15 and July 15, 2000. The range of ΔT is wider than the non-wind case, but smaller than the non-fluxes experiment.

The temporal evolution of ΔT is depicted as follow. On January 15, 2000, ΔT has both positive and negative values, but the BS basin shows no differences. At the head of Liaodong Gulf, the tides are responsible for a cooling effect of about -0.5°C, but have also warming features (~ 0.5°C). The head of Bohai Gulf presents a cooling effect as well, but its entrance shows a warm spot. The deeper region near the Bohai Strait has cooling. At the central basin, there are two pair of cooling and warming spots. A range of ΔT (-0.2°C to 0.2°C) dominates the BS. At the mid-depth, the difference field has some changes compared with the surface field. On April 15, 2000, at the head of the gulfs and the western central basin, there is warming due to the tidal effect, which is more than 0.2°C. At the north part of the central basin, there is a large region that has a cooling effect due to the tides. Bohai Strait is dominated by the cooling effect as well. In the deeper region and east of Bohai Strait, there is a strong and warming spot with ΔT of about 0.5°C. At mid-depth, there is a small amount of warming in the central basin and in the deeper region near Bohai Strait. At the bottom, the ΔT field presents the warming effect in the central basin and at the spot near the open boundary. On July 15, 2000 the range of ΔT increases, which indicates enhancement of tidal mixing. The west coast of the central basin and the head of Bohai Gulf, suffer the strongest warming due to tides. Near the open boundary and at the south, there is a cooling spot with ΔT smaller than -5°C. The east coast of the BS and the Bohai Strait has a cooling effect. At the mid-depth, the tides are responsible for warming the central basin. At the bottom, the entire BS

presents a warming effect by the tidal mixing, but this is affected less in shallow waters. On October 15, 2000, there is a dominance of warming effects in the BS. Near the eastern boundary, a strong and cooling region is present with ΔT smaller than -1°C.

The vertical dependence of ΔT is represented by zonal (Figure 60) and meridional (Figure 61) cross-sections. The plots ratify that there is some stratification in winter, spring and summer. In the winter (Figures 60a and 61a), at the gulfs there is a spot warming at the surface and cooling at the bottom. On April 15, 2000 (Figures 60b and 61b), and on July 15, 2000 (Figures 60c and 61c), there is cooling at the surface layer and warming in the deeper with the absolute value of ΔT increasing with depth. On October 15, 2000 (Figures 60d and 61d), away from the open boundary, the tidal effect over the temperature is vertically uniform.

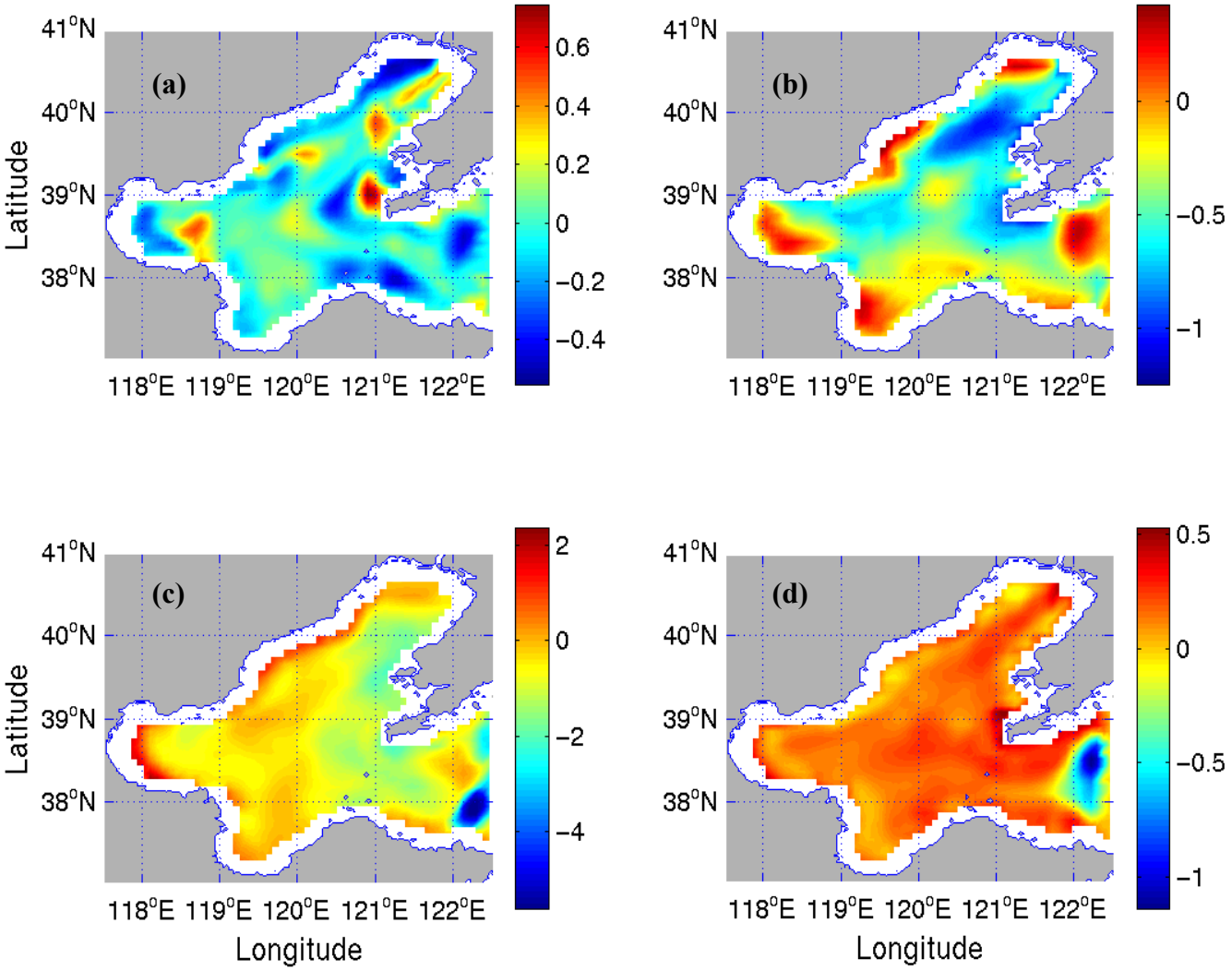

Figure 57. Temperature difference (°C) field (Run-1 minus Run-4) at the surface on (a) January 15, (b) April 15, (c) July 15 and (d) October 15, 2000.

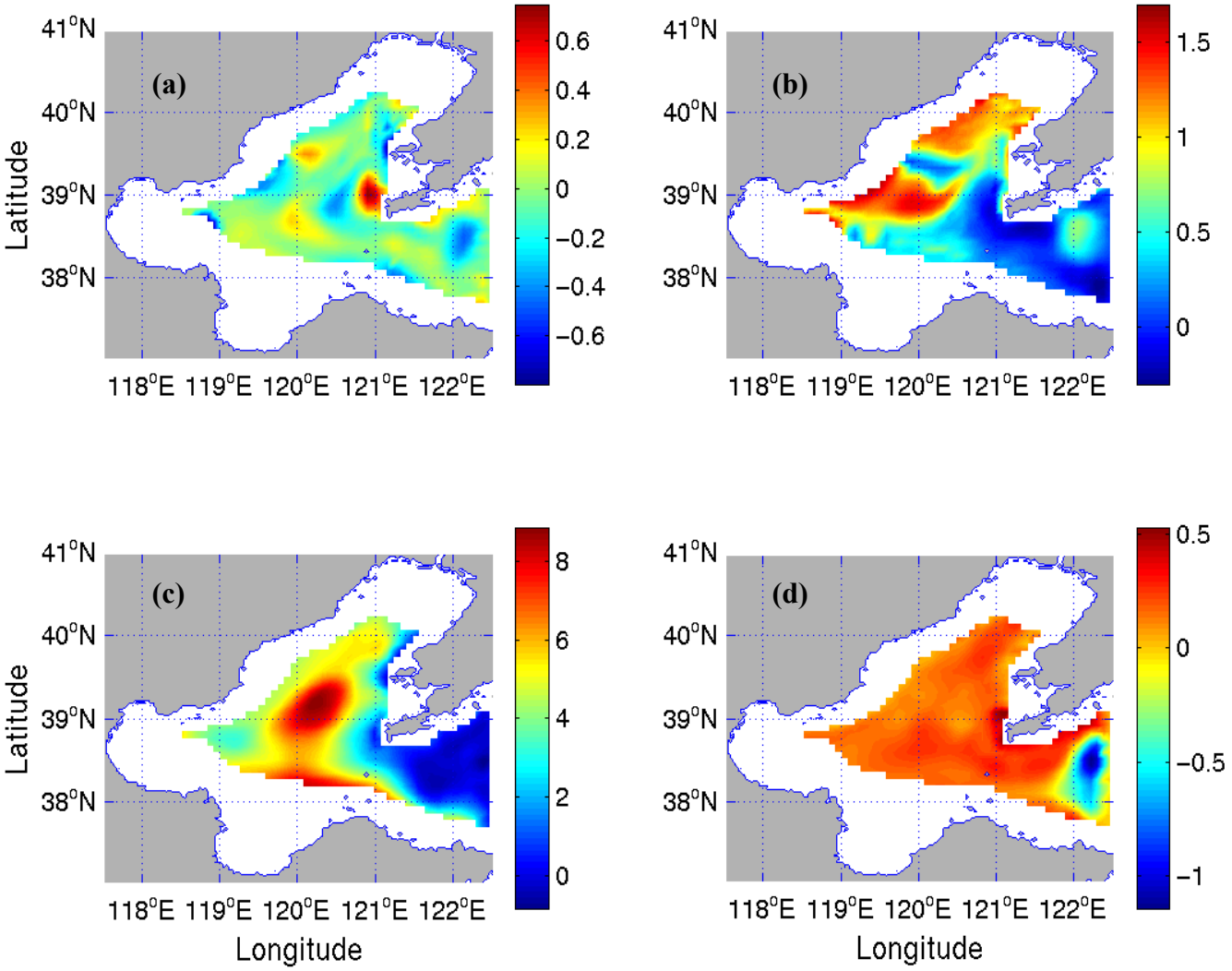

Figure 58. Temperature difference (°C) field (Run-1 minus Run-4) at 20 m depth on (a) January 15, (b) April 15, (c) July 15 and (d) October 15, 2000.

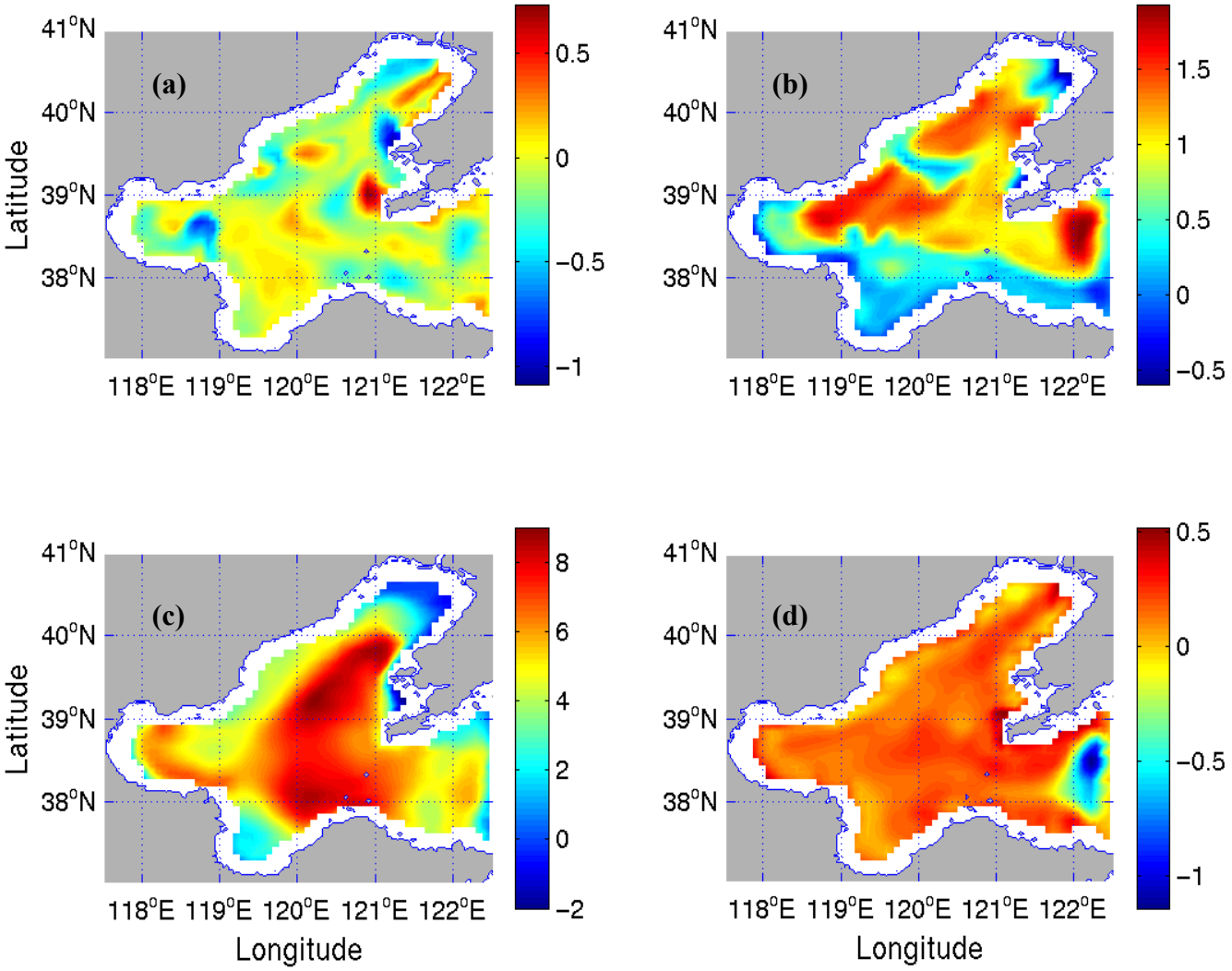

Figure 59. Temperature difference (°C) field (Run-1 minus Run-4) at the bottom on (a) January 15, (b) April 15, (c) July 15 and (d) October 15, 2000.

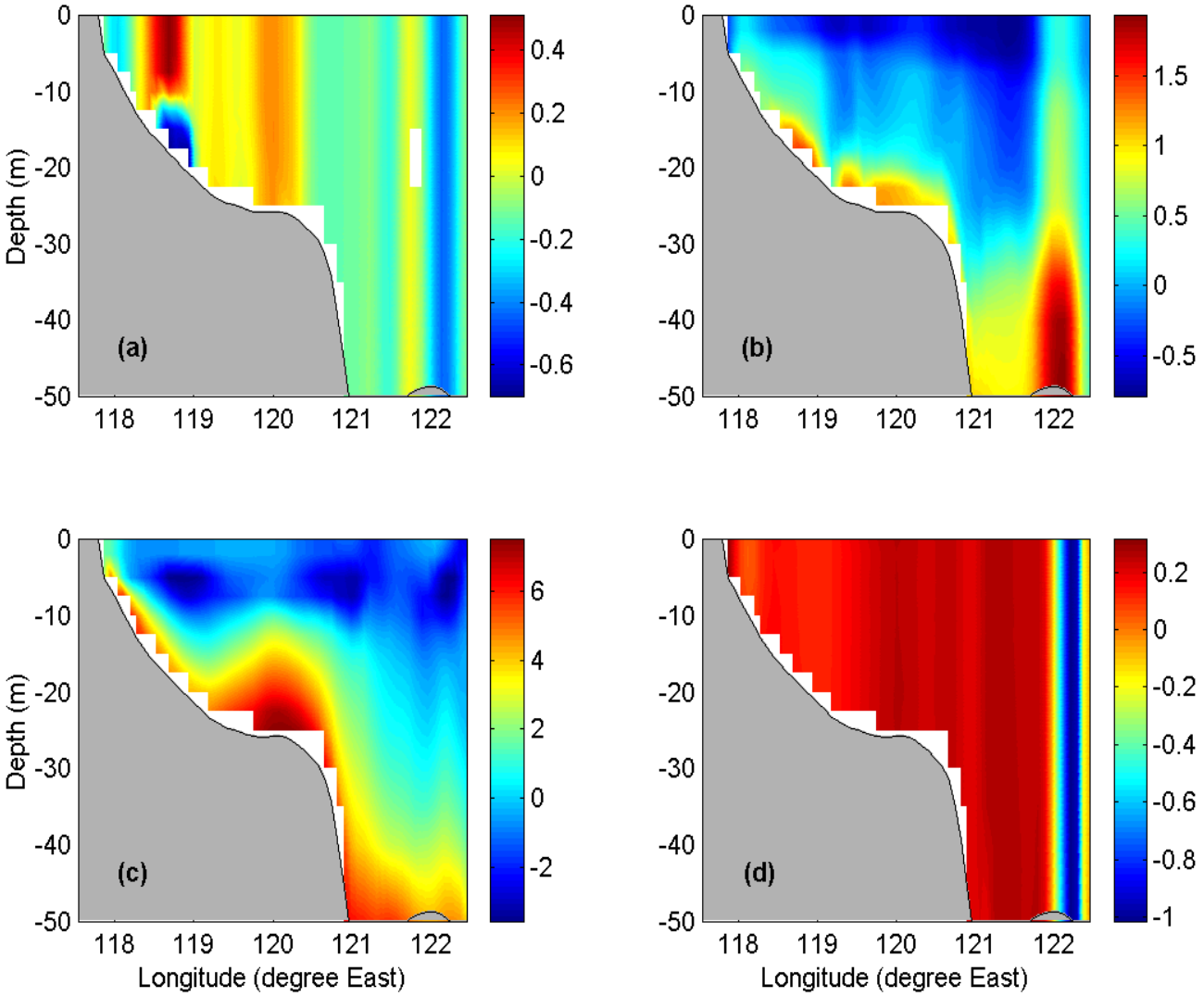

Figure 60. Zonal cross-section of the temperature (^{o}C) difference (Run-1 minus Run-4) along 38°35.52'N on (a) January 15, (b) April 15, (c) July 15 and (d) October 15, 2000.

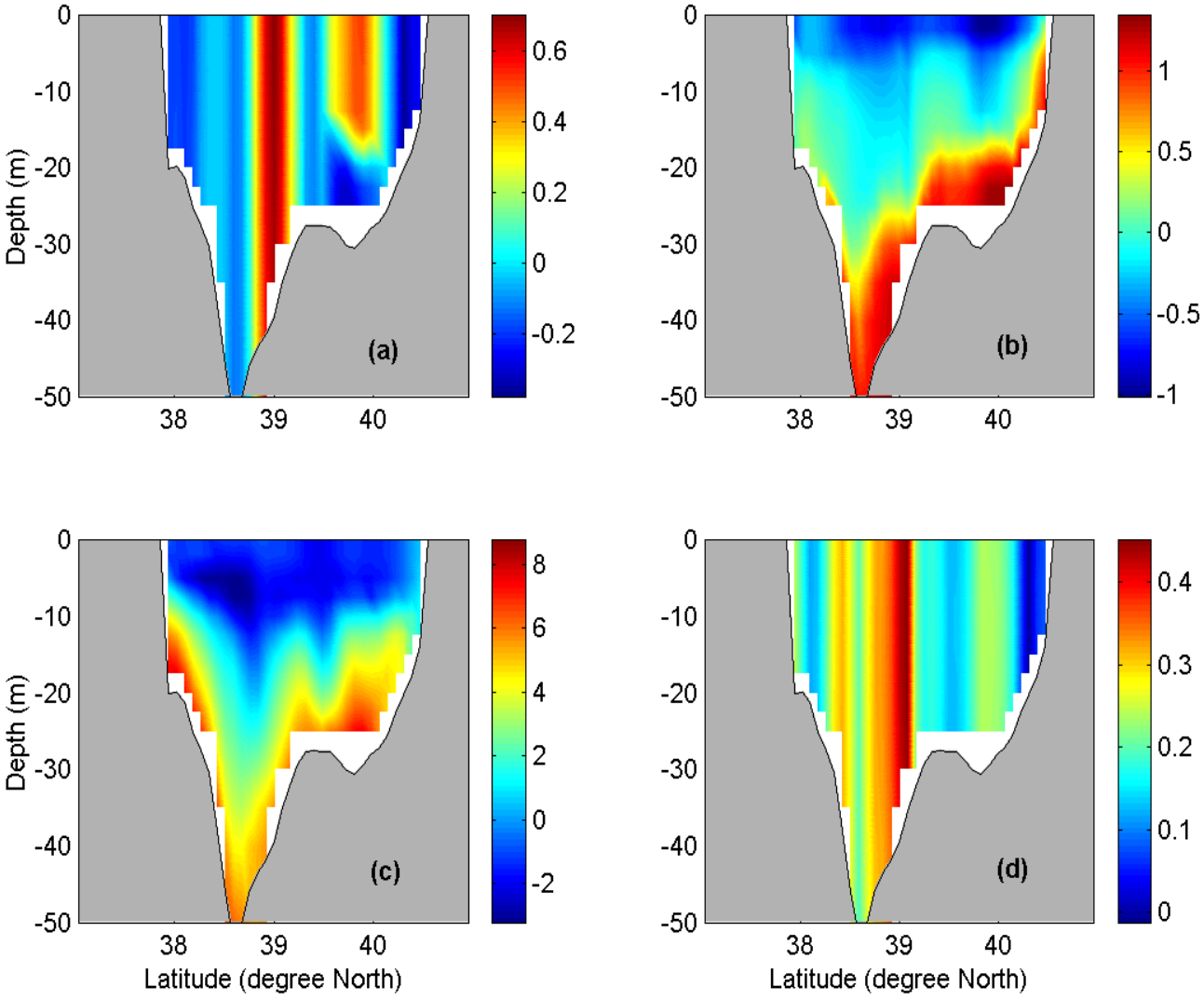

Figure 61. Meridional cross-section of the temperature (^{o}C) difference (Run-1 minus Run-4) along 121°01.5'E on (a) January 15, (b) April 15, (c) July 15 and (d) October 15, 2000.

C. EFFECTS ON SALINITY

The effect of tidal mixing over the salinity field is to increase the salinity in January and April, and to decrease the salinity in July and October (Figures 62-64). There is not much difference in ΔS values at the surface, mid-depth (20 m), and bottom on October 15, 2000. There are, however, evident differences in ΔS values at the surface, mid-depth (20 m), and bottom on January 15, April 15 and July 15, 2000. The salinity is more affected by the tidal mixing than the wind and surface thermohaline forcing in most seasons (a greater range of ΔS) except for the surface thermohaline forcing in October.

The temporal evolution of ΔS is described as follow. On January 15, 2000, most BS basin values of ΔS are between -0.2 and 0.2 psu. In the central basin, there is great variability, where the tides produce positive (more saline) and negative (less saline) ΔS. At the bottom, there are some different features compared with the surface field. On April 15, 2000, the tidal mixing is responsible for the increase of the salinity in the middle of the central basin more than January 15 and for the decrease of the salinity in the southern part of the central basin. At mid-depth and at the bottom, there are some features different from the surface field. On July 15, 2000, the tidal mixing effect on the salinity is to decrease the values in the deeper region near the Bohai Strait, in the central basin and at the northern part of BS. At the head of Bohai Gulf, tidal mixing increases the salinity ($\Delta S \approx 1$ psu). At the mid-depth and at the bottom, the ΔS values indicate some differences from the surface field. On October 15, 2000, the tides increase the salinity at the Bohai Gulf more than on July 15. There is great variability during this season. At the Bohai Strait, the salinity increases due to the tidal forcing. At mid-depth and at the bottom, there is not much difference from the surface field.

The vertical dependence of ΔS is represented by zonal (Figure 65) and meridional (Figure 66) cross-sections. The tidal mixing is responsible for the increase of the salinity at Bohai Gulf. In the winter (Figures 65a and 66a), the effect of the tidal mixing over the salinity field is almost vertically uniform. At the entrances of the gulfs, there are two regions where the salinity at the surface is higher than on the bottom. On April 15, 2000 (Figures 65b and 66b), the ΔS, generally, increases slowly with depth due to the tidal

forcing. In the summer (Figures 65c and 66c), the salinity decreases at the surface layer and increases in the deeper layer due to the tides. On October 15, 2000 (Figures 65d and 66d), the tides affect the salinity vertical structure uniformly.

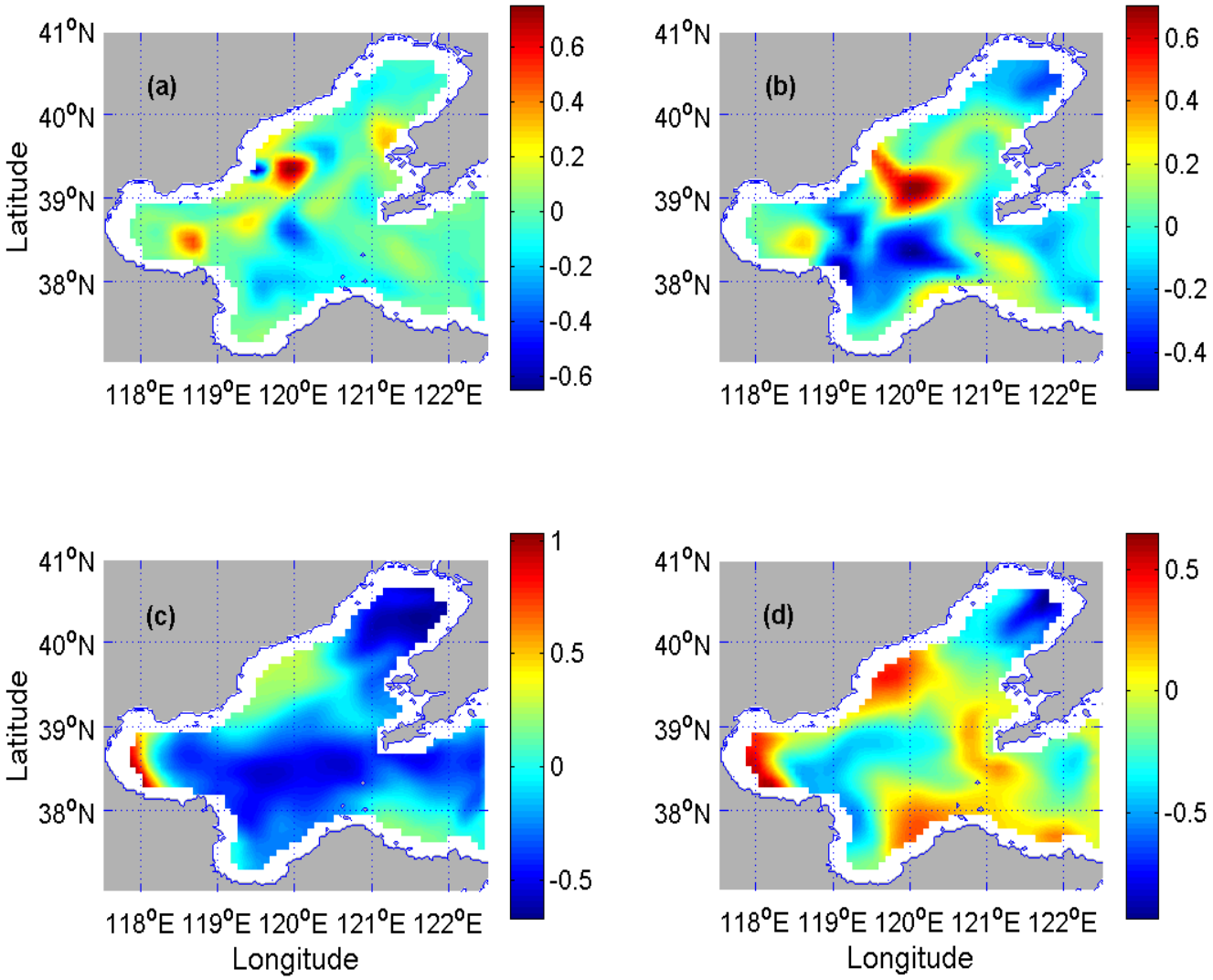

Figure 62. Salinity difference (psu) field (Run-1 minus Run-4) at the surface on (a) January 15, (b) April 15, (c) July 15 and (d) October 15, 2000.

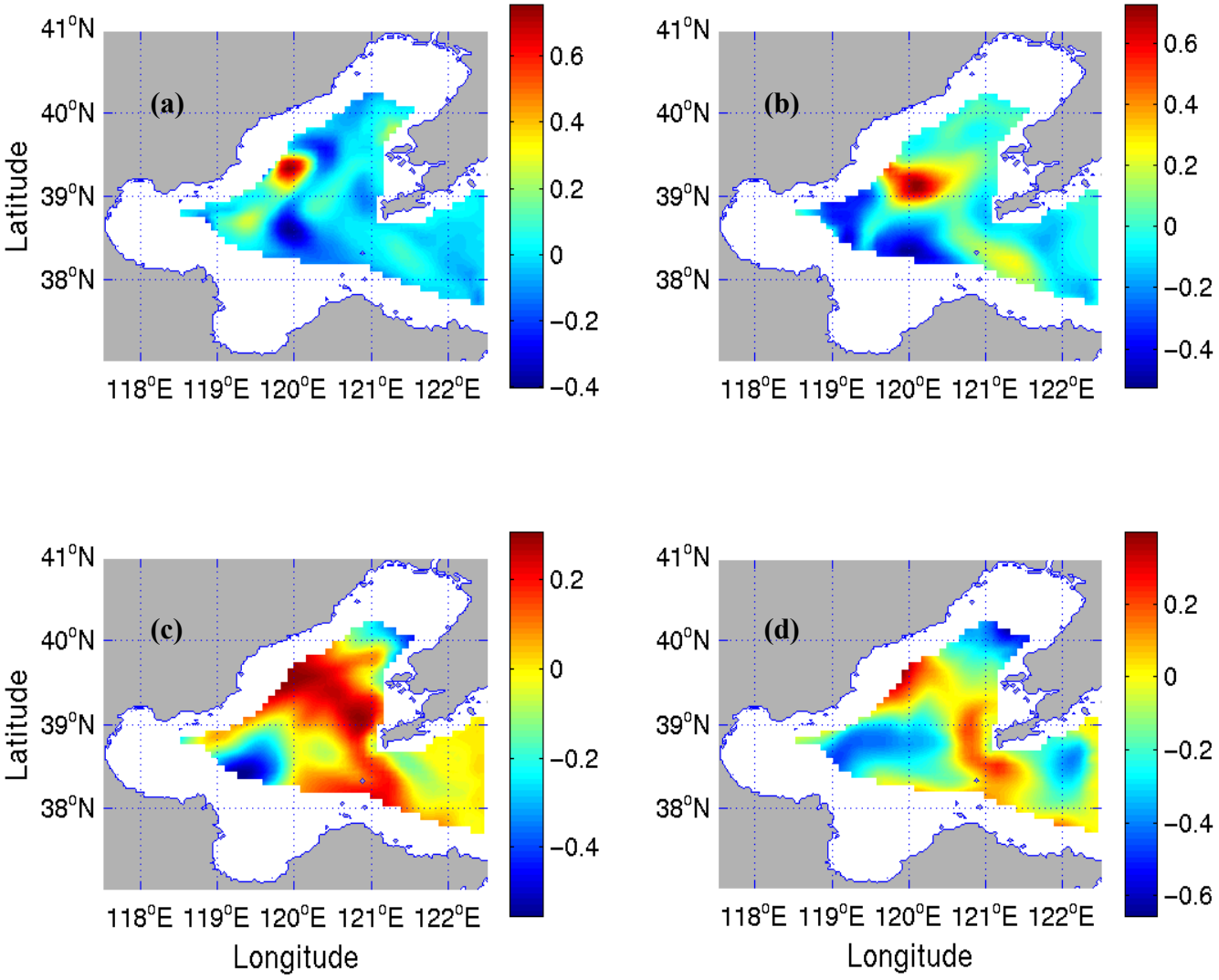

Figure 63. Salinity difference (psu) field (Run-1 minus Run-4) at 20 m depth on (a) January 15, (b) April 15, (c) July 15 and (d) October 15, 2000.

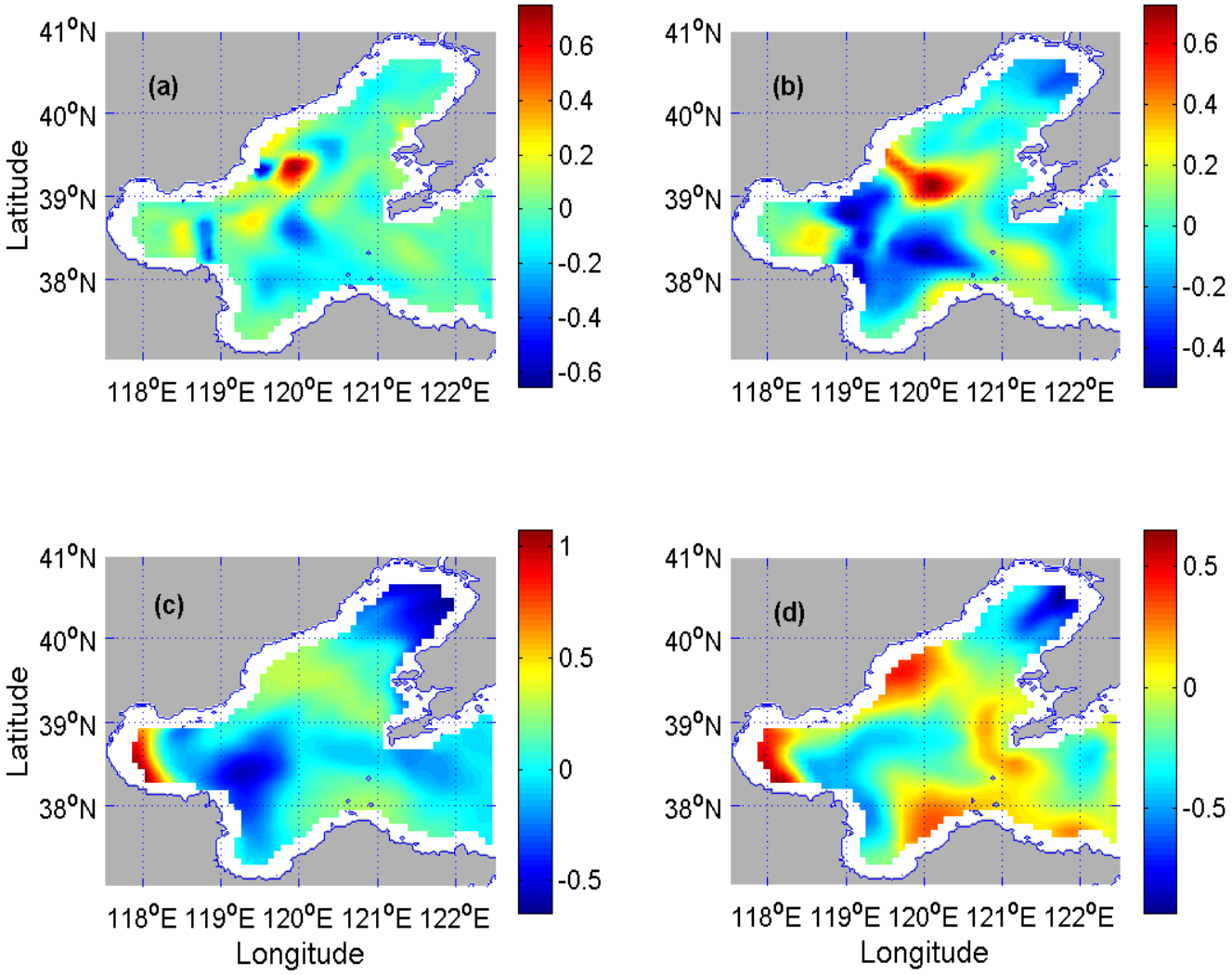

Figure 64. Salinity difference (psu) field (Run-1 minus Run-4) at the bottom on (a) January 15, (b) April 15, (c) July 15 and (d) October 15, 2000.

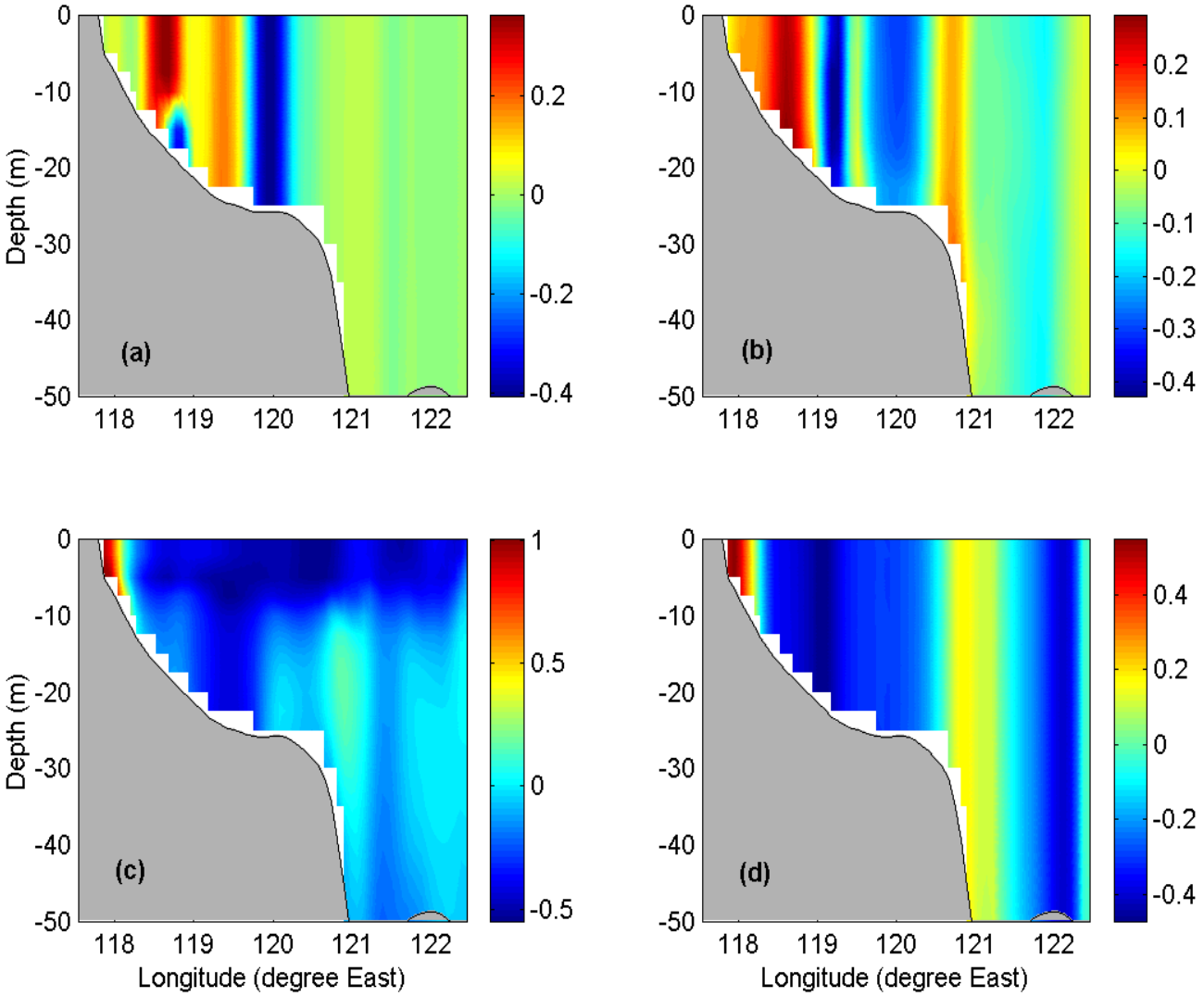

Figure 65. Zonal cross-section of the salinity (psu) difference (Run-1 minus Run-4) along 38°35.52'N on (a) January 15, (b) April 15, (c) July 15 and (d) October 15, 2000.

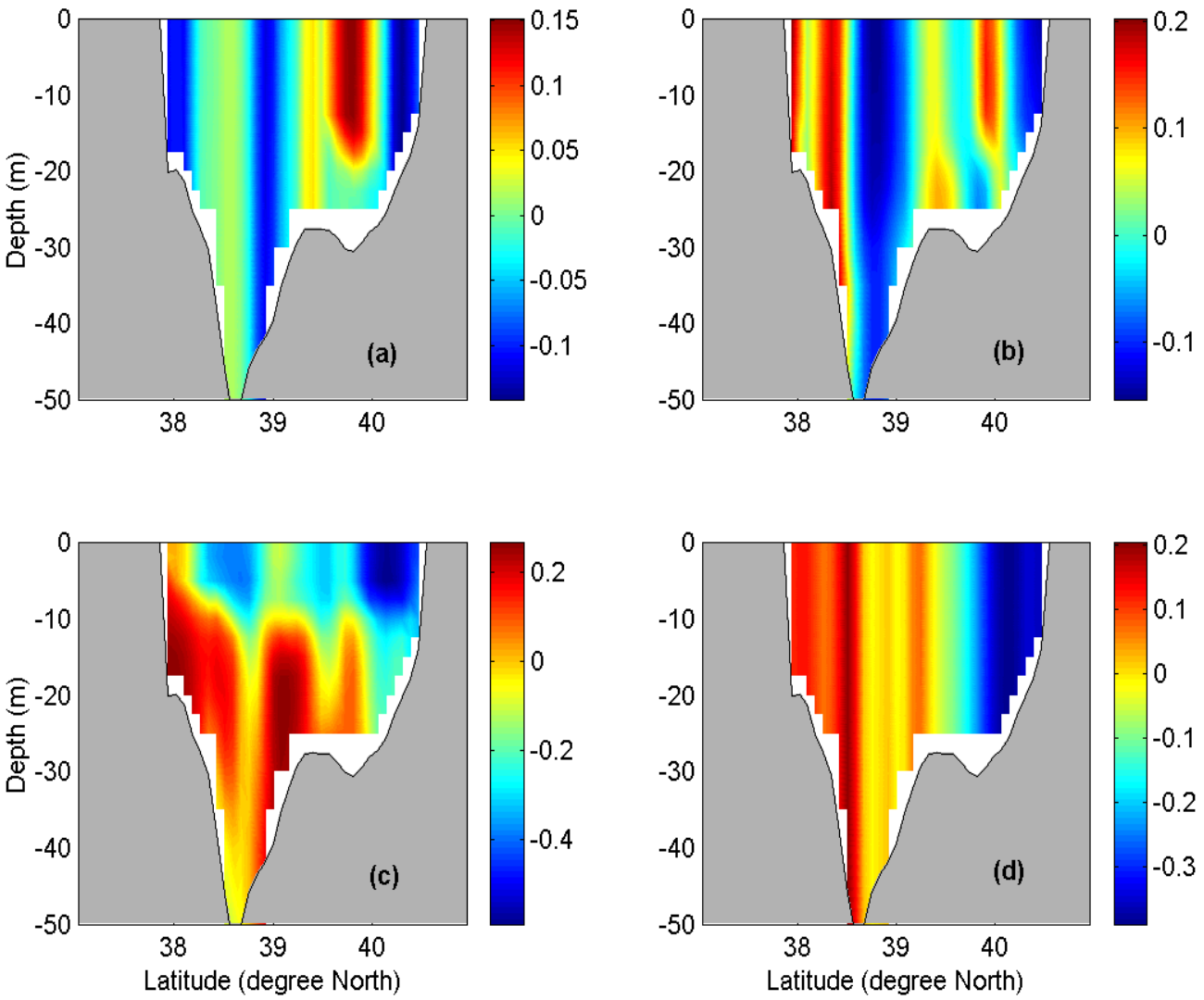

Figure 66. Meridional cross-section of the salinity (psu) difference (Run-1 minus Run-4) along 121°01.5'E on (a) January 15, (b) April 15, (c) July 15 and (d) October 15, 2000.

THIS PAGE INTENTIONALLY LEFT BLANK

VIII. TWO TURBULENCE SCHEMES

Vertical eddy viscosity and diffusivity are parameterized using Richardson number formulations, flow-dependent formulations, or turbulence closure schemes. There are two commonly used turbulence closure schemes: "*k*-*l*" (or called level 2.5) scheme (Mellor and Yamada, 1982) and "*k*-ε" scheme (Luyten et al., 1996). The "*k*-*l*" scheme uses the "Kolmogorov-Prandtl" mixing length (*l*) and TKE to determine the vertical eddy viscosity and diffusivity, and parameterizes the dissipation rate. The "*k*- ε" scheme avoids the mixing length concept and uses the dissipation rate (ε) to determine *k* and the vertical eddy viscosity and diffusivity.

What is the difference between the two schemes? A comparison of TKE between Run-1 and Run-5 provides the answer. Six points distributed in BS (Figure 67) are selected for the comparison: Point-a (38°21'N 122°24'E) represents the eastern boundary, Point-b (38°36'N 121°12'E) the northern part of Bohai Strait, Point-c (39°02'N 120°15'E) the middle of the central basin, Point-d (39°50'N 120°59'E) the Liaodong Gulf, Point-e (38°35'N 118°32'E) the Bohai Gulf, Point-f (37°46'N 119°40'E) the Laizhou Bay. Point-c (central basin) is selected for studying the TKE diurnal variation.

A. VERTICAL VARIABILITY OF TKE

Vertical profiles of January (Figure 68) and July (Figure 69) 2000 mean TKE for the six locations show a similar vertical dependency, same order of magnitude, but higher values (of TKE) simulated using the *k*-*l* scheme than the *k*-ε scheme for all depths. In January, a maximum TKE value appears at the surface and a minimum occurs at the bottom except at Point-f, where a maximum TKE appears at the bottom and a minimum at 5 m depth. TKE values at Points-a, Point-b, and Point-d have the same range between 0.2 and 1.4×10^{-3} m^2/s^2, and have smaller values at Point-c (from 0.2 to 0.8×10^{-3} m^2/s^2) and smallest values at Point-e and Point-f (below 0.3×10^{-3} m^2/s^2). The maximum TKE difference generally appears at 5 m depth. Only at Point-c (central basin) does the

maximum TKE difference occur at the surface. The stations at Bohai Gulf (Point-e) and Laizhou Gulf (Point-f) have higher TKE differences.

The vertical variability of the mean TKE is larger in July (Figure 69) than in January (Figure 68). In July, the maximum mean TKE for the six selected points appears at the surface and reaches 1.5×10^{-3} m^2/s^2 at the northern Bohai Strait (Point-b). Minimum mean TKE values occur at the bottom at Point-b, Point-c, and Point-d, and at 40 m (Point-a), 14 m (Point-e), and 9 m (Point-f).

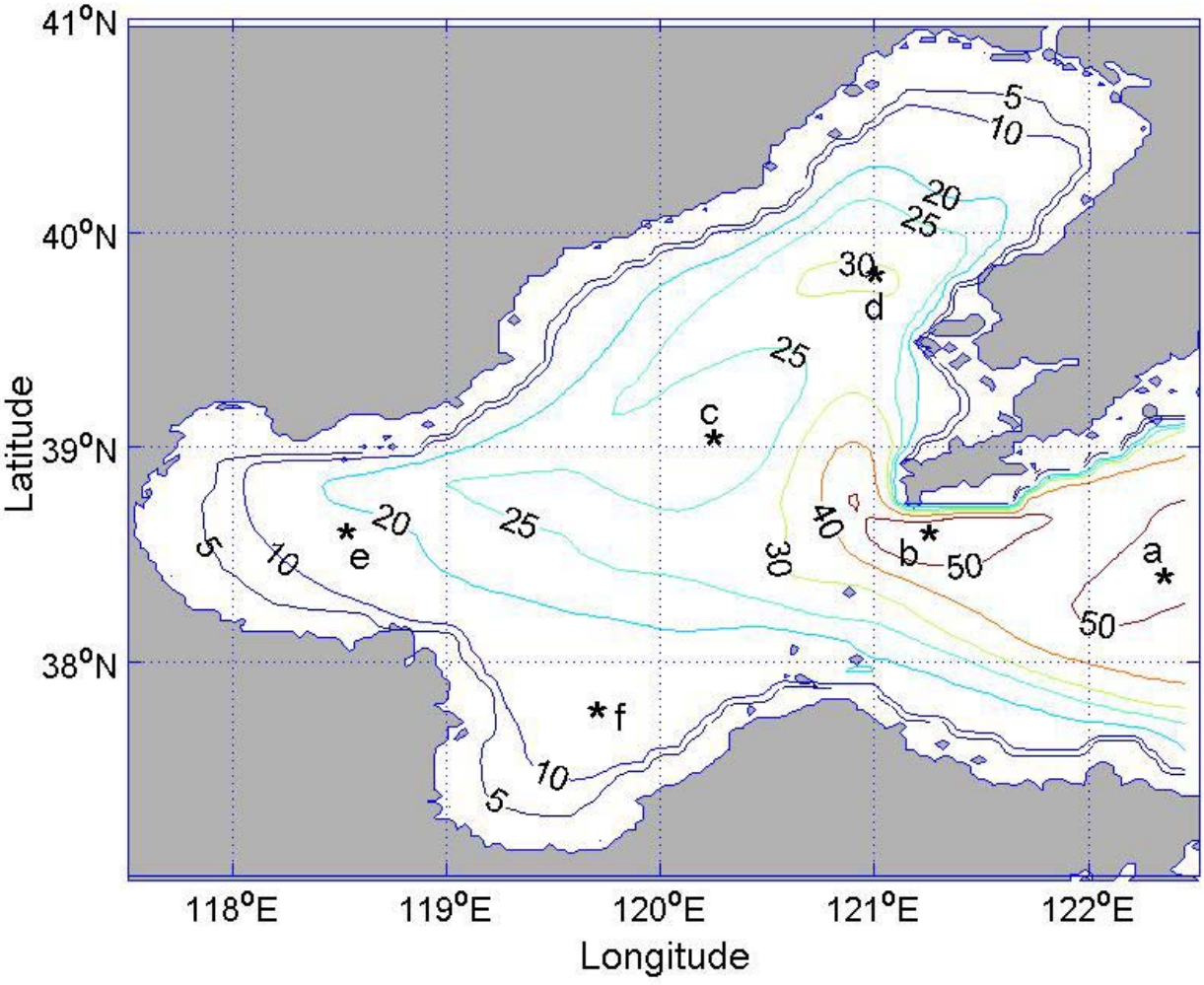

Figure 67. Points selected for turbulence closure scheme study. Bathymetry is represented by the isobaths in meters.

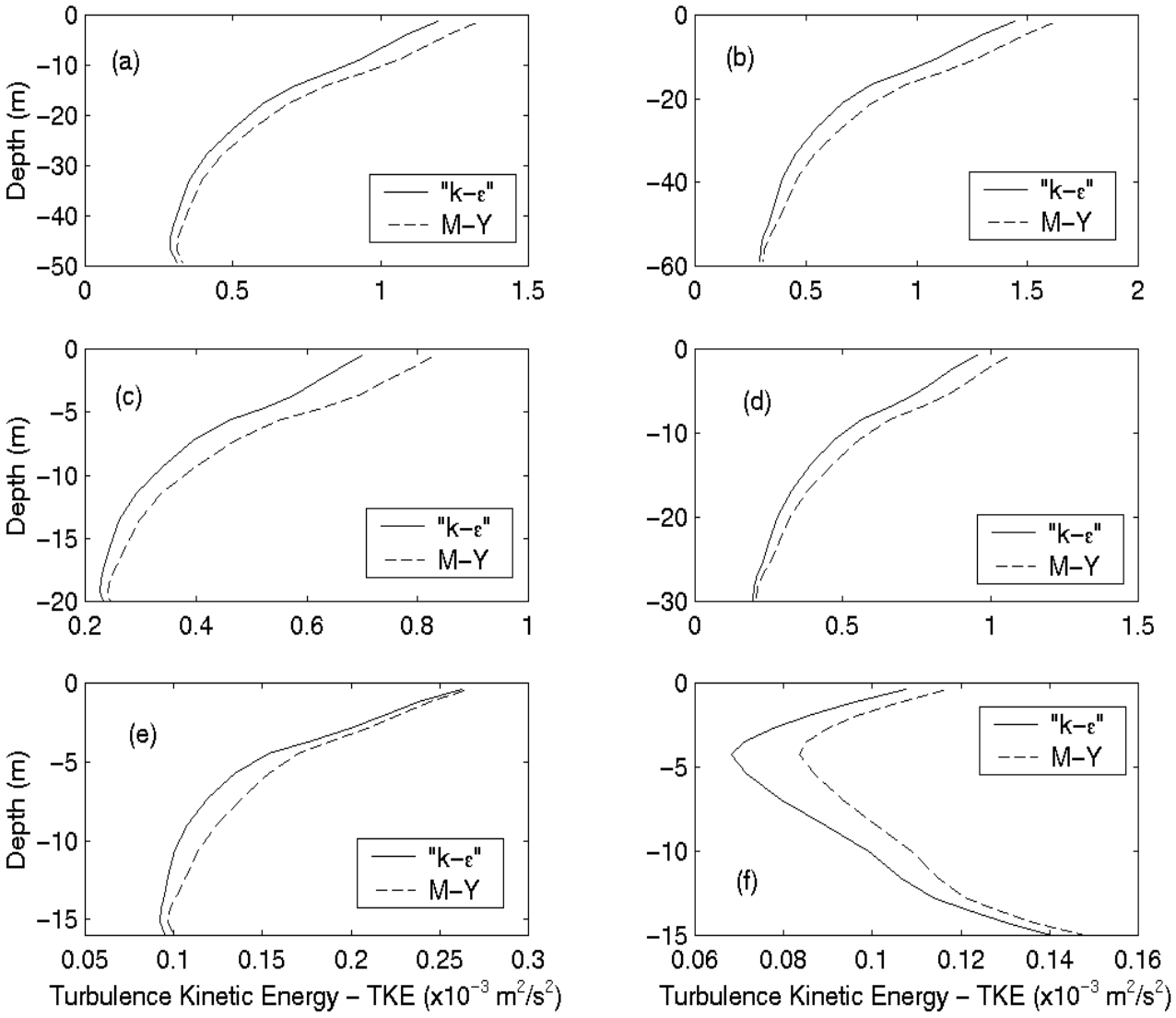

Figure 68. Monthly mean turbulence kinetic energy at each point in January 2000.

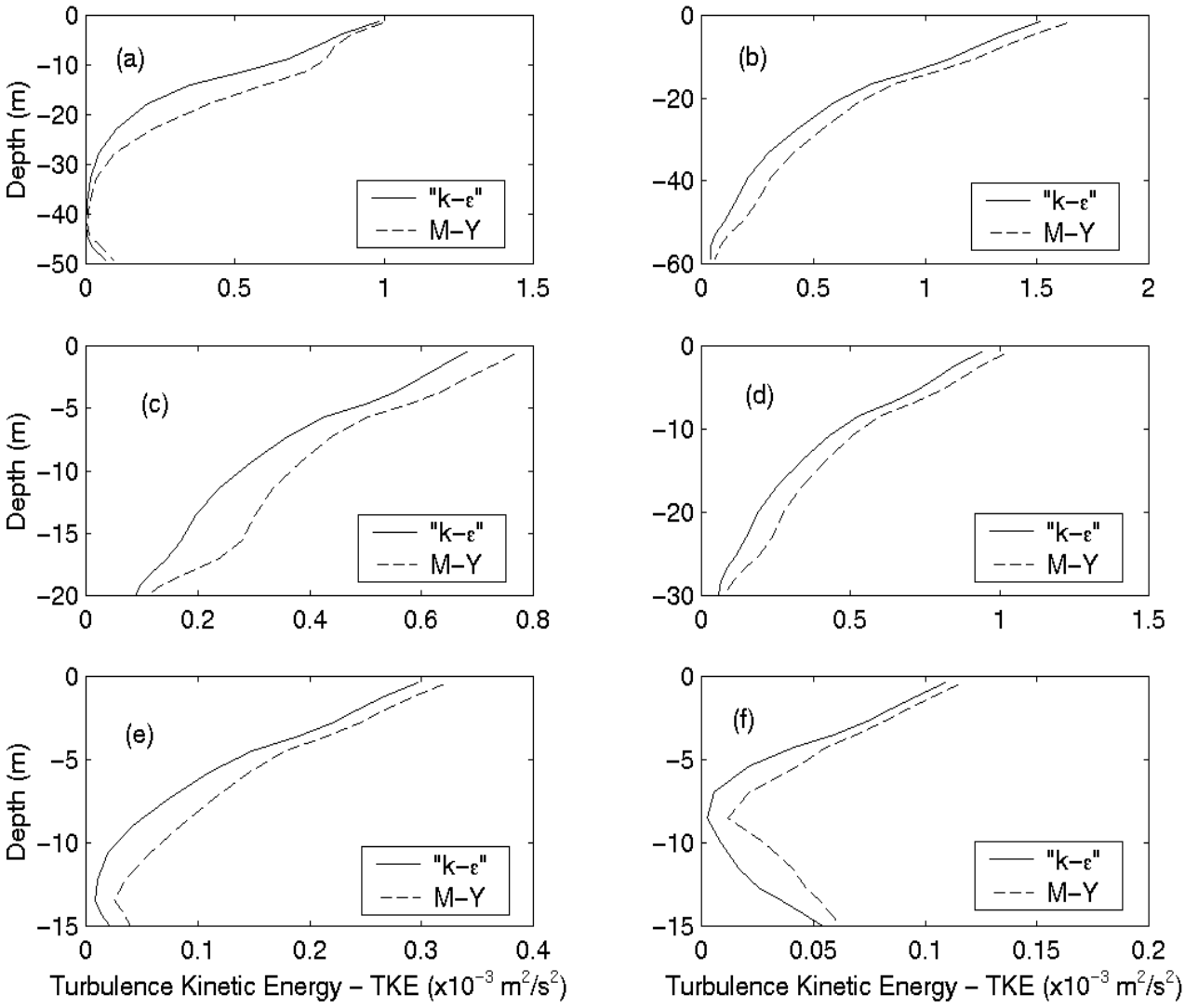

Figure 69. Monthly mean turbulence kinetic energy at each point in July 2000.

B. DIURNAL AND SEASONAL TKE VARIATIONS

The January 15 and July 15 dates are selected for the analysis of TKE diurnal variation and for the examination of the TKE differences using the two schemes. Figures 70-75 illustrate hourly TKE computed using the "*k-ε*" scheme on January 15 and July 15 at the selected points. Figures 76-81 illustrate hourly TKE computed using the "*k-l*" scheme on January 15 and July 15. Both formulations present the same variation and tendency. On the TKE decreasing phase, the profile is approximately a straight sloping line. When the TKE weakens, the gradient decreases and at the surface layer the curve bends to a lower value. The curve subsequently appears to approximate a parabola with a maximum TKE values of ~0.5 $\times 10^{-3}$ m^2/s^2 located between 10 and 20 m depth, and with a minimum TKE value close to zero. The parabola tends to decrease its curvature and to form a straight vertical line. On the TKE increasing phase, the surface layer TKE acquires a positive gradient, while the deeper layer becomes uniform. Both layers subsequently increase their gradient, with the surface layer greater and thicker. The deeper layer then bend to a higher gradient and the curve becomes again nearly a straight line with a strong gradient. For both schemes, the TKE is stronger in July than in January. Table 1 displays a comparison between the schemes of maximum TKE at each point, for the surface and at the bottom.

Scheme	"k-ε"		"k-l"	
Level	Surface	Bottom	Surface	Bottom
Point a	5.1	0.5	6.1	0.6
Point b	8.1	0.9	8.9	0.9
Point c	3.1	0.3	3.6	0.3
Point d	3.3	0.3	3.7	0.3
Point e	1.2	0.1	1.3	0.1
Point f	0.3	0.16	0.3	0.19

Table 1. Maximum TKE at the surface and at the bottom for both turbulence closure schemes. Values are expressed in 10^{-3} m^2/s^2.

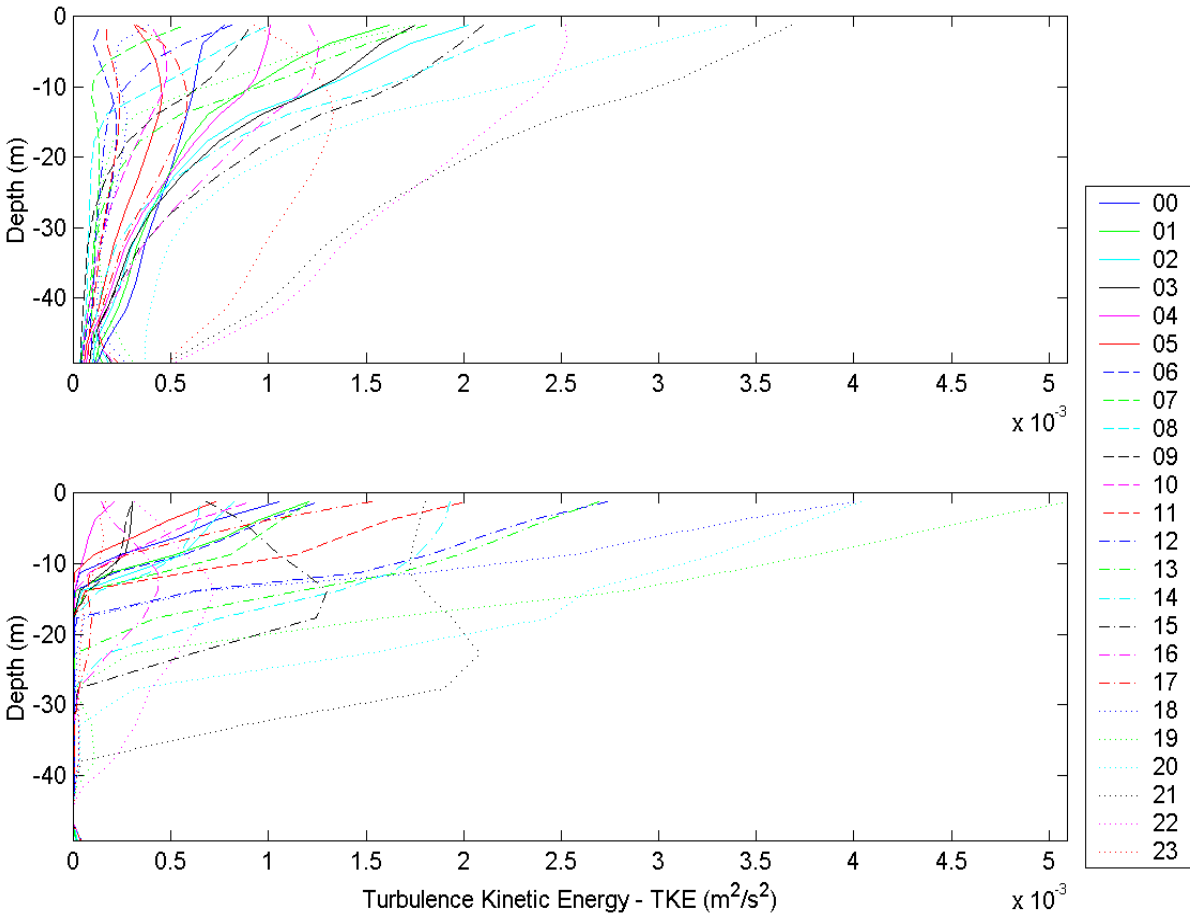

Figure 70. Hourly TKE computed at Point-a using the "k-ε" scheme on January 15 (above) and July 15 (below), 2000.

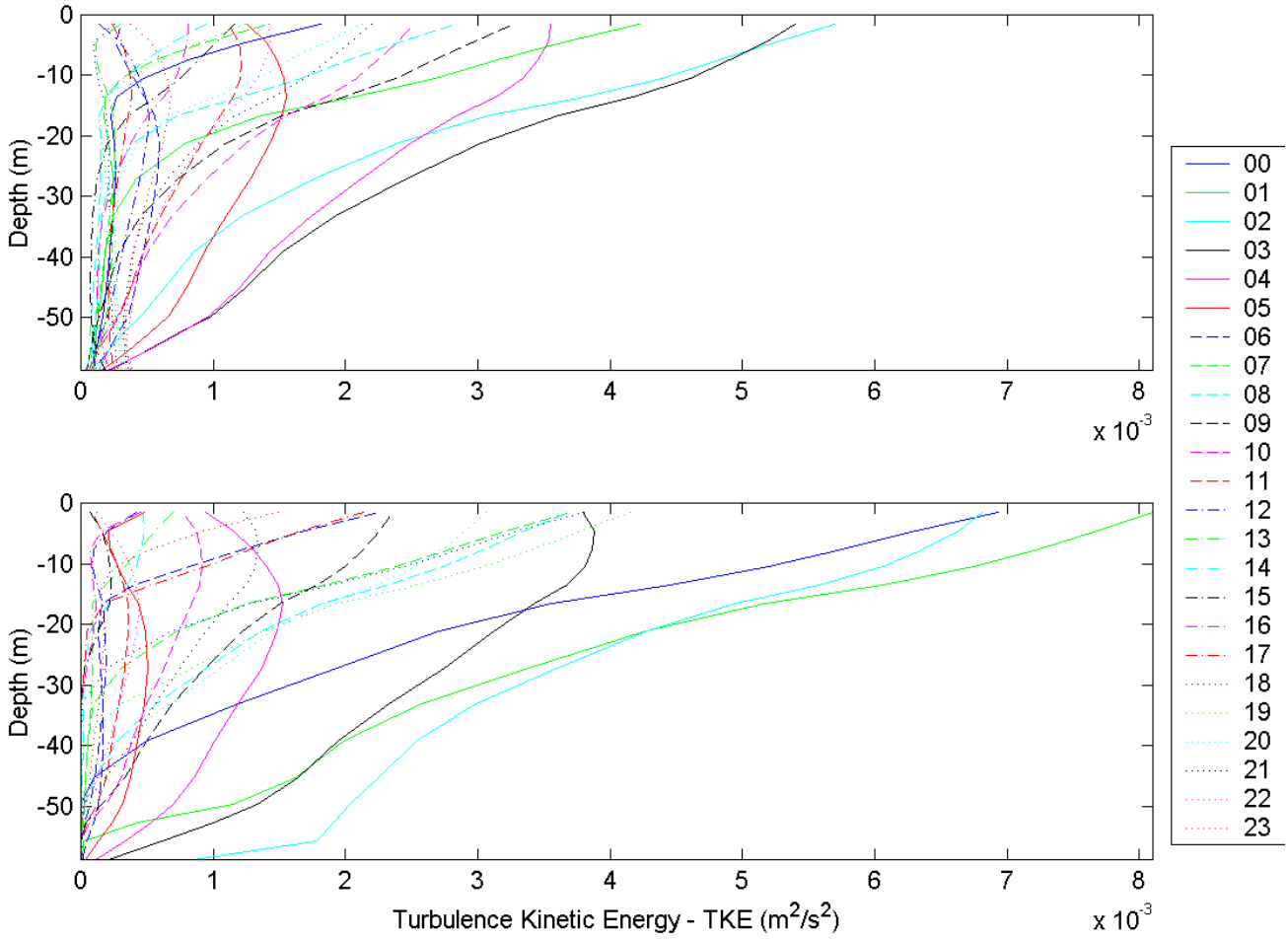

Figure 71. Hourly TKE computed at Point-b using the "k-ε" scheme on January 15 (above) and July 15 (below), 2000.

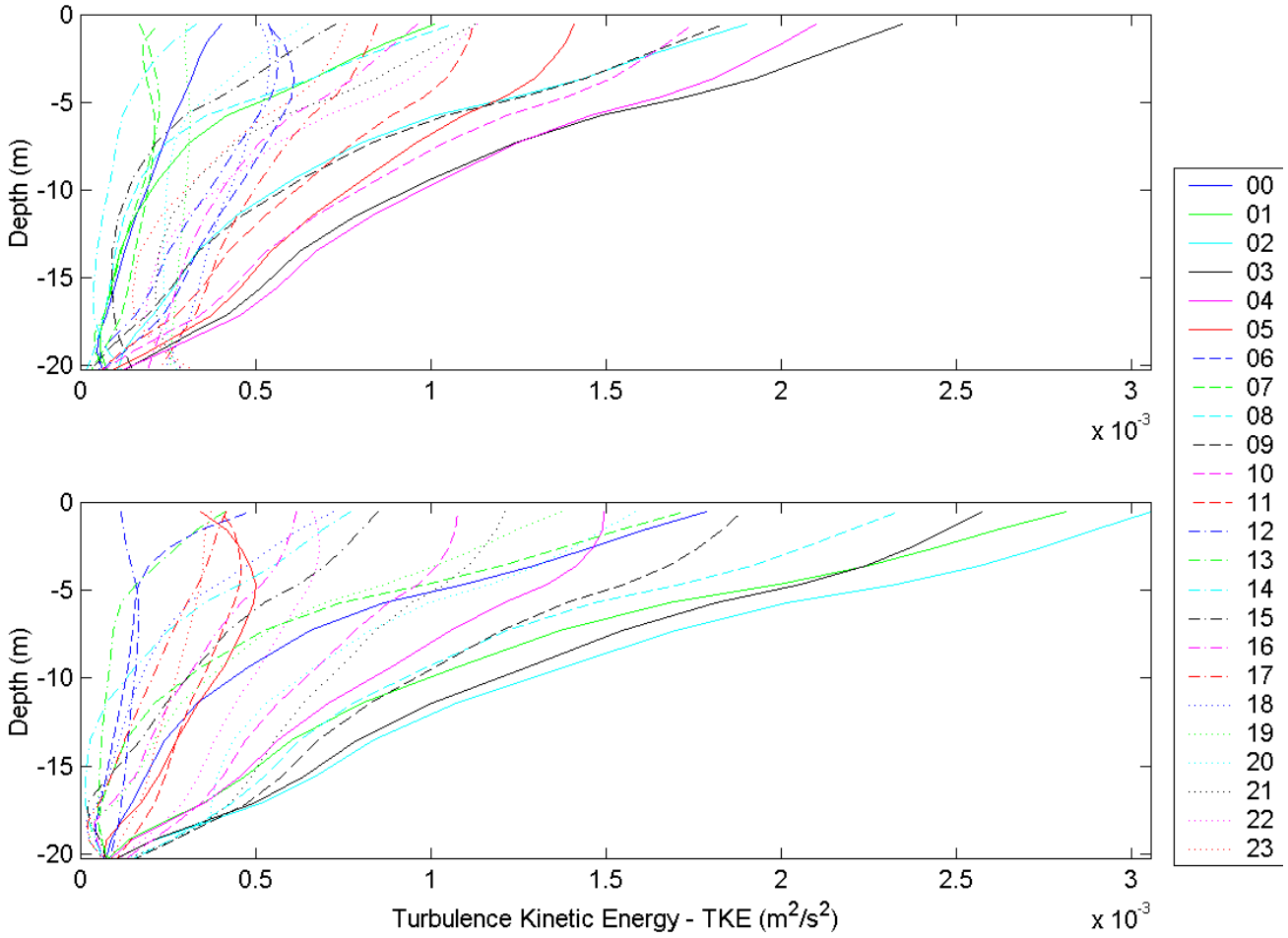

Figure 72. Hourly TKE computed at Point-c using the "k-ε" scheme on January 15 (above) and July 15 (below), 2000.

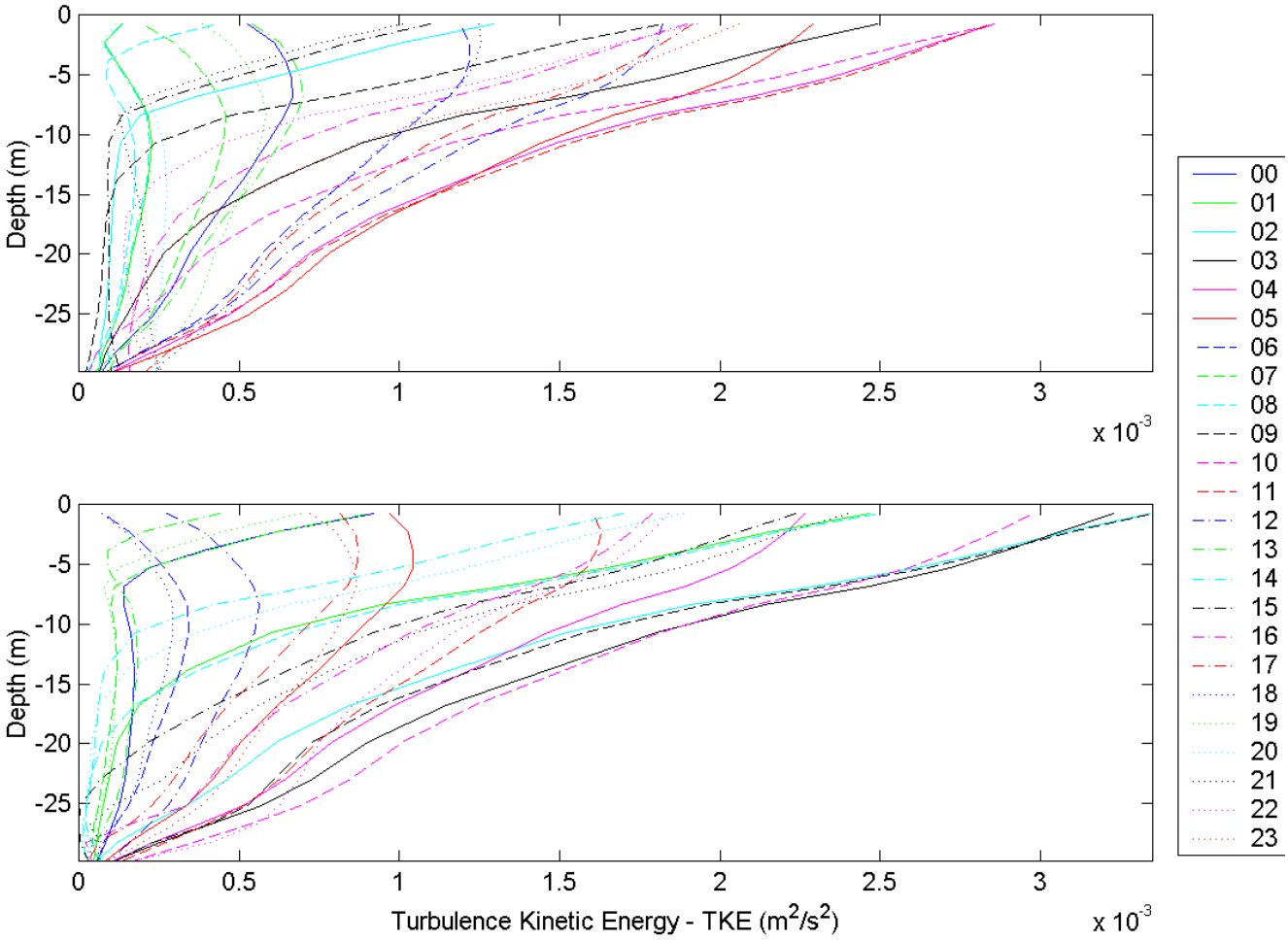

Figure 73. Hourly TKE computed at Point-d using the "k-ε" scheme on January 15 (above) and July 15 (below), 2000.

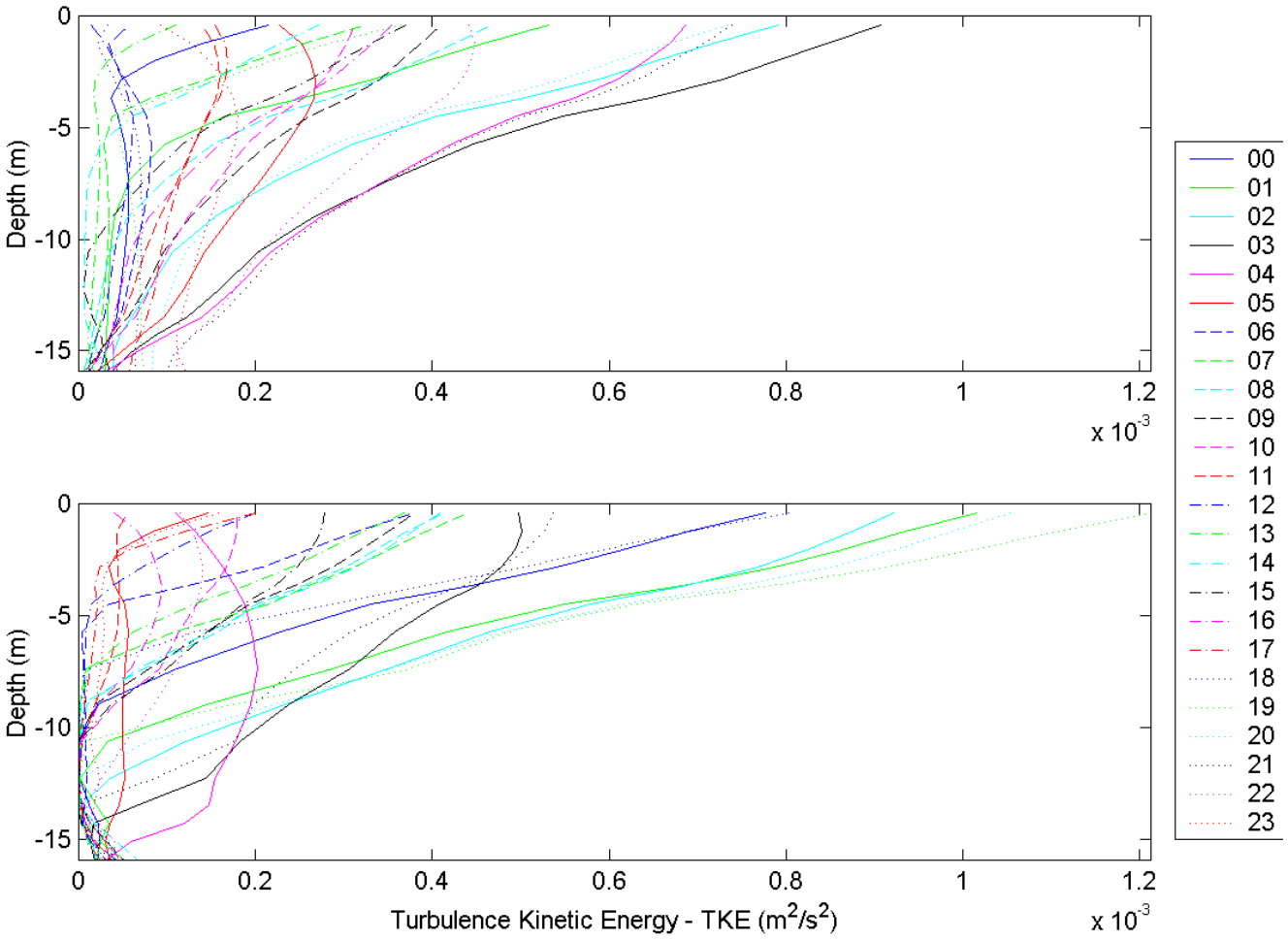

Figure 74. Hourly TKE computed at Point-e using the "k-ε" scheme on January 15 (above) and July 15 (below), 2000.

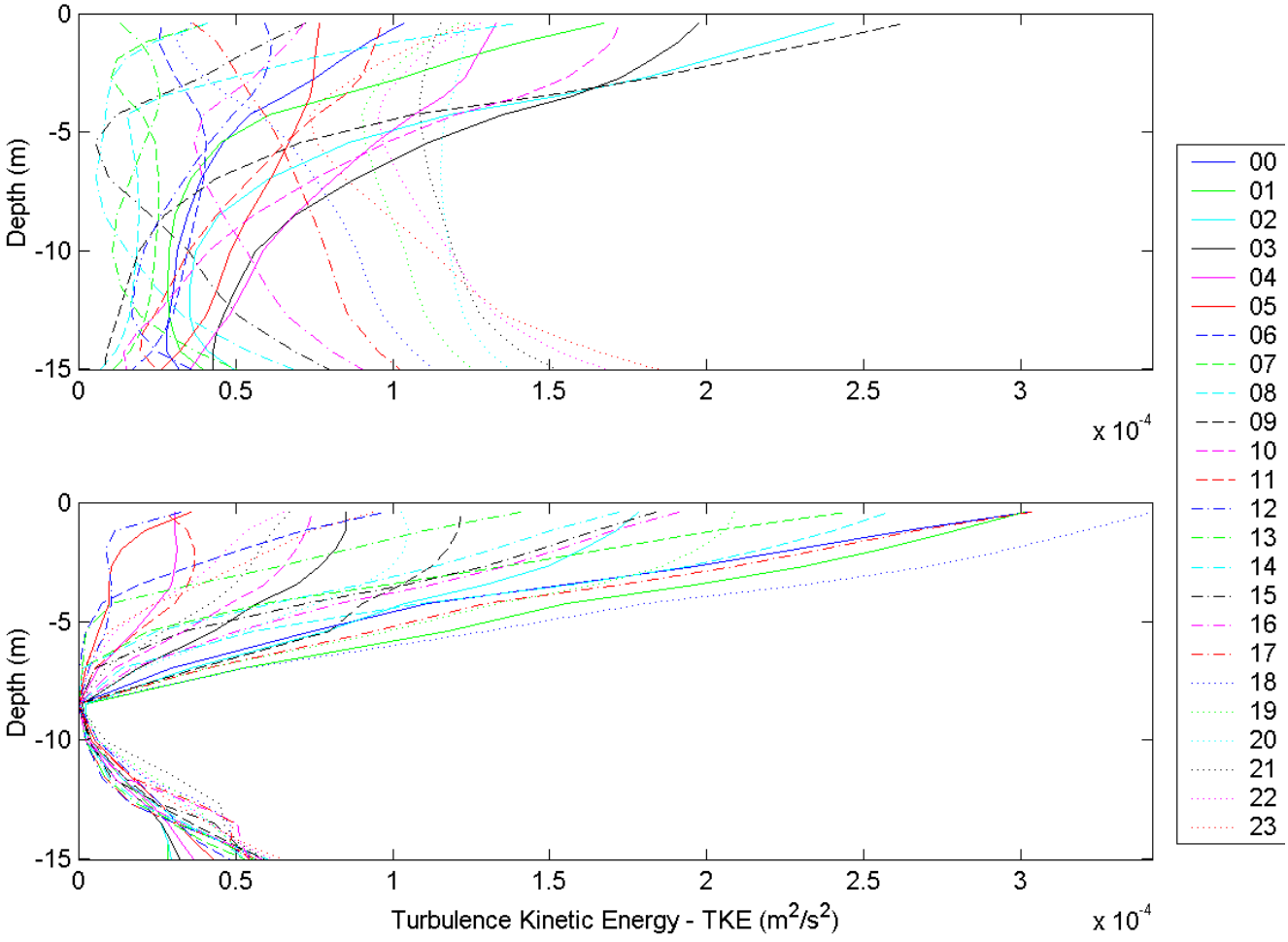

Figure 75. Hourly TKE computed at Point-f using the "k-ε" scheme on January 15 (above) and July 15 (below), 2000.

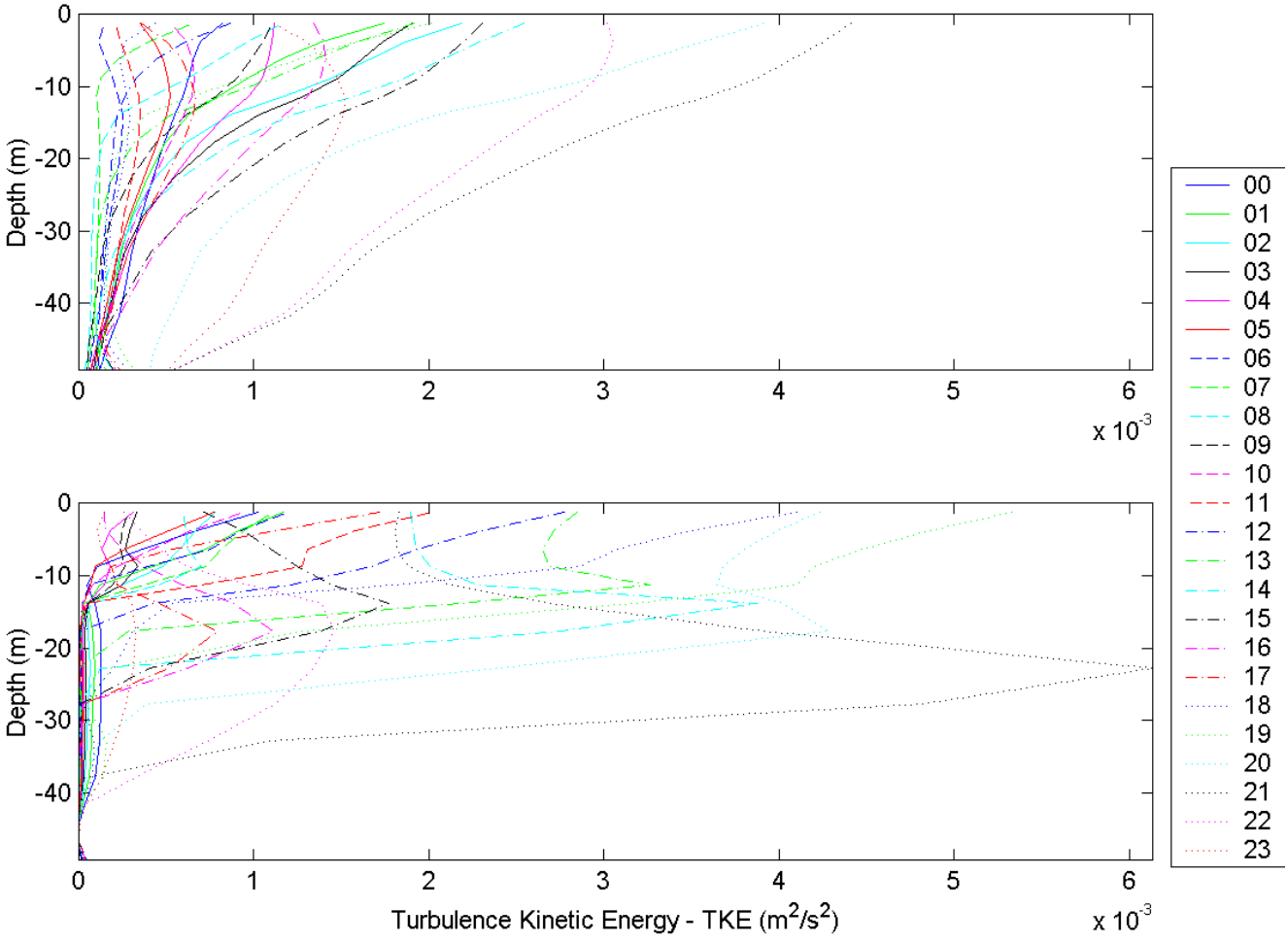

Figure 76. Hourly TKE computed at Point-a using the "k-l" scheme on January 15 (above) and July 15 (below), 2000.

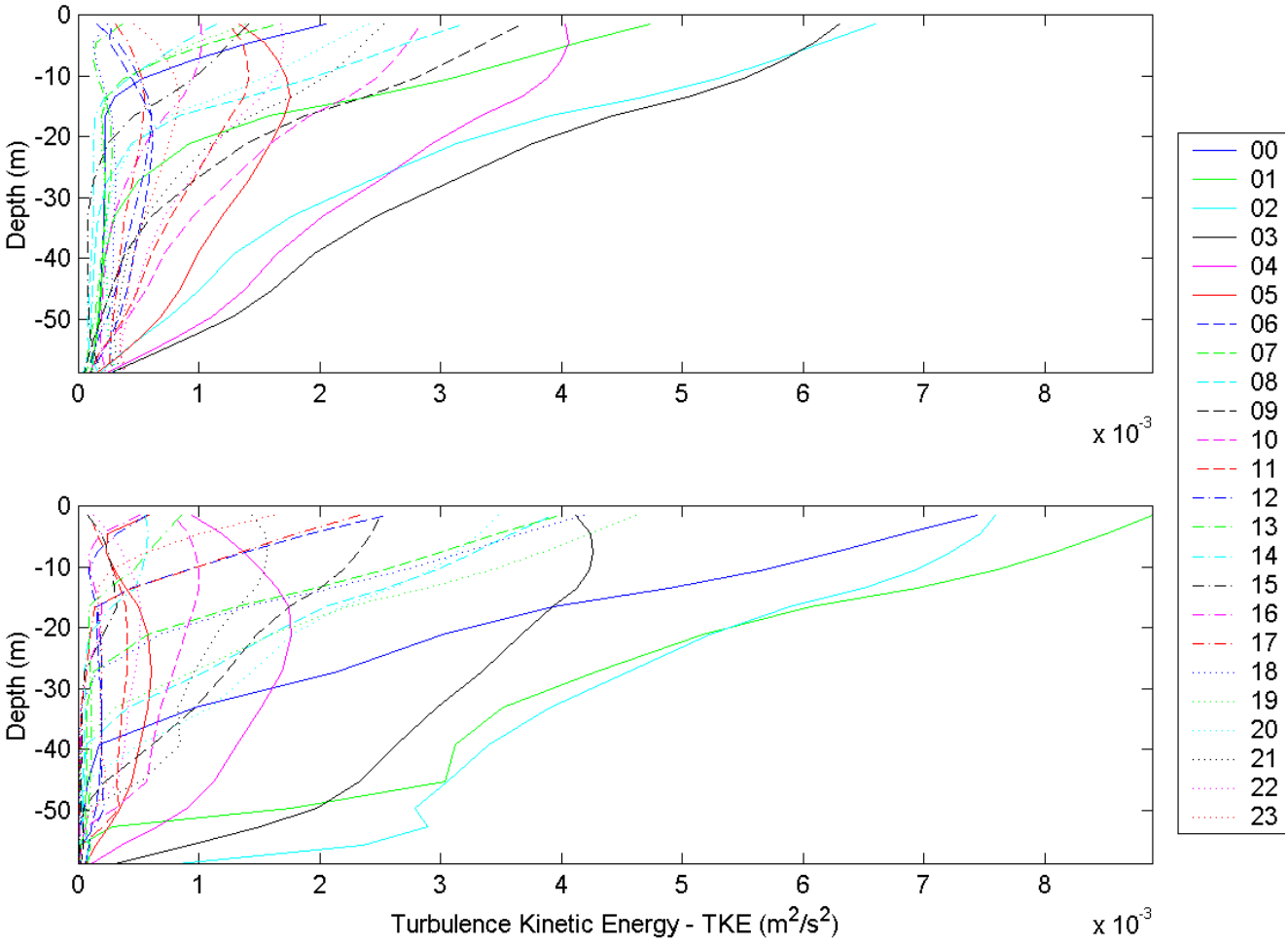

Figure 77. Hourly TKE computed at Point-b using the "k-l" scheme on January 15 (above) and July 15 (below), 2000.

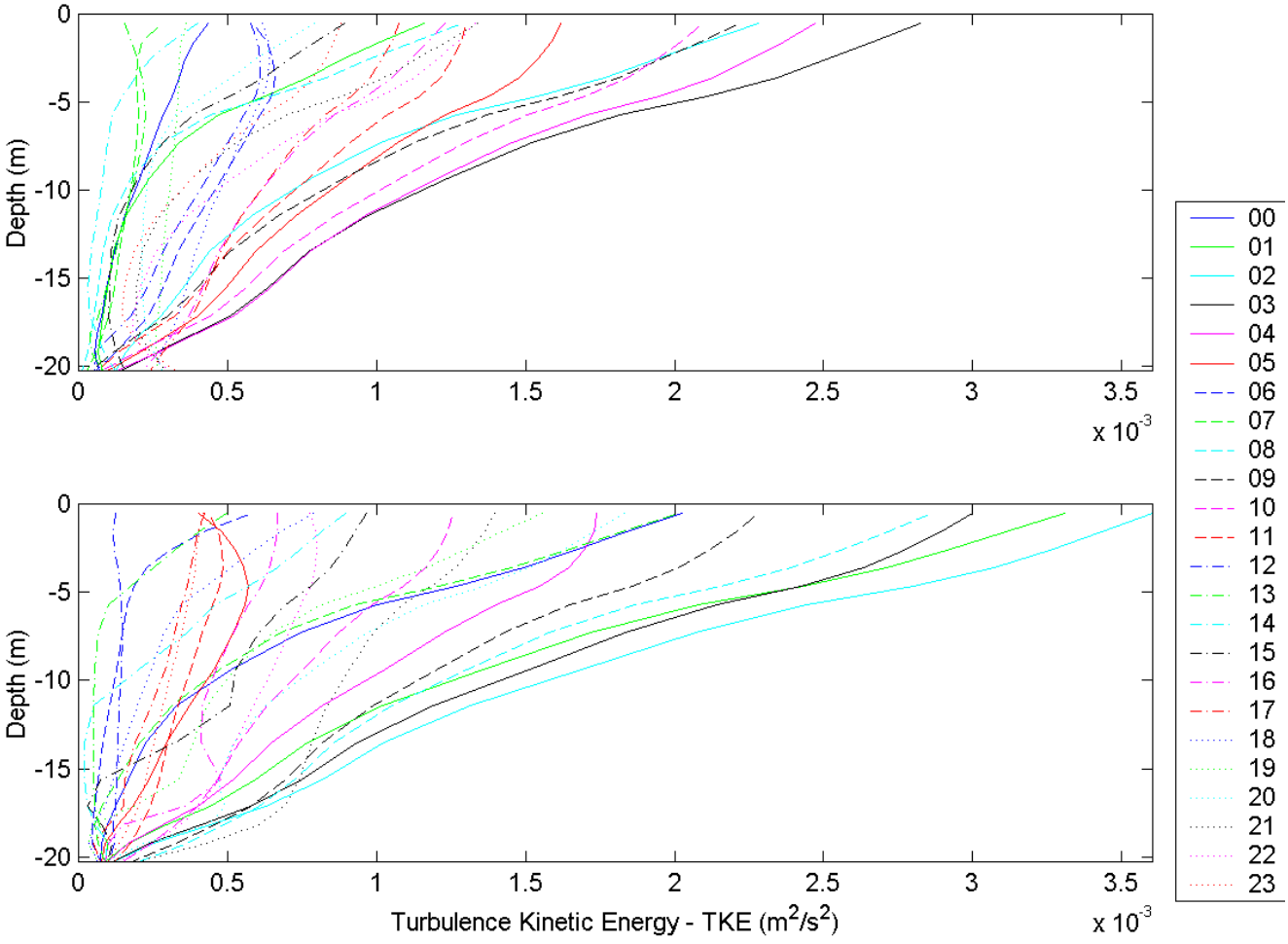

Figure 78. Hourly TKE computed at Point-c using the "k-l" scheme on January 15 (above) and July 15 (below), 2000.

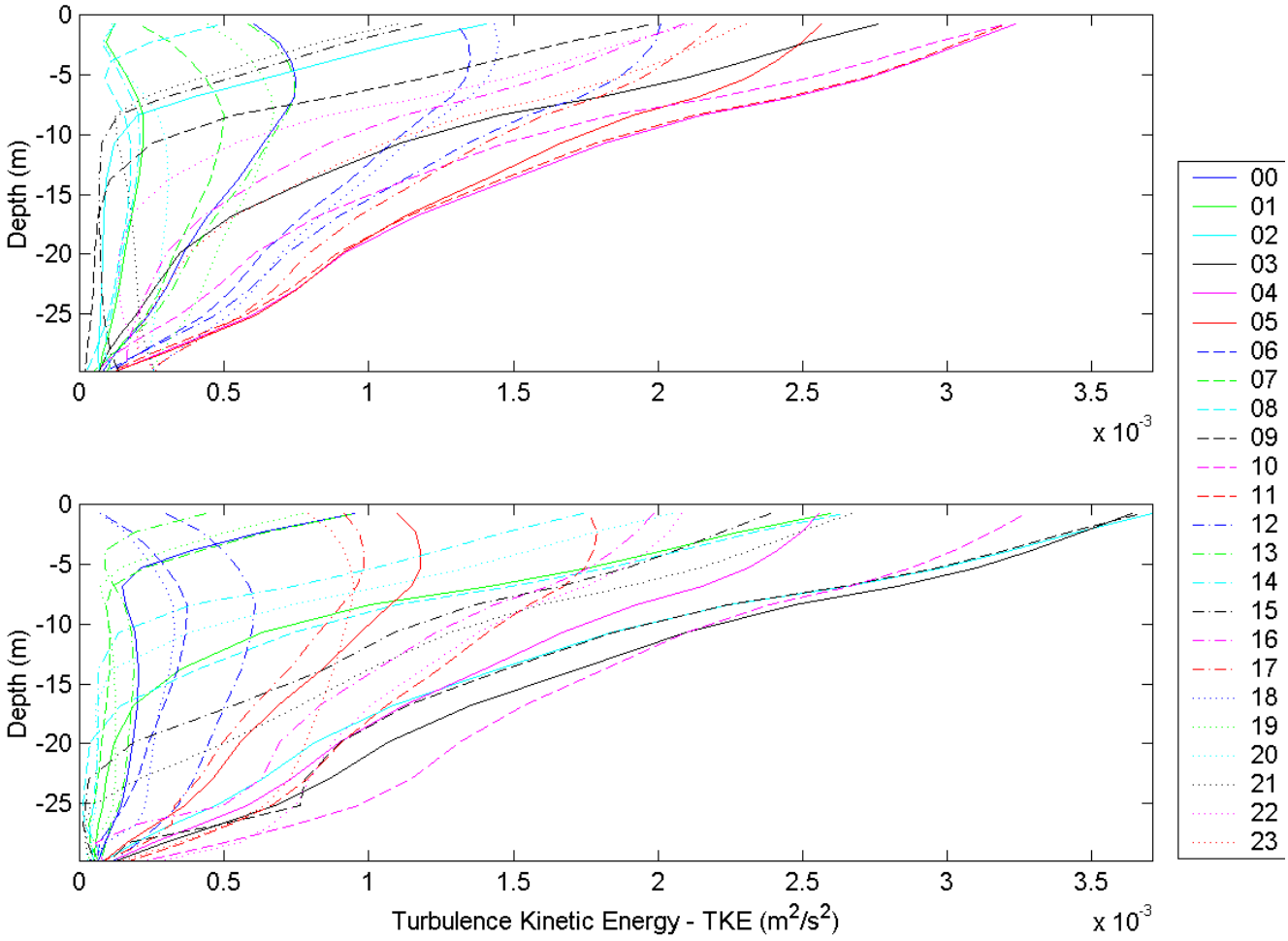

Figure 79. Hourly TKE computed at Point-d using the "k-l" scheme on January 15 (above) and July 15 (below), 2000.

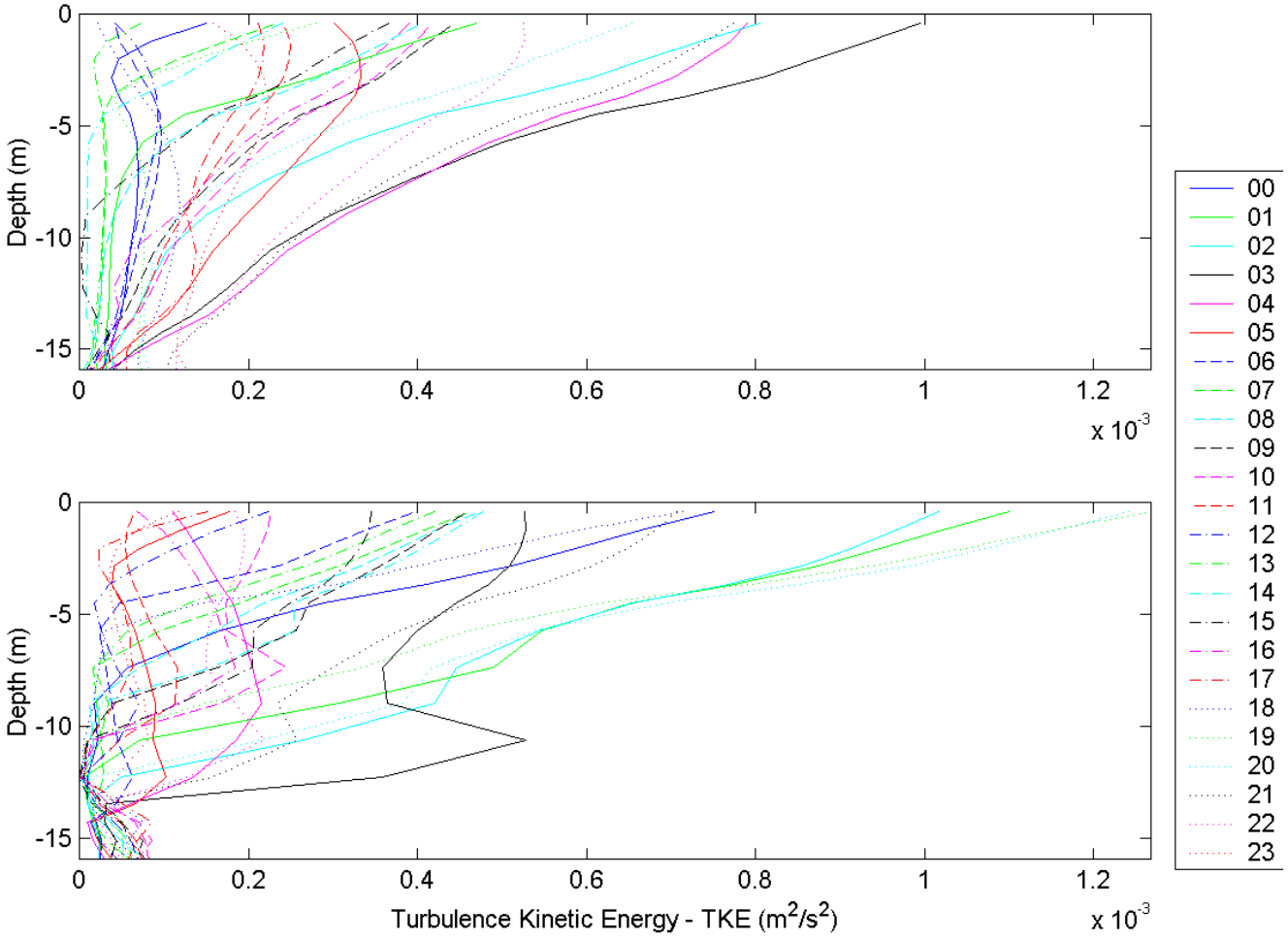

Figure 80. Hourly TKE computed at Point-e using the "k-l" scheme on January 15 (above) and July 15 (below), 2000.

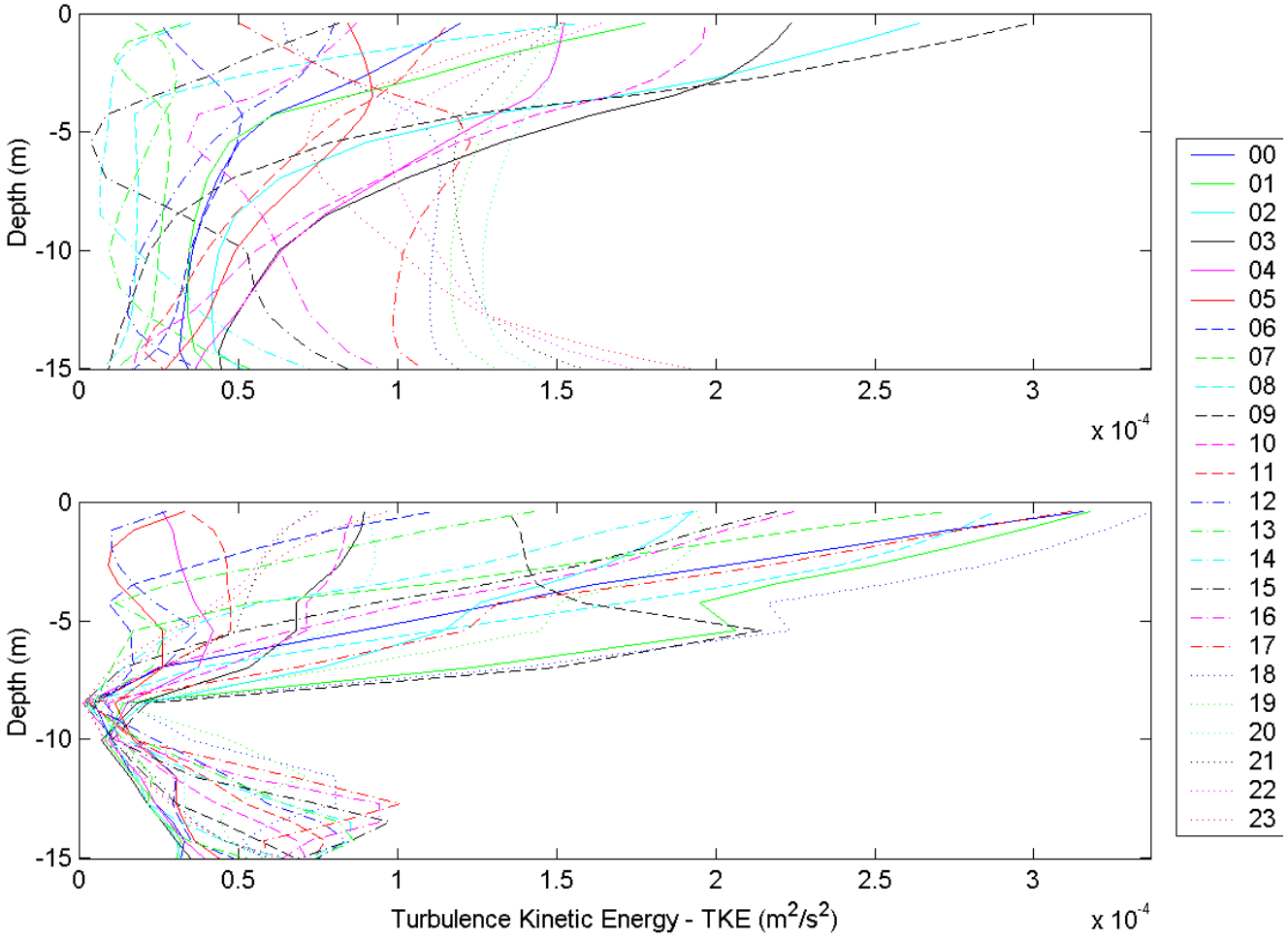

Figure 81. Hourly TKE computed at Point-f using the "k-l" scheme on January 15 (above) and July 15 (below), 2000.

THIS PAGE INTENTIONALLY LEFT BLANK

VIII. CONCLUSIONS

Although there are many renowned regional ocean models, the COHERENS model was specifically designed for shelf seas and manifests a huge flexibility due to the possibility of selecting the appropriate formulations from a variety of available schemes. Because of these advantages, the COHERENS ocean model was used to conduct a numerical simulation in the Bohai Sea and to develop sensitivity studies about the role of atmospheric data, winds and tides in the generation of currents and mesoscale features. Results indicate that the model simulates well the seasonal variability of the circulation pattern and the thermal structure. This study has shown that the use of four-time daily reanalysis atmospheric data can produce results qualitatively agreeable with previous observational studies and the Chinese atlas climatological data. We should, however, note that uncertainties in the reanalysis atmospheric data such as surface winds, relative humidity, atmospheric pressure, precipitation rate and cloudiness may distort the simulation.

The surface currents seem to be primarily wind-driven, while the compensating sub-surface circulation assumes an opposite direction and is restrained by the bottom topography. The northern part of the Bohai Strait throughout the year has a strong westward current. The circulation pattern is consistent with studies of Huang et al. (1995), where near the open boundary there is a surface cyclonic motion during the winter monsoon and a sub-surface anticyclonic circulation during the summer monsoon. This result may explain the water transport between the BS and the YS. In winter, the surface inflow occurs in the northern Bohai Strait and the outflow in the south at all layers, while in summer, the inflow is below the surface through the southern part and flows out through the north. At the mid-depth and at the bottom, the currents are stronger in the northern part of the central basin and at Liaodong Gulf during the winter and the summer monsoons. During the transition seasons, the sub-surface velocities are stronger in the southern part of the central basin and at Bohai Strait.

In January, April and October, the model simulated a vertically uniform thermohaline structure, while in July it presented a multi-layer structure. In January and

October, due to cooling, temperatures are lower in the shallow-water regions such as Liaodong Gulf, Bohai Gulf and Laizhou Bay than in the deep-water regions. In April and July, the shallow-water regions warm up faster than the deep-water regions. In the summer, a multi-layer structure is simulated with thermocline occurring at ~ 10 m depth.

The vertical salinity structure has similar features to the temperature structure. Only during the summer monsoon, is there some stratification in the surface layer. Throughout the year, it was found that the salinity values had a slow increase, even with forcing at the eastern open boundary. The salinity field was not as well simulated as the temperature, probably because the river runoff was not considered. The use of the Huanghe River discharge may adjust the salinity to expected values.

The wind effect is the major forcing driving the surface currents. This can be explained by the fact that differences found for the velocities at the surface in the wind experiment are greater than the surface thermohaline forcing and the tidal mixing cases. Only during April, at the east coast of the central basin and in the deeper regions of the Bohai Strait, where the currents found to be dominated by the tides.

The major effect of the surface thermohaline fluxes is to cool (warm) the BS in the winter (summer) for the whole water column. This effect becomes stronger at the gulfs and at Laizhou Bay due to the shallow depth, and quite weak near the eastern boundary in Bohai Strait. This effect does not change with depth in most seasons except in the summer when the effect weakens with the depth. Nevertheless, this effect has a large seasonal variability in shallow-water regions such as Liaodong Gulf (from -3^{o}C on 15 January 2000 to 7^{o}C on 15 July 2000) than the deep-water regions such as the central BS basin (from -2^{o}C on 15 January 2000 and 3-4^{o}C on 15 July 2000).

The tidal effect does not dominate the seasonal circulation at the surface, but it is responsible for some cyclonic and anticyclonic motions found at the gulfs and at the Laizhou Bay. The tidal mixing is responsible for the deep layer thermohaline characteristics. It cools the surface layer and warms the deeper layer in the summer as a result of vertical mixing.

The "*k*-*l*" turbulence closure scheme is found to have higher TKE than the "*k*-*ε*" scheme. Both schemes, however, provide similar TKE characteristics: (a) TKE has maximum values at the surface and decreases with depth rapidly in the surface layer and slowly below the surface layer; and (b) at the deeper layer TKE is weaker in the summer than in the winter.

Since this study did not account for the sediment, contaminant and biological models available in COHERENS, the inclusion of all of them or some of them would provide better understanding of these mechanisms in a crucial region for the Chinese economy. Future investigations could also include a detailed study of the tidal effect on the surface elevation and of the main harmonic constituents.

THIS PAGE INTENTIONALLY LEFT BLANK

LIST OF REFERENCES

Arakawa, A., and V. R. Lamb, 1977: Computational Design of the Basic Dynamical Processes of the UCLA General Circulation Model. *M. Comp Phys*., **17**, 173-265.

Dou Z., Yang L. and J. Ozer, 1994: Numerical simulation of three-dimensional tidal current in the Bohai Sea. *Acta Oceanologica Sinica*, **13(2)**, 155-172.

EU Marine Science and Technology (MAST) Programme, 1999: COHERENS – A Coupled Hydrodynamical-Ecological Model for Regional and Shelf Seas.

Fang, G., 1994: Tides and tidal currents in East China Sea, Huanghai Sea and Bohai Sea. *Oceanology of China Seas*, Vol. 1, Kluwer Academic Publishers, 101-112.

Feng, S., S. Zhang and P. Xi, 1994: A Lagrangian model of circulation in Bohai Sea. *Oceanology of China Seas*, Vol. 1, Kluwer Academic Publishers, 83-93.

Galperian, B., Kantha, L. H., Hassid, S. and Rossati, A., 1988: A quasi-equilibrium turbulent energy model for geophysical flows. *J. Atmos. Sci*., **45**, 55-62.

Guan, B., 1994: Patterns and structures of the currents in Bohai, Huanghai and East China Seas. *Oceanology of China Seas*, Vol. 1, Kluwer Academic Publishers, 17-93.

Huang D., Chen Z. and Su J., 1995: Modelling of the barotropic processes in the Bohai Sea. *Acta Oceanologica Sinica*, **14(3)**, 337-353.

Huang D., Su J. and Chen Z., 1995: Simulation of the thermal structure in the Bohai Sea. *Acta Oceanologica Sinica*, **14(4)**, 461-474.

Jin M., Wang Z. and Xu B., 1993. Three-dimensional numerical prediction of vertical temperature structure of the Huanghai and Bohai Seas. *Acta Oceanologica Sinica*, **12(4)**, 511-520.

Li L., Dou Z. and Zhang C., 1998: Numerical modeling of the Lagrangian residual current in the Bohai Sea. *Acta Oceanologica Sinica*, **7(2)**, 186-194.

Luyten, P. J., Deleersnijeder, E., Ozer, J. and Ruddick, K. G., 1996: Presentation of a family of turbulence closure models for stratified water flows and preliminary application to the Rhine outflow region. *Cont. Shelf Res.*, 16, 101-130.

Mellor, G. L. and T. Yamada, 1982: Development of a turbulence closure model for geophysical fluid problems. *Rev. Geophys. Space Phys*., **20**, 851-875.

Miao J. and Liu X., 1989: Some numerical experiments of the dynamics of the wintertime circulation in the Northern Huanghai Sea and the Bohai Sea. *Acta Oceanologica Sinica*, **8(3)**, 327-336.

Orlanski, I., 1976: A simple boundary condition for unbounded hyperbolic flows. *J. Comp. Phys*., **21**, 251-269.

Phillips, N. A., 1957: A coordinate system having some special advantages for numerical forecasting. *J.Meteor*., **14**, 184-185.

Smagorinsky, J., 1963: General circulation experiments with the primitive equations. I: The basic experiment. *Mon. Wea. Rev*., **91**, 99-164.

State Oceanic Administration of China, 1992: Marine Atlas of Bohai Sea, Yellow Sea and East China Sea Hydrology, Beijing, China Ocean Press, 524 pp.

Su Jilan, 1998: Circulation dynamics of the China Seas north of 18°N. *The Sea*, Vol. 11, Allan R. Robinson and Kenneth H. Brick, 483-505.

Su Y. and Weng X., 1994: Water masses in China Seas. *Oceanology of China Seas*, Vol. 1, Kluwer Academic Publishers, 3-16.

Sun W. and Wang Z., 1994: A quasi-three-dimensional numerical prediction model of salinity structure in Bohai Sea and Huanghai Sea. *Acta Oceanologica Sinica*, **3(4)**, 485-494.

Wang Hui, Su Z., Feng S. and Sun W., 1993: A three-dimensional numerical calculation of the wind-driven thermohaline and tide-induced Lagrangian residual current in the Bohai Sea. *Acta Oceanologica Sinica*, **12(2)**, 169-182.

Wang Zongshan, Xu B., Jin. M., Zou E. and Li F., 1998: A numerical prediction model of strong thermocline in the Bohai and the Huanghai Seas. *Acta Oceanologica Sinica*, **17(2)**, 141-154.

Wu H., Bai S. and Zhang Z., 1998: Numerical sea ice prediction in China. *Acta Oceanologica Sinica*, **17(2)**, 167-185.

Zhang Y. and Wang Y., 1992: Numerical modeling of the depth variation and the fluctuation of the thermocline under the effects of wind in the Bohai Sea. *Acta Oceanologica Sinica*, **11(3)**, 331-341.

Zhao Baoren, 1989: Basic characteristics and forming mechanism of the sharp thermocline in the Bohai Sea, Huanghai Sea and northern East China Sea. *Acta Oceanologica Sinica*, **8(4)**, 497-510.

Zhao J. and Shi M., 1994: Study on short-range numerical forecasting of ocean current in the East China Sea – II. *Acta Oceanologica Sinica*, **12(2)**, 173-188.

THIS PAGE INTENTIONALLY LEFT BLANK

INITIAL DISTRIBUTION LIST

1. Defense Technical Information Center
   Ft. Belvoir, Virginia

2. Dudley Knox Library
   Naval Postgraduate School
   Monterey, California

3. Chairman
   Department of Oceanography
   Naval Postgraduate School
   Monterey, California

4. Oceanographer of the Navy
   Naval Observatory
   Washington, D.C.

5. Commander
   Naval Meteorological and Oceanography Command
   Stennis Space Center, MS

6. Commanding Officer
   Naval Oceanographic Office
   Stennis Space Center, MS

7. Chief of Naval Research
   800 North Quincy Street
   Arlington, VA

8. Dr. Peter C. Chu
   Department of Oceanography
   Naval Postgraduate School
   Monterey, California

9. Dr. Don Durham
   Commander
   Naval Meteorological and Oceanography Command
   Stennis Space Center, MS

10. CDR Eric Gottshall
    SPAWAR, PMW-155

11. Mr. Steve D. Haeger
Naval Oceanographic Office
Stennis Space Center, MS

12. Dr. Edward Johnson
Naval Oceanographic Office
Stennis Space Center, MS

13. CDR Eric Long
Chief of Naval Operations, N752
Washington, D.C.

14. Mr. Mark Null
Naval Oceanographic Office
Stennis Space Center, MS

15. Dr. Richard Spinrad
CNO-N96
Naval Observatory
Washington, D.C.

16. LCDR Rodrigo de S. Obino
Rua Lopes Quintas, 200 Bl I 405
Rio de Janeiro, R.J.
Brazil

17. Diretor do Centro de Hidrografia da Marinha
Av. Vital de Oliveira, s/n Ponta da Armação
Niterói, R.J.
Brazil

18. Superintendente de Previsão Ambiental
Centro de Hidrografia da Marinha
Av. Vital de Oliveira, s/n Ponta da Armação
Niterói, R.J.
Brazil

19. Superintendente de Ensino
Diretoria de Hidrografia e Navegação
Av. Vital de Oliveira, s/n Ponta da Armação
Niterói, R.J.
Brazil